Investigation of Modes of Current Transfer to Cathodes of Glow and Arc Discharges

TESE DE DOUTORAMENTO

Pedro Jorge Gomes Camacho de Almeida
DOUTORAMENTO EM FÍSICA

UNIVERSIDADE da MADEIRA
A Nossa Universidade
www.uma.pt

Maio | 2011

Io ritornai da la santissima onda
rifatto sì come piante novelle
rinovellate di novella fronda,
puro e disposto a salire a le stelle.

From that most holy water I returned,
remade, in the manner of new plants
That are renewed with new-sprung leaves,
Pure and disposed to mount unto the stars.

Dante Alighieri, *Divina commedia*
Canto XXXIII, Purgatorio

Acknowledgements

I wish to thank my supervisor, Professor Mikhail Benilov, who taught me much more than just physics. I had the privilege of meeting Professor Benilov in 1998, when I was still a Physics undergraduate student at Universidade da Madeira. He has influenced my life in many, many ways, probably in more than I can think of. During this work he has always been available to discuss physics and always did his best to keep me motivated. I thank him for that, for the opportunities he gave me, for the chance of becoming a member of the Physics Group of Universidade da Madeira and for his continuous effort to pass me some of his scientific brilliance. Professor Benilov set the academic standard to which I aspire. I have great pride in being one of his PhD students.

I acknowledge fruitfull collaboration with my colleagues Mário Cunha and Maria José Faria. Mário provided the numerical results given in chapter 4; MJ provided results from bifurcation theory and stability analysis mentioned throughout the thesis.

I am grateful to Professor Marco Haverlag, to Dr. Lars Dabringhausen and to Philips Lighting for supplying lamps with different electrode diameter and without coils used in the experiments, and for supplying X-ray photographs of the electrodes. I thank also Dr. Henk van Esveld of Philips Lighting, Mr. Loek Baede of Eindhoven Technical University and, in particular, Dr. Lars Dabringhausen of Philips Lighting for their valuable support to construction of the experimental setup in Universidade da Madeira.

I thank Professor Jurgen Mentel and Oliver Langenscheidt for discussions concerning the experiments in Bochum University and for their support during my stay in Bochum. I also thank Professor Joost van der Mullen and Dr. Tanya Nimalasuriya for discussions concerning experiments with COST-529 standard lamps in Eindhoven Technical University and for their support during my stay in Eindhoven.

I also thank Vasco Guerra and Carlos Pintassilgo for very useful discussions concerning kinetic schemes of argon. I am grateful to George Petrov and Professor Carlos Matos Ferreira for supplying extensive data on argon kinetics.

Thanks are due to Mário Cunha, my colleague and friend, for his recurrent availability to listen to me rambling about my work and for countless discussions which have contributed decisively to my understanding of physics. His incentive played and important role.

I thank Nelson Almeida for his availability to temporarily take over my classes during the final stages of the preparation of the thesis and for his help with LaTeX problems.

I thank my bonsai master, Mr. Nobuichi Urushibata, who showed me the importance of humbleness in one's life. Oyakata Urushibata helped me clear my mind during the time I spent with him in Japan, which constituted a crucial break from the work leading to this thesis.

To all my family and friends, who always had some encouraging words for me in the most difficult times. Maurício Reis and Nélio 'Nilio' Ferreira, who were working towards their PhDs in Mathematics, showed me the hilarious world of PhD Comics. I thank them for laughing sessions in their company, which I believe to have held the three of us at acceptable levels of sanity, and for sharing their "always look on the bright side of life" philosophy with me.

I thank my parents and my grandparents for their constant support, for teaching me the

benefits of working hard and for nurturing my interest in science since I was a little toothless boy. I also thank all of my in-laws for their valuable support.

To Julie, the Basset Hound who owns me, for some very insightful moments spent in her company. To my wife Andreia, who always tolerated my grumpiness and replied with her disarming smile, especially during the long months of numerical calculations. I cannot imagine how could anyone be as supportive as she is.

Preamble

The work leading to this thesis was performed within activities of:

- PhD Fellowship SFRH/BD/30598/2006 from Fundação para a Ciência e a Tecnologia.
- Project POCTI/FIS/32411/2000 *Theory and modelling of plasma-cathode interaction in high-pressure arc discharges* of the program POCTI of FCT and FEDER.
- Project POCI/FIS/60526/2004 *Modes of current transfer to cathodes of high-pressure arc discharges and their stability* of Fundação para a Ciência e a Tecnologia, POCI 2010 and FEDER.
- Project PTDC/FIS/68609/2006 *Cathode spots in high-pressure DC gas discharges: self-organization phenomena* of Fundação para a Ciência e a Tecnologia and FEDER.
- *Centro de Ciências Matemáticas* of Fundação para a Ciência e a Tecnologia, POCTI-219 and FEDER.

Most of the results presented in this thesis are published in the following articles:

- P. G. C. Almeida, M. S. Benilov, and M. D. Cunha, Formation of stationary and transient spots on thermionic cathodes and its prevention (2008), J. Phys. D: Appl. Phys. 41 No. 14 144004-1-9
- P. G. C. Almeida, M. S. Benilov, and M. D. Cunha, Transient spots on cathodes of high-pressure arc discharges (2008) IEEE Trans. Plasma Sci. 36, No. 4 1032-1033
- P. G. C. Almeida, M. S. Benilov, and M. J. Faria, Multiple solutions in the theory of dc glow discharges (2010) Plasma Sources Sci. Technol. 19 No. 2 025019-1-13
- P. G. C. Almeida, M. S. Benilov, and M. J. Faria, 3D Modeling of self-organization in DC glow microdischarges (2011) IEEE Trans. Plasma Sci. 39 No. 4 to appear

Results presented in this thesis were reported at the following conferences:

- P. G. C. Almeida, M. S. Benilov and M. D. Cunha, Transient spots on thermionic arc cathodes II. Experiment and comparison, Proc. 11th Symposium on the Science and Technology of Light Sources (May 20-25, 2007, Shanghai, China), ed. by M. Q. Liu and R. Devonshire, ISBN 978-0-9555445-0-7, pp. 579-580
- P. G. C. Almeida, M. S. Benilov, and M. D. Cunha, Mode changes on thermionic cathodes: II. Preventing transient spots, Proc. 28th ICPIG (July 15-20, 2007, Prague, Czech Republic), ed. by J. Schmidt, M. Simek, S. Pekárek, and V. Prukner, Institute of Plasma Physics AS CR, ISBN 978-80-87026-01-4, pp. 1815-1818

- P. G. C. Almeida, M. S. Benilov, and M. D. Cunha, Preventing transient spots on thermionic cathodes, Proc. 60th Gaseous Electronics (October 2-5, 2007; Arlington, Virginia, USA), Bull. Amer. Phys. Soc., vol. 52, No. 8, p. 31

- Pedro G. C. Almeida and Mikhail S. Benilov, Multiple solutions in the theory of near-cathode layers and self-organization on DC glow cathodes, Abstracts of 2008 IEEE International Conference on Plasma Science (June 15-19, 2008, Karlsruhe, Germany), ISBN 978-1-4244-1930-2, p. 456

- P. G. C. Almeida and M. S. Benilov, Self-consistent modelling of self-organization on DC glow cathodes, Abstracts of the 19th Europhysics Sectional Conference on the Atomic and Molecular Physics of Ionized Gases (ESCAMPIG) (July 15-19, 2008, Granada, Spain), p. 2-27

- P. G. C. Almeida and M. S. Benilov, Multiple Solutions in the Theory of DC Glow Discharges, In Proc. European COMSOL Conference (November 4-6, 2008, Hannover, Germany)

- P. G. C. Almeida, M. S. Benilov, and M. J. Faria, Modelling self-organization on DC glow cathodes, Proceedings of XXIX International Conference on Phenomena in Ionized Gases (July 12-17, 2009, Cancun, Mexico), PB4-2

- P. G. C. Almeida, M.S. Benilov, and M. J. Faria, Modelling self-organization in DC glow microdischarges in xenon and argon, Proc. 63rd Gaseous Electronics Conf. and 7th Int. Conf. on Reactive Plasmas (October 4-8, 2010, Paris, France), Bull. Amer. Phys. Soc., vol. 55, No. 7, p. 166

Resumo

Este trabalho é dedicado à modelação de diferentes modos de transferência de corrente aos cátodos de descargas luminescentes e à investigação experimental da formação de manchas transitórias em cátodos termiónicos de descargas de arco.

Múltiplas soluções estacionárias existentes na teoria da descarga luminescente foram calculadas numericamente pela primeira vez. A modelação foi realizada no âmbito do modelo básico da descarga luminescente e no âmbito de um modelo detalhado. O modelo básico contém equações de conservação de uma espécie iónica e dos electrões, equações de transporte dos iões e electrões escritas na aproximação local e a equação de Poisson. O modelo detalhado leva em conta iões atómicos e moleculares, estados excitados dos átomos, dímeros excitados e não-localidade dos coeficientes de transporte e cinéticos dos electrões. As múltiplas soluções descrevem modos com uma mancha normal e modos com padrões de várias manchas semelhantes aos observados nas experiências com micro-descargas em xénon. Demonstra-se que modos com mais que uma mancha podem, em princípio, ocorrer em descargas noutros gases que não o xénon.

A formação de manchas transitórias em cátodos termiónicos foi estudada em experiências com lâmpadas HID padrão, COST-529. Existe uma concordância genéricamente boa entre os resultados experimentais e da modelação numérica. Uma possibilidade de prevenção do aparecimento de manchas transitórias através da breve redução da corrente da descarga logo após um salto na corrente é proposta e justificada. Demonstra-se que o principal mecanismo de escurecimento das lâmpadas HID que acompanha a formação de manchas catódicas é a evaporação do material do cátodo.

Palavras chave: Interacção plasma-cátodo, Auto-organização, Descargas luminescentes, Descarga normal, Cátodos termiónicos, Manchas catódicas

Abstract

This work is dedicated to modelling of different modes of current transfer to cathodes of glow discharges and to experimental investigation of formation of transient spots on thermionic arc cathodes.

Multiple steady-state solutions in the theory of DC glow discharge have been found for the first time. The modelling was performed in the framework of the basic model of glow discharges and also in the framework of a more detailed model. The basic model comprises equations of conservation of a single ion species and the electrons, transport equations for the ions and the electrons written in the local approximation, and the Poisson equation. The detailed model takes into account atomic and molecular ions, atomic excited states, excimers, and non-locality of electron transport and kinetic coefficients. These multiple solutions describe modes with a normal spot as well as modes with patterns of several spots similar to those observed in experiments with microdischarges in xenon. It is shown that modes with more than one spot can, in principle, occur not only in xenon but also in other plasma-producing gases.

Formation of transient spots on thermionic cathodes was studied in experiments with COST-529 standard HID lamps. There is a generally good agreement between experiment and results of numerical modelling. A possibility of prevention of appearance of transient spots by means of a brief reduction of the arc current shortly after the initial current increase is proposed and justified. It is shown that the main mechanism of blackening of burners of HID lamps that accompanies appearance of transient cathode spots is evaporation of the cathode material and not sputtering.

Keywords: Plasma-cathode interaction, Self-organization, Glow discharges, Normal glow discharges, Thermionic cathodes, Cathodic spots

Contents

List of Figures

Chapter 1

Introduction

1.1 Observations of multiple modes of current transfer to cathodes of DC discharges

The oldest and perhaps best known example of the existence of multiple modes of steady-state current transfer to cathodes of DC discharges can be found in DC glow discharges: current transfer can occur in the abnormal mode or in the mode with a normal spot, e.g., [1, 2]. In the abnormal mode the cathode is almost completely covered with current and the distribution of discharge parameters varies along the axis of the discharge while remaining more or less uniform in the radial direction. In the normal mode, only a part of the cathode surface is covered with current - a spot is present. The abnormal mode is realized for high discharge currents up to the transition to the arc discharge. The normal mode is realized at lower currents, from the transition to the abnormal mode down to currents at which a transition the Townsend dark discharge occurs, via the quasi-stationary subnormal mode or oscillations.

In the abnormal mode an increase of discharge current results in an increase of the discharge voltage and the corresponding section of the current-voltage characteristic (CVC) is rising. In the normal mode variations of the discharge current take place through proportional variations of the area of the cathode covered with current, while the current density at the cathode and the discharge voltage remain virtually unchanged - the corresponding section of the CVC is horizontal. The constancy of current density over the cathode in the normal mode is known as the effect of normal current density. Figure 1.1 shows examples of normal glow discharges for different gases [3]. In this figure, the (wire) electrode at the top of the discharges is the anode; the plane square cathode is at the bottom. The expansion of the cathode spot as the current is increased can be seen.

The transition from normal to abnormal mode is usually continuous: when the current spot occupies the whole surface of the cathode a further increase of discharge current can take place only at the expense of a higher discharge voltage. The transition from the normal mode to the Townsend dark discharge is usually accompanied by intermittency and by a sharp rise in the voltage.

Recently, other steady-state modes of current transfer have been discovered in so-called DC

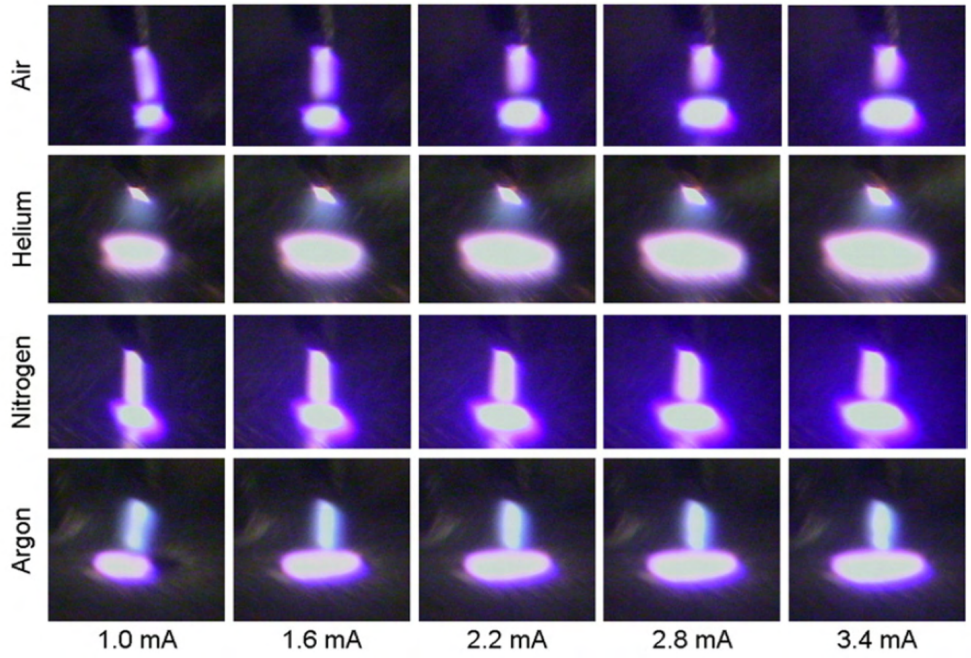

Figure 1.1: Images of discharges in various gases at atmospheric pressure vs. discharge current. Electrode spacing of 0.4 mm. From [3].

glow microdischarges[1] [5–11]. These modes comprise regular patterns of two or more cathode spots that seem to appear at the transition from the normal mode to the abnormal mode in xenon. Examples of the observed modes are shown in figures 1.2 and 1.3, taken from [5] and [10], respectively. The images in these figures are photographs of the cathode surface taken from the anode opening.

Most of the results were obtained in cathode boundary layer discharges. A schematic is shown in figure 1.4, taken from [10]. It is important to stress, however, that similar self-organized patterns have been observed in DC glow microdischarges between parallel-plane electrodes [8]. It is interesting that self-organization patterns have been observed in xenon but not argon [6, 12].

A diffuse mode and a mode with a spot have been observed also on cathodes of high-pressure arc discharges [13, 14]; see [15, 16] for further references. The diffuse mode is realized for high discharge currents, while the spot mode is realized for lower currents. Transitions between these modes are usually accompanied by hysteresis, see e.g. [17]. An example is shown in figure 1.5, taken from [17]. Here are shown photos of the cathode operating under exactly the same conditions, including the same arc current. In one of the photos the cathode operates in the diffuse mode, and in the other in the spot mode.

Different modes of current transfer were observed in other gas discharges, see [18] for a review and many references. The best known example is the formation of patterns of filaments in dielectric barrier discharges (DBD), e.g. [19–22]. Considerable effort was invested in production and investigation of patterns of filaments in sandwich-like gas-discharge systems, which comprise

[1] Glow microdischarges can be operated in DC or AC modes and take place in vessels with characteristic length scales ranging from a few dozens of micrometers up to the order of one milimeter and pressures between several dozens of Torr up to atmospheric pressure. A variety of configurations have been proposed, see review [4].

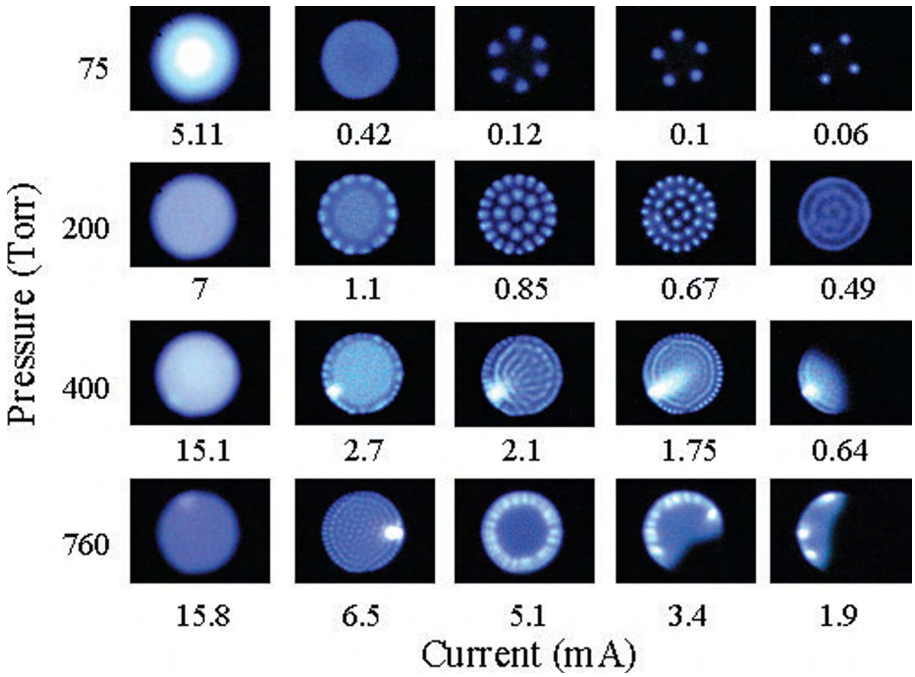

Figure 1.2: Patterns of spots observed for different currents and pressures in a cathode boundary layer discharge in xenon with diameter 0.75 mm. From [5].

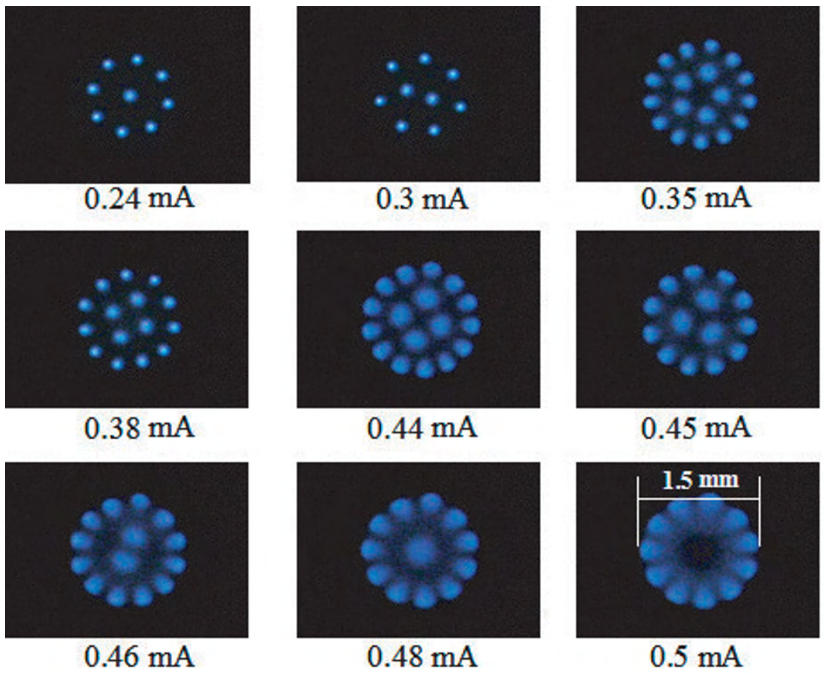

Figure 1.3: Patterns of spots observed for different currents in a cathode boundary layer discharge in xenon with diameter of 1.5 mm and pressure of 75 torr. From [5].

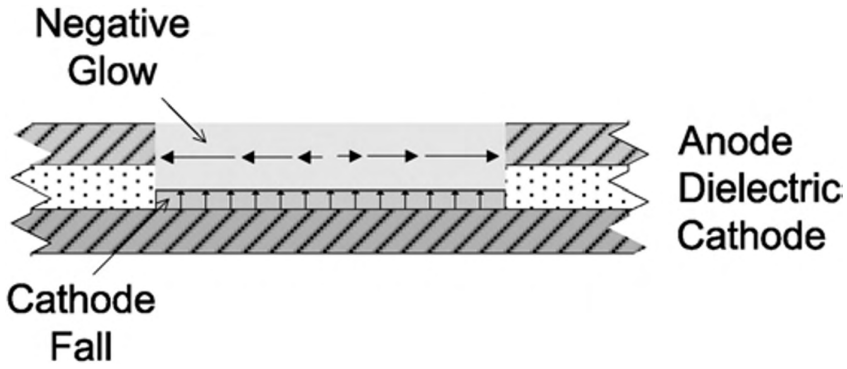

Figure 1.4: Schematics of a cathode boundary layer discharge. From [10].

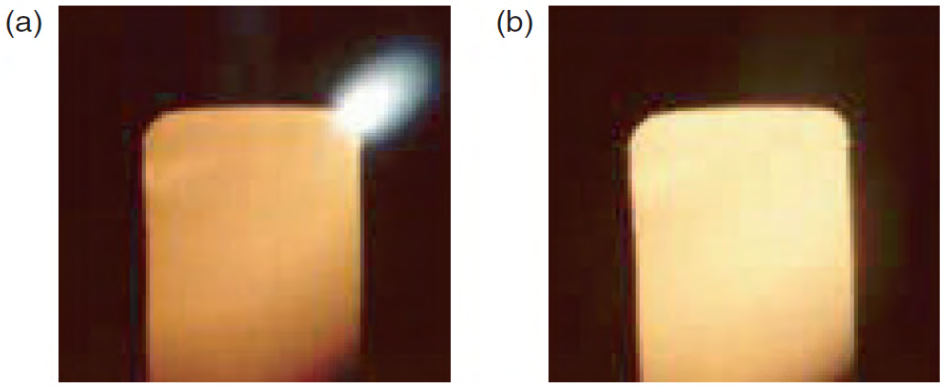

Figure 1.5: Photos of a tungsten thermionic arc cathode operating in the spot mode (a) and diffuse mode (b) in argon. The diameter of the cathode is 1.5 mm and the length is 20 mm. Gas pressure is 4.5×10^5 Pa and discharge current is 2.5 A. From [17].

a layer of a semiconductor and a layer of gas, see [23–25] and references therein. The α and γ modes of capacitively coupled radio-frequency (CCRF) discharges represent another example; see [2] and references therein. An effect analogous to the effect of normal current density in DC glow discharges has been observed in DBD [26] and in the α mode of CCRF discharges [2]. Modes with more than one spot have been observed also on cathodes of non-self sustained DC glow discharges [27–29]. These topics are, however, out of the scope of this thesis.

1.2 Theoretical description of multiple modes of current transfer to cathodes of DC glow and arc discharges

Multiple modes of current transfer to cathodes of DC discharges represent a scientifically very interesting phenomenon. In the case of the glow discharge, the normal and abnormal modes were discussed already in 1934 by von Engel and Steenbeck [30][2]. In the case of the arc discharge, the existence of diffuse and spot modes has been under constant discussion since the 1950s. The aim of this section is to give a brief account of the current state of the art of theoretical approaches to description of multiple modes of current transfer to cathodes of DC glow and arc discharges.

The outline of this section is as follows. In subsection 1.2.1, a retrospective is given of traditional theoretical approaches to description of modes of current transfer to cathodes of DC glow discharges. In subsection 1.2.2, a theoretical approach based on the hypothesis of existence of multiple solutions in the theory of glow discharges is discussed. A brief account of the current state of the art of theoretical approaches to description of modes of current transfer to cathodes of arc discharges is given in subsection 1.2.3.

1.2.1 Glow discharge: conventional approaches

A strongly simplified one-dimensional theory of the cathode voltage drop was proposed by von Engel and Steenbeck in 1934 [30]. The theory yields a current density-voltage characteristic (CDVC) of the cathode layer, $U(j)$, that is U-shaped, i.e., comprises a falling section and a rising section separated by a point of minimum $j = j_{\min}$. While the solution obtained in the framework of this simple model succeeds in describing the qualitative behaviour of the cathode region in the abnormal mode, at $j > j_{\min}$, it cannot be used to describe the normal mode, since the latter is a multi-dimensional feature. It was assumed that states with $j < j_{\min}$ are not realized and the justification given for this assumption was that these states belong to the falling section of the CDVC. We note, however, that this argument is not very convincing since states belonging to falling sections of the CVC of arc discharges can be stable [31, 32] and in fact have been observed in experiments, e.g. [17].

It was noted in [30] that an agreement by order of magnitude with experimental data is possible by postulating that the minimum voltage drop, $U(j_{\min})$, corresponds to parameters of the normal mode. This assumption is based on a conjecture that states which are realized in

[2] The 1934 book by von Engel and Steenbeck [30] is available in German only. In this work, it is cited according to [1, 2].

current-controlled gas discharges are those which require the lowest possible discharge voltage to be maintained[3].

In 1965 von Engel stressed in his book [1, p. 224] that the nature of the normal mode and the effect of normal current density were not understood. The action of forces of unknown nature and the minimum power principle were invoked: "*Neither the fact that the normal current density at the cathode nor that the normal thickness of the dark space is approximately constant can be explained in simple terms without invoking dicta like the minimum energy principle. It can be assumed that the rise of the emitting cathode area is controlled by dispersive forces acting radially outwards, viz. electric fields originating from space charges rather than diffusion and by inward forces the nature of which is unknown.*"

It is noted in [37] that the value of the normal current density measured experimentally systematically exceeds $j_{\min}$ by a factor of $2 \sim 20$ for different gases. This fact contradicts the postulate that $j_{\min}$ corresponds to the normal current density. A value V_n for the normal cathodic voltage drop different from $U(j_{\min})$ was proposed in 1972 [38]. This value is calculated from balance of electrons in the cathode layer: the electron (ambipolar) diffusion flux in the radial direction is set equal to the difference between the rates of ionization and of removal of electrons from the cathode layer by the field. Solutions to the equation thus obtained that correspond to a discharge occupying part of the cathode surface are possible only when $U = V_n$, which in turn allows calculation of the normal current density j_n. This simple model provides values of j_n which qualitatively agree with the experiments [38]. A helpful discussion of results [37, 38] in the light of subsequent results can be found in [2, p.185], where conclusions were drawn that: i) the voltage drop corresponding to the normal mode is larger than $U(j_{\min})$ and corresponds to a state in the rising section of the CDVC which describes the abnormal mode; ii) diffusion is the stabilizing mechanism of the edge of the normal spot in the sense that diffusion flux into the edge of the spot compensates insufficient charge production at the edge. (In other words, this electron diffusion flux has a stabilizing effect since the Townsend self-sustainment condition does not hold at the edge of the normal spot due an increase of the thickness of the space charge sheath, which leads to reduction of the electric field and, consequently, of the ionization rate.) Interestingly, von Engel and co-workers in 1972 suggested [39], in contradiction to the former conclusion, that stability of the discharge in the normal mode may be due to the radial electric field in the space charge sheath which retains electrons in the core of the discharge and draws ions away from it.

[3] This conjecture is known as Steenbeck's principle of minimum power or voltage. It was proposed by Max Steenbeck in 1932 [33] for the particular case of a current-controlled cylindrical arc discharge: Steenbeck assumed that parameters of this discharge adjust themselves in a way that the axial electric field in the arc attains a minimum value. (The 1932 paper by Steenbeck [33] is available in German only. In this work, it is cited according to [34].) At present, this principle is used in a more general form: it is assumed that states of gas discharges which are realized are those which require the lowest power (or voltage) to be maintained. It is argued in [2, 35] that this principle is not a consequence of any fundamental law and the agreement with the experiment resulting from its use is merely fortuitous. Some authors believe, on the basis of the work [36], that this principle is a corollary of the principle of minimum entropy production, well known in irreversible thermodynamics. (Once again, the paper [36] is available in German only and is cited according to [34].) However, it was shown [34] that there is a grave error in the work [36] invalidating the derivation, so Steenbeck's minimum principle is not a corollary of the principle of minimum entropy production. Not being a corollary of mathematical models of gas discharges, this principle in fact contradicts the mathematical models. Its usage may result in unacceptably large errors. An extended discussion, examples of evaluation of the error incurred by using the minimum principle and further references can be found in [34].

1. Introduction

The first self-consistent one-dimensional simulations of the cathode layer were reported by Ward in 1958 and 1962 [40, 41]. In these simulations, the Poisson equation coupled with so-called Townsend's ionization equation governing the electron current density were solved. Diffusion was neglected. The electron energy distribution function (EEDF) was assumed to be governed by the local electric field, which means that the transport and kinetic coefficients of the electrons are assumed to depend solely on the local electric field. One ion species was included in the model and one channel of ionization was considered. Recombination was neglected. Dependent variables for which the problem has been solved were the electric potential and density of electrons; the density of ions was eliminated from the Poisson equation by means of expressing it in terms of the ion (drift) flux and using electric current conservation. The simulations [40, 41] in a way justified approximations made in von Engel and Steenbeck's theory (e.g. the assumption of an approximately linear variation of the electric field in the cathode layer) and the calculated CDVC had the same shape as the CDVC found by von Engel and Steenbeck. Since the modelling was 1D, the normal current density effect remained unexplained.

A significant step forward was taken in the 1980s, when the first self-consistent two-dimensional simulations [42–45] have appeared, which were followed by more elaborate simulations in the next two decades, e.g. [46–49]. Simulations [42] were based on the Poisson equation coupled with conservation and transport equations for the electrons and ions and were performed in the planar geometry. Diffusion of charged particles was neglected. The simulations [42] were not brought to an absolute steady-state due to the lack of sufficient computer time. However, the structure of a normal spot has been calculated. This result is in apparent contradiction with the model [38], which suggests that diffusion plays a fundamental role. This contradiction was discussed by Raizer in 1986 [35]. In 1987 and 1988 Raizer and Surzhikov performed two-dimensional axially-symmetric simulations both with and without account of diffusion [43, 44][4]. Dissociative recombination was taken into account. The simulations confirmed the appearance of a normal spot and the presence of the effect of normal current density even when diffusion was not taken into account. However, it was argued by the authors [43, 44] that when diffusion is not taken into account the spot is stabilized in the modelling by the so-called computational diffusion, which originates in the approximation error. The authors concluded that diffusion, either physical or computational - whichever is greater, plays a dominant role in the stabilization of the normal spot.

Also in 1988, Boeuf has performed two-dimensional planar simulations based on the drift-diffusion equations for one ionic species and electrons coupled with the Poisson equation [45]. The goal of this work was to study not only the radial structure of the normal mode, but also the transition from the normal mode to the abnormal mode. Except for dissociative recombination, which was not taken into account, the model [45] was similar to the one in [43, 44]. In [45] a CVC was obtained which comprises a rising section corresponding to the abnormal mode and a plateau corresponding to the normal mode. It was concluded, in agreement with [39] but contrary to [43, 44], that the radial electric field plays an important role in the stabilization of the discharge in the normal mode.

In our view, the results of these simulations suggest that basic mechanisms of glow discharges,

[4] Writing transport equations of charged particles with account of drift and diffusion but not inertia is usually referred to as the drift-diffusion approximation, e.g. review [50].

which are ionization, recombination and transport of charged particles suffice to capture the relevant physics of the normal mode of the glow discharge and of the effect of normal current density. Note that it is pointed out in [35] that non-local effects need to be accounted for in order to obtain from modelling a correct qualitative picture of the longitudinal structure of the near cathode layer. However, the possible influence of non-local effects on the structure of the normal spot or on the effect of normal current density was not mentioned in [35]; in fact it is indicated in [2, p.188] that nonlocal effects are "*unrelated to the problem of normal current density*".

Results similar to those reported in [42–45] were obtained in subsequent two-dimensional simulations [46–49]. (Note that the goal of the works [46–49] was to study general properties of DC glow discharges and not specifically the effect of normal current density.) In [46] nonlocal effects in the ionization source term are taken into account by means of a Monte Carlo simulation. Calculations in [47] were performed using both the local approximation for electrons and a Monte Carlo simulation to account for nonlocal effects in the ionization source term. In [48] nonlocal effects are taken into account by means of a differential equation of conservation of electron energy. (The EEDF is obtained from solving the Boltzmann equation in the two-term spherical harmonic expansion. Electron transport and reaction rate coefficients are then obtained as functions of electron energy by integration, using the EEDF as weight function.) Apart from electrons and ions, the model also includes atoms in the ground state and in metastable states. Heating of the discharge gas is taken into account in [49]. All these simulations revealed a steady-state solution which exists at all discharge currents and describes the abnormal mode at high currents and the normal mode at lower currents.

The solution computed in [43–49] is qualitatively different from the von Engel and Steenbeck solution: it predicts the normal mode where the mode associated with the falling section of the CDVC is predicted by the von Engel and Steenbeck solution. This discrepancy is very interesting, however it apparently has not been discussed. Moreover, note that the essential difference between one- and two-dimensional models is allowance for fluxes in the radial direction. Estimates reveal that the characteristic time scale of transport of charged particles in the radial direction exceeds by several orders of magnitude the characteristic time scale of transport along the discharge axis. Hence, fluxes of the ions and electrons in the radial direction represent a weak effect, and a question arises how can this weak effect produce such a dramatic difference in solutions. This question has, apparently, remained unnoticed.

In summary, one can say that after almost eighty years and much effort to understand the nature of the effect of normal current density, computational methods exist that allow for simulation of this effect, however there are still questions to which purely computational approaches do not provide answers. The limitations of purely computational approaches became even more evident since 2004 when steady-state modes with more than one cathodic spot have been observed [5–11] in DC glow microdischarges. These modes have not been calculated. A qualitative discussion of physical mechanisms that can be responsible for the appearance of patterns with multiple spots was given in [5, 7]; an increasing dependence of the effective secondary emission coefficient on the reduced electric field and/or heating of the gas were mentioned.

1.2.2 Glow discharge: hypothesis of multiple solutions

In 1988, a hypothesis was proposed [51] that a self-consistent theoretical model of a near-cathode region in a DC glow discharge must admit multiple steady-state solutions describing different modes of current transfer. In the simplest case where transport of the ions and the electrons in the near-cathode region is dominated by drift, one of these multiple solutions is 1D and describes distributions of parameters that vary along the axis of the discharge but are uniform in the radial direction. This solution exists at all values of the discharge current and represents an analogue of the solution of von Engel and Steenbeck. The other solutions are multidimensional and their pattern was suggested in [51] on the basis of bifurcation analysis and general trends of self-organization in bistable nonlinear dissipative systems: the mode described by each solution exists in a limited range of discharge currents, some of these solutions describe modes with one normal spot and other solutions describe modes with patterns of multiple spots.

From the point of view of the hypothesis of multiple solutions, the existence of different modes of current transfer in DC glow discharges is a manifestation of phenomena of self-organization, and this includes also the normal mode. This is different from the traditional point of view: the effect of normal current density is not generally viewed as a consequence of self-organization and most efforts in research have been focused on physical mechanisms, as discussed in the preceding section.

Since the numerical modelling [43–49] has shown the capacity to reproduce the effect of normal current density as it is observed in the experiment, there was apparently no necessity in the hypothesis of multiple solutions describing different modes of current transfer to cathodes of DC glow discharges and this hypothesis was not explored during a long time. The situation changed relatively recently, after patterns with multiple spots, similar to those predicted by the theory [51], have been observed in DC glow microdischarges [5–11]: these observations were interpreted [52] as an argument in favour of the hypothesis of multiple solutions.

An attempt to find multiple solutions was undertaken in [53]. Simulations [53] have been performed for a discharge between parallel electrodes with a single ion species and transport of the ions and the electrons dominated by drift, without account of complex effects such as a nonlocal electron energy distribution or the presence of multiple ion and neutral species with a complex chemistry. The conclusion was that "*the system never relaxes to a spatially structured time-independent state*", meaning that no other steady-state solutions except the 1D one have been found. In other words, no multiple solutions describing different steady-state modes have been detected in [53]. However, the bifurcation analysis [54] has shown that multiple steady-state solutions must exist even in the framework of this simple model.

Multiple solutions have not been calculated so far and the question remains open. It is the objective of this work to compute these solutions for the first time. Then a pertinent question is why these solutions have not been found in preceding works and what should be done in order to find them.

One of the reasons why multiple solutions have not been found in preceding works is as follows: according to the previous experience of calculations of multiple modes on thermionic cathodes, one needs to know what these solutions are like and where to look for them. In other words, the

question of initial approximation is critical in problems with multiple solutions since it is just the choice of initial approximation what determines to which one of the multiple solutions will the code converge. This is described in detail in the tutorial of the free online tool for simulation of diffuse and axially symmetric spot modes of current transfer from high-pressure plasmas to thermionic cathodes [55]. (This tool is discussed in some detail in the next section.) In the present work, this information will be obtained with the use of the bifurcation theory, again similarly to how it is done in the modelling of multiple modes of current transfer from high-pressure plasmas to thermionic cathodes.

Another reason why multiple solutions have not been found in preceding works is likely to be as follows. Steady-state solutions in these works were found by means of nonstationary solvers: an initial state of the discharge is specified and its relaxation over time is followed by means of a nonstationary solver until a stationary state has been attained. The difficulty is that nonstationary solvers do not allow decoupling questions of numerical and physical stability. In other words, if a nonstationary solver, while starting from different initial states, produces only one stationary solution corresponding, for example, to a normal spot, this does not mean that steady-state solutions with multiple spots do not exist: it may be that such solutions do exist but are unstable for the external circuit considered.

In this work steady-state solvers of commercial software Comsol Multiphysics are used. Previous experience of application of this software to finding multiple solutions describing different modes of current transfer to cathodes of high-pressure arc discharges was quite positive: steady-state solvers of Comsol Multiphysics allow one to find the whole pattern of multiple modes; e.g. [56].

The pattern of multiple modes of current transfer to cathodes of high-pressure arc discharges is rather complex; e.g. figures 1 and 2 of [56]. An important feature of this pattern is that some modes exist in a limited range of discharge currents and possess turning points and their CVC possess extrema. The use of discharge voltage as an input parameter does not allow one to find a mode past an extreme point of its CVC. A possible solution is to introduce an external circuit and consider the electromotive force and the ballast resistance as input parameters. On the other hand, Comsol Multiphysics allows one to directly specify the discharge current as an input parameter, and computation times of models using as input parameters the discharge voltage and current were close, in spite of changes of the structure of the matrix of the system of linear equations in finite elements. Conversely, the use of discharge current as an input parameter does not allow finding the mode past a turning point, and it is natural to use discharge voltage as an input parameter in such situations.

Comsol Multiphysics offers a possibility to easily switch between the discharge current and voltage as an input parameter, and the pattern of multiple modes of current transfer to cathodes of high-pressure arc discharges [56] was calculated in this way. This procedure will be used also in this work.

1.2.3 Arc discharge

The existence of multiple modes of current transfer to cathodes of arc discharges is a subject of great interest not only from the point of view of fundamental science, but also from the point of view of technological applications: the mode of current transfer to cathodes of arc discharges has a huge effect on the performance and lifetime of arc devices. During the last decade and due essentially to the interest by the industry, this topic received considerable attention and many papers were published, reporting both experimental and theoretical results. As opposed to the situation in glow discharges, a universally accepted theoretical approach to the description of modes of current transfer to cathodes of arc discharges has already been developed, e.g. review [15] and references therein. This approach treats modes of current transfer to cathodes of arc discharges as self-organization phenomena, and this is the very reason of its success. The theory of plasma-cathode interaction in arc discharges is developed to the point that it is possible to use it for industrial applications.

The above-mentioned theoretical description of different modes of current transfer to cathodes of arc discharges is based on the model of non-linear surface heating, e.g. [15] and references therein. This model was proposed in 1963 and a hypothesis was suggested that the model admits multiple solutions [57]. However, no proof of this hypothesis was given. Besides, the work [57] is a technical report and was not easily available during many years. A detailed description of the model of non-linear surface heating was given in 1987 in the book [58], however, the hypothesis of existence of multiple solutions was not mentioned.

The existence of multiple solutions in the framework of the model of non-linear surface heating was proved in 1988 [59] by means of bifurcation analysis and numerical calculations. It was shown that one of these solutions describes a diffuse mode, while other solutions describe modes with one or more spots. The work [59] was essentially of a mathematical nature and contained no calculations for conditions of arc cathodes.

In 1998 [60] the bifurcation analysis [59] was extended to conditions typical of thermionic cathodes of arc discharges. Bifurcations were found and it was concluded that multiple solutions describing different modes of current transfer to cathodes of arc discharges should exist. Multiple solutions were indeed computed in a number of subsequent papers, see e.g. [56, 61–64]. At present, the adequacy of theoretical description of diffuse and spot modes of current transfer to thermionic cathodes of arc discharges in high-pressure plasmas is common knowledge.

The model of non-linear surface heating may be briefly described as follows, see [15] and references therein for a more detailed presentation of this model. The arc plasma-cathode interaction is described theoretically in two steps. At the first step, densities of energy flux and electric current from the plasma to the active part of the cathode surface are calculated. These quantities are governed by a thin near-cathode layer, which comprises the space-charge sheath and the ionization layer, and are assumed to depend only on the cathode surface temperature and on the cathodic voltage drop. Since the thickness of the near-cathode layer is much smaller than the typical diameter of the cathode or of the spots, the problem comprising the first step is assumed to be one-dimensional. At the second step, the equation of heat conduction governing the temperature distribution in the cathode body is solved with boundary conditions at the cath-

ode surface expressed in terms of the densities found at the first step. Joule heating can usually be neglected in conditions typical of low-current arc discharges and one does not need to solve the current continuity equation. If the cathodic voltage drop is the control parameter, then the boundary condition on the active part of the cathode surface is written in terms of energy flux density. If discharge current is the control parameter, another condition on the active part of the cathode appears, which is written in terms of current density.

The decoupling of the equation of heat conduction in the cathode body from the equations governing the near-cathode layer is possible since the characteristic thickness of the layer is much smaller than the characteristic diameter of the cathode or the spots.

It should be stressed that what is specified as a boundary condition for the heat conduction equation at the cathode surface is a functional dependence between the density of energy flux and the local temperature of the cathode surface. This is different from specifying a distribution of energy flux over the cathode surface. In other words, the density of energy flux for, e.g., the spot mode is not introduced by hand in an artificial way, but it is rather a result of calculations.

Note that the appearance of spots on cathodes of arc discharges was interpreted for many years as a manifestation of different electron emission mechanisms [2]: for relatively low temperatures of the arc cathode material, typical of the diffuse mode, thermo-field emission was thought to be the dominant mechanism, while for high temperatures, typical of the spot mode, thermionic emission was thought to be the dominant mechanism. In the framework of the model of nonlinear surface heating, the existence of diffuse and spot modes is understood as a result of non-uniqueness of thermal balance in the cathode body.

The modelling of 2D modes of current transfer to cathodes of arc discharges is developed to the point that it can be automated. An example is the free online tool for simulation of diffuse and axially symmetric spot modes of current transfer [55]. The tool allows one to simulate diffuse and axially symmetric spot modes of current transfer from high-pressure plasmas to cylindrical thermionic cathodes in a wide range of arc currents, cathode materials and dimensions, and plasma compositions. An example is given of a situation in which the tool can be used to find four different solutions for the same value of the cathodic voltage drop, two of these solutions corresponding to the diffuse mode and the other two to the spot mode.

It is interesting to note the rapid development and recognition of the theoretical description of different modes of current transfer to cathodes of DC arc discharges based on the hypothesis of multiple solutions. Only a decade, roughly, was needed to get to the point where the theory is universally accepted and widely used by the industry. One should acknowledge a highly important support received by the theory from experimental work at Bochum University.

1.3 This work

The main goals of this work are as follows. As far as modes of current transfer to cathodes of glow discharges are concerned, the aim is to compute multiple solutions describing different modes and characterize them. The following questions will be answered, among others: if these multiple solutions describe modes with a normal spot as well as modes with patterns of several spots similar to those observed in the experiment [5–11]; how does the weak effect of transport

of charged particles in directions transversal to the axis of the discharge produce a dramatic difference in the CVC and distribution of current on the cathode surface; how important is effect of kinetics over multiple modes; whether modes with more than one spot can occur not only in xenon but also in other plasma-producing gases.

As far as modes of current transfer to cathodes of arc discharges are concerned, the aim is to characterize appearance on cathodes of high-intensity discharge (HID) lamps of transient spots induced by rapid variations of the arc current. To this end, an experimental setup with COST-529 standard lamps[5] is built up. The experiments are performed in parallel and coordinated with numerical simulations. The questions to be answered include: whether it is possible to prevent the appearance of the transient spots by means of an intelligent power supply; whether the main mechanism of blackening of burners of HID lamps that accompanies the appearance of transient cathode spots is evaporation of the cathode material or sputtering.

The work leading to this thesis was performed within activities of a larger research project ongoing in Universidade da Madeira. This thesis is concerned with modelling of DC glow discharges and experiments on transient spots on cathodes of HID lamps. On the other hand, results on bifurcations and stability, mentioned throughout this thesis for completeness and clarity, were obtained not by the author of the thesis. The same is true with respect to numerical results on transient spots on cathodes of HID lamps cited in chapter 4.

The most part of the thesis is a compilation of papers already published [66–68] or accepted for publication [69].

The text is organized in five chapters. The first chapter represents an introduction.

In chapter 2, corresponding to [69, 70], multiple steady-state solutions existing in the theory of glow discharges are computed for the first time. The simulations are performed in 2D and 3D in the framework of the basic model, which accounts for a single ion species and employs the local approximation. Solutions describing up to twelve different modes were found in the case where losses of the ions and the electrons due to neutralization at the wall were neglected. One mode is 1D, exists at all values of the discharge current, and represents in essence the well-known solution of von Engel and Steenbeck. Eight of the other modes are axially symmetric and three modes are 3D. All the multidimensional modes exist in limited ranges of the discharge current and are associated with different patterns of current spots on the cathode. The mode with a spot at the centre of the cathode and a 3D mode with a spot at the pheriphery of the cathode exhibit a well pronounced effect of normal current density. Modes with multiple spots exhibit patterns which represent analogues of those observed in DC glow microdischarges in xenon. 3D modes exhibit a minimum or a maximum of the current density at the centre of the cathode, which cannot be predicted by the bifurcation theory and is in qualitative agreement with the experiments. Account of neutralization at the wall affects the solutions dramatically: a mode appears that exists at all discharge currents and comprises the Townsend, subnormal, normal and abnormal discharges; the number of solutions is reduced.

In chapter 3, multiple steady-state solutions are studied existing in the framework of a model

[5] These experimental lamps were produced by Philips in the framework of action 529 of programme COST of the EU and are described in [65]. The lamps used in this work were a modified version of the standard lamps which had no coils around the electrodes.

which takes into account multiple ionic species, atomic excited states, excimers, and non-locality of electron transport and kinetic coefficients. The simulations in the framework of this model are performed for xenon and argon. A complex behaviour of glow microdischarges is found in apparently simple situations, even setting aside the existence of multiple solutions, which seems to be reported for the first time. Fortes and weaknesses of Comsol Multiphysics as a tool for modelling of glow discharges are identified and discussed. Solutions describing three different 2D modes in xenon microdischarges are shown. It is found that these modes are qualitatively similar to 2D modes computed in the framework of the basic model of glow discharge. The conclusion is that the inclusion of a detailed kinetic scheme and non-locality of electron energy is not likely to affect the pattern of multiple modes found in chapter 2 in the framework of the basic model. Modelling results show that conditions of argon microdischarges are less favourable for the appearance of self-organization than the conditions of xenon microdischarges, which is due to lower cross sections of elastic collisions between electrons and atoms. Results from bifurcation theory for argon and helium indicate that it should be possible to observe formation of self-organized patterns also in these plasma-producing gases provided that the pressure is sufficiently high and the discharge radius is large enough.

In chapter 4, corresponding to [66, 67], spots on cathodes of high-pressure arc discharges induced by a rapid increase in the arc current are studied in experiments with COST-529 standard lamps. Appearance of spots is analyzed in the context of the general pattern of steady-state modes of current transfer to thermionic cathodes and their stability. Modelling and experimental results are in a reasonable agreement. A method to prevent formation of transient spots on cathodes of high-pressure arc discharges by means of short negative rectangular current pulses is proposed and validated experimentally. Experimental indications are found that the main mechanism of blackening of burners of HID lamps that accompanies appearance of transient cathode spots is evaporation of the cathode material and not sputtering.

In chapter 5 conclusions of this work are given and possible directions of future research discussed.

Chapter 2

Multiple modes of current transfer in DC glow discharges

2.1 Introduction

In this chapter, multiple axially symmetric (2D) and 3D solutions describing different modes of current transfer to the cathode of DC glow discharges are computed for the first time. The basic model of glow discharge is used with xenon, which accounts for a single ion species with electron transport and kinetic coefficients assumed to be governed by the local electric field.

In agreement with the discussion in Introduction, section 1.2.2, one of the questions to be answered is whether the normal discharge mode and modes associated with patterns comprising several spots, similar to those observed in the experiment [5–11], can be computed in the framework of the same model. Another question concerns losses of the charged particles due to their neutralization at the wall: how can this weak effect produce a dramatic difference which exists between the von Engel and Steenbeck solution and the 2D solutions computed in [43–49]?

The modelling reported in this chapter may show the way to a self-consistent description of patterns observed in [5–11] and is in line with the recent trend to model self-organization in gas discharges from the first principles; see, for example, the modelling of 3D patterns in a DBD [22, 71–73].

The outline of the chapter is as follows. The model is briefly introduced in section 2.2. Multiple solutions without neutralization of the charged particles at the wall describing 2D and 3D modes are given and discussed in section 2.3. Also studied in this section are the effect of variation of the tube radius and the role of diffusion of charged particles. Effect over the multiple solutions produced by neutralization of the charged particles at the wall is analyzed in section 2.4. Concluding remarks are given in section 2.5.

Results on axially symmetric modes reported in this chapter were published in [68, 74]. 3D modes are reported in the paper [69], which has been accepted for publication.

2.2 The model

Let us consider a mathematical model of a DC glow discharge comprising equations of conservation of a single ion species and the electrons, transport equations for the ions and the electrons written in the drift-diffusion approximation, and the Poisson equation:

$$\nabla \cdot \mathbf{J}_i = n_e \, \alpha \, \mu_e \, E - \beta \, n_e \, n_i, \quad \mathbf{J}_i = -D_i \, \nabla n_i - n_i \, \mu_i \, \nabla \varphi, \tag{2.1}$$

$$\nabla \cdot \mathbf{J}_e = n_e \, \alpha \, \mu_e \, E - \beta \, n_e \, n_i, \quad \mathbf{J}_e = -D_e \, \nabla n_e + n_e \, \mu_e \, \nabla \varphi, \tag{2.2}$$

$$\varepsilon_0 \, \nabla^2 \varphi = -e \, (n_i - n_e) \, . \tag{2.3}$$

Here n_i, n_e, $\mathbf{J}_i$, $\mathbf{J}_e$, D_i, D_e, μ_i, and μ_e are number densities, densities of transport fluxes, diffusion coefficients, and mobilities of the ions and electrons, respectively; α is Townsend's ionization coefficient; β is coefficient of dissociative recombination; φ is electrostatic potential, $E = |\nabla \varphi|$ is electric field strength; ε_0 is permittivity of free space; and e is elementary charge.

Boundary conditions at the cathode and anode are written in the conventional form: diffusion fluxes of the attracted particles are neglected compared to drift; the normal flux of the electrons emitted by the cathode is related to the flux of incident ions in terms of the effective secondary emission coefficient γ, which is assumed to characterize all mechanisms of electron emission (due to ion, photon, and excited atom bombardment) [2]; density of ions vanishes at the anode; electrostatic potentials of both electrodes are given. One boundary condition at the wall of the discharge vessel is the conventional condition of zero electric current density. Two boundary conditions are used alternatively for n_i and n_e at the wall, corresponding to the cases *i)* where neutralization of charged particles the wall are neglected, and *ii)* where neutralization is taken into account. Let us consider a discharge vessel in the form of a right circular cylinder of a radius R and of a height h, and introduce cylindrical coordinates (r, ϕ, z) with the origin at the centre of the cathode and the z-axis coinciding with the axis of the vessel. Then the boundary conditions read

$$z = 0: \quad \frac{\partial \, n_i}{\partial \, z} = 0, \quad J_{ez} = -\gamma J_{iz}, \quad \varphi = 0 \, ; \tag{2.4}$$

$$z = h: \quad n_i = 0, \quad \frac{\partial \, n_e}{\partial \, z} = 0 \, , \quad \varphi = U; \tag{2.5}$$

$$r = R: \quad \begin{array}{ll} i) & \frac{\partial n_i}{\partial r} = \frac{\partial n_e}{\partial r} = 0 \\ ii) & n_i = n_e = 0 \end{array} \, , \quad J_{ir} - J_{er} = 0. \tag{2.6}$$

Here U is the discharge voltage, the subscripts r and z denote radial and axial projections of corresponding vectors.

The input parameter for the model can be the discharge voltage U or the discharge current I. Both possibilities had to be used in the modelling. To this end, the switching between U and I in the course of calculations has been implemented while building the model. I was used in states where the slope of the current-voltage characteristics (CVC) of the discharge, $U\,(I)$, is small, in particular, in the vicinity of extreme points of the CVC, on the normal and Townsend discharges. U was used as the input parameter in states where the slope is large, in particular, in the vicinity of turning points and on the subnormal discharge.

It is interesting to note that computation times of models using as input parameters U or I were close, in spite of changes of the structure of the matrix of the system of linear equations in finite elements.

The problem (2.1)-(2.6) is well known and represents the most basic self-consistent model of a DC glow discharge. Without account of neutralization [i.e., with boundary condition *i)* in (2.6)], the problem admits a 1D solution of the form $f = f(z)$ (here f is any of the quantities n_i, n_e, and φ), which is in essence the well-known solution of von Engel and Steenbeck [2]. Under certain conditions, the problem admits also 2D (axially symmetric) solutions, $f = f(r, z)$, and 3D solutions, $f = f(r, \phi, z)$. With account of neutralization [i.e., with boundary condition *ii)* in (2.6)], the problem admits a 2D solution which was computed in [44–49]. Under certain conditions, the problem admits also other 2D solutions and 3D ones. In this work, multiple 2D solutions are found, both with and without account of neutralization of charged particles at the wall. As an example, 3D solutions are also found without neutralization.

In each case computed in this work, there is one and only one mode that exists at all values of the discharge current: in the case without neutralization at the wall, this is the 1D mode which is similar to the solution of von Engel and Steenbeck; in the case with neutralization, this is the 2D mode computed in [44–49]. This mode is of special importance and will be called the fundamental mode.

Numerical results reported in this work have been calculated with the use of a steady-state solver of the commercial finite element software Comsol Multiphysics. Note that iterative processes in steady-state solvers need not be equivalent to relaxation in time. In particular, the solver being used allows one to decouple questions of numerical and physical stability. For example, one can without any difficulty calculate states on falling branches of CVC treating U as a control parameter, i.e., without a ballast resistance required by solvers based on relaxation in time. Note that this feature is characteristic not only to the Comsol Multiphysics solver being used, but also to other steady-state solvers based on the Newton linearization with a direct solution of linear equations in finite elements or differences, such as the one used in the online tool simulating plasma-cathode interaction in high-pressure arc discharges [55].

The fundamental mode may be found as a matter of routine. However, other solutions are not easy to find: one needs to know in advance what these solutions are like and where they should be sought. This topic will be discussed in some detail in the next sections.

Results reported in this chapter refer to a discharge in xenon under the pressure of 30 torr. The interelectrode gap is $h = 0.5$ mm and the radius of the discharge tube R is between 1.5 mm and 0.5 mm. The (only) ionic species considered is Xe_2^+. The mobility of Xe_2^+ ions in xenon was evaluated by means of the formula $\mu_i = 2.1 \times 10^{21}\,\mathrm{m^{-1}\,V^{-1}\,s^{-1}}/n_n$ (here n_n is the density of the neutral gas), which is an approximation of the measurements [75]. The mobility of the electrons was evaluated as $\mu_e = 17\,\mathrm{torr\ m^2\,V^{-1}\,s^{-1}}/p$, where p is the pressure of the plasma; Townsend's ionization coefficient α was evaluated as

$$\alpha = Cp \exp\left[-D\,(p/E)^{1/2}\right], \tag{2.7}$$

with $C = 6.53 \times 10^3\,\mathrm{m^{-1}\,torr^{-1}}$ and $D = 3.61 \times 10^2\,\mathrm{V^{1/2}\,(m\,torr)^{-1/2}}$ [2]. (Note that this way of evaluation of μ_e and α yields results in good agreement with those given by the zero-dimensional

Boltzmann solver BOLSIG+ [76].) The diffusion coefficients were evaluated by means of Einstein's law, $D_{i,e} = k\,T_{i,e}\,\mu_{i,e}\,/e$, where k is Boltzmann's constant and T_i and T_e are temperatures of the heavy particles and electrons, respectively: $T_i = 300\,\mathrm{K}$ and $T_e = 1\,\mathrm{eV}$. The coefficient of dissociative recombination of molecular ions Xe_2^+ was set equal to $2 \times 10^{-13}\,\mathrm{m^3\,s^{-1}}$[77, 78]. The effective secondary emission coefficient was set equal to 0.03.

2.3 Solutions without neutralization of charged particles at the wall of the discharge vessel

In this section, 2D and 3D solutions are considered without account of neutralization, i.e., with boundary condition *i)* in (2.6). Information on what these solutions are like and where they should be sought was obtained by means of finding bifurcation points where 2D and 3D modes branch off from the fundamental (1D) mode. Calculation of each 2D or 3D mode was started in the vicinity of the corresponding bifurcation point with an initial approximation obtained by adding to the 1D solution a small radial perturbation governed by a Bessel function [74]. When a state belonging to the desired 2D or 3D mode has been found, the next step is to vary the input parameter (U or I) in order to find the mode in the whole range of its existence.

The 1D eigenvalue problem governing the location of bifurcation points in the framework of the present model is similar to the one considered in [54], except that the diffusion terms are taken into account in the transport equations for the ions and the electrons in the present work[1].

2.3.1 Axially symmetric solutions

Results reported in this section refer to a discharge tube of the radius $R = 1.5\,\mathrm{mm}$. Multiple solutions describing nine different modes were detected in this case, a 1D mode and eight 2D modes. The CVCs of the 1D mode and five 2D modes are shown in figure 2.1. Here $\langle j \rangle$ is the average value of the axial component of the electric current density evaluated over the whole surface of the cathode or, equivalently, over a whole (circular) cross section of the discharge vessel. The 1D mode exists at all values of the discharge current and is termed fundamental mode; this is an analogue of the well-known solution of von Engel and Steenbeck [2]. Each of the 2D modes exists in a limited range of the discharge current and its CVC represents a closed curve. For each of the 2D modes, there are two states in which functions n_i, n_e, and φ vary with z but not with r, i.e., $n_{i,e} = n_{i,e}\,(z)$ and $\varphi = \varphi\,(z)$. These states are marked by circles in figure 2.1 and subsequent figures. One of these two states is close to the point of minimum of the CVC of the fundamental mode and is designated a_i $(i = 1, 2, .., 8)$, the other is designated b_i and located at lower currents. These states belong not only to the 2D mode being considered, but also to the fundamental mode. In other words, the solutions describing the 2D mode and the fundamental mode coincide at these states. This phenomenon is well known in mathematical physics and called bifurcation, or branching, of solutions, and states where it occurs are called bifurcation points.

[1] It is once again stressed that a solution to this problem is out of the scope of this thesis. Some results obtained from the solution of this eigenvalue problem will be shown and discussed in the current chapter for the sake of readability and completeness.

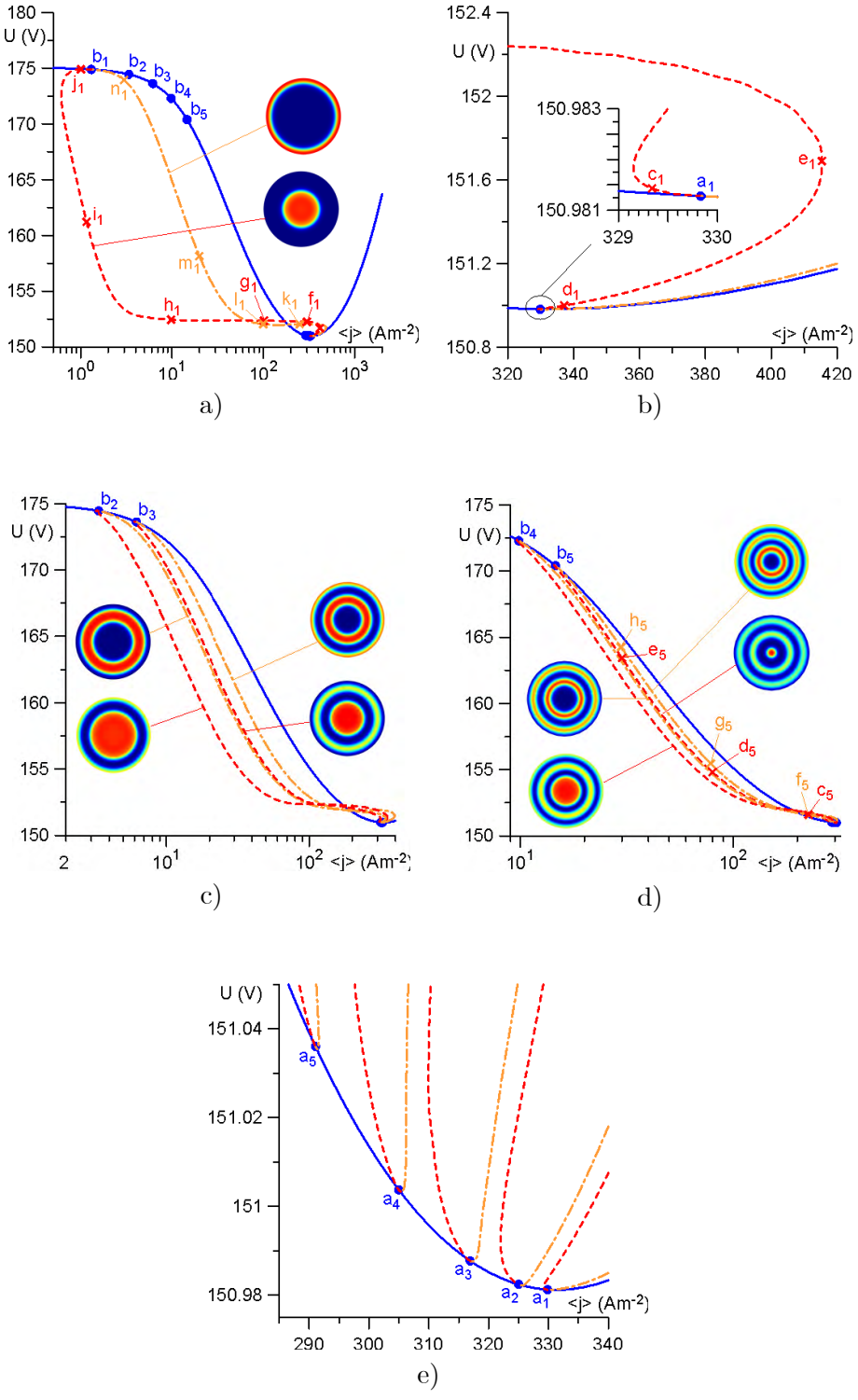

Figure 2.1: CVCs. $R = 1.5\,\mathrm{mm}$, neutralization neglected. Solid: the fundamental mode. Dashed: branches of 2D modes associated with patterns comprising a spot at the centre of the cathode. Dashed-dotted: branches of 2D modes associated with patterns without a central spot. (a) The first 2D mode and the fundamental mode; (b) details of the CVC of the first 2D mode near the bifurcation point a1; (c) the second and third 2D modes and the fundamental mode; (d) the fourth and fifth 2D modes and the fundamental mode; (e) details of the CVCs near the minimum of the CVC of the fundamental mode.

The point of minimum of the CVC of the fundamental mode, found by means of the 2D simulations, is $j_{\min} \approx 325\,\mathrm{A\,m^{-2}}$. The two nearest bifurcation points determined in the above-described way (i.e., as states belonging to 2D modes where distributions of parameters become 1D) are located at $j \approx 329\,\mathrm{A\,m^{-2}}$ and $j \approx 325\,\mathrm{A\,m^{-2}}$. One could think that the first bifurcation point is positioned on the section of the fundamental mode with a rising CVC. However, the numerical accuracy of the 2D modelling is insufficient to judge. An alternative way of finding bifurcation points is to solve the 1D eigenvalue problem mentioned in the beginning of section 2.3. The bifurcation points determined in this way which are the nearest to the point of minimum of the CVC of the fundamental mode are located at $j = 327\,\mathrm{A\,m^{-2}}$ and $j = 322\,\mathrm{A\,m^{-2}}$ and the point of minimum found by means of 1D simulations is $j_{\min} = 328\,\mathrm{A\,m^{-2}}$. These values are accurate and one can see that the bifurcation points are positioned on the section of the fundamental mode with a falling CVC, which is a usual situation.

Let us designate by $I(a_i)$ and $I(b_i)$ values of the discharge current that correspond to bifurcation points a_i or, respectively, b_i. We number the bifurcation points so as $I(b_1) < I(b_2) < \cdots < I(b_8) < I(a_8) < I(a_7) < \cdots < I(a_1)$. Analysis of figure 2.1 with necessary magnifications reveals that the 2D mode that bifurcates at a_1 is the same that bifurcates at b_1. In the following, this mode will be referred to as the first 2D mode. Similarly, the 2D mode that bifurcates at a_2 is the same that bifurcates at b_2; the second 2D mode *etc.*

The (two) bifurcation points positioned on each 2D mode divide this mode into two branches. Schematics in figure 2.1 illustrate current density distributions over the cathode surface corresponding to each branch. One of the branches of the first 2D mode is associated with a pattern comprising a spot at the centre of the cathode, the other branch is associated with a pattern comprising a ring spot at the periphery. One of the branches of the second 2D mode is associated with a pattern comprising a spot at the centre and a ring spot at the periphery, the other branch with a pattern comprising a ring spot in the interior of the cathode. One of the branches of the third 2D mode is associated with patterns comprising a spot at the centre and an interior ring spot, the other with an interior ring spot and a spot at the periphery. One of the branches of the fourth 2D mode is associated with patterns comprising a spot at the centre, an interior ring spot, and a spot at the periphery, the other with two interior ring spots. One of the branches of the fifth 2D mode is associated with patterns comprising a spot at the centre and two interior ring spots, the other with two interior ring spots and a spot at the periphery. Generalizing, one can say that one of the two branches of each 2D mode is associated with a pattern comprising a spot at the centre of the cathode and the other with a pattern without a central spot.

In the vicinity of each bifurcation point, e.g., the point a_i, the bifurcating 2D mode exists at currents both below and above $I(a_i)$. (This can be seen from figure 2.1b as far as the point a_1 is concerned, from figure 2.1e as far as the points a_2, a_3, a_4, a_5 are concerned; from figure 2.1a as far as the point b_1 is concerned; and from appropriate magnifications of the vicinities of points b_2, b_3, b_4, b_5 in figures 2.1c and 2.1d.) In other words, if a branch of an i-th 2D mode bifurcates into the current range $I < I(a_i)$, then the other branch of the same mode bifurcates into the range $I > I(a_i)$. Furthermore, it can be seen that the branch of an i-th mode associated with a pattern comprising a spot at the centre bifurcates into the range $I < I(a_i)$ in the vicinity of the bifurcation point a_i and into the range $I < I(b_i)$ in the vicinity of the bifurcation point b_i, while

the branch associated with a pattern without a central spot bifurcates into the ranges $I > I(a_i)$ and $I > I(b_i)$.

According to the bifurcation theory [54], a solution describing an i-th 2D mode in the vicinity of both bifurcation points a_i and b_i represents a superposition of a 1D solution and a small 2D perturbation with the radial variation governed by the Bessel function of the first kind of order zero, $J_0(k\,r)$, where $k = 3.832/R$, $k = 7.016/R$, $k = 10.17/R$, $k = 13.32/R$, and $k = 16.47/R$ for the first, second, third, fourth, and fifth 2D modes, respectively. [Note that numbers 3.832, 7.016, 10.17, 13.32 and 16.47 represent abscissas of the first five extrema of the function $J_0(x)$.] This variation is indeed seen in the numerical results.

The complexity of the patterns associated with the 2D modes increases with i or, equivalently, with a decrease of the range of existence of the corresponding mode. This is a behavior typical for bistable nonlinear dissipative systems. Note that the two stable regimes of the glow discharge are represented by the 1D abnormal discharge and the case where the discharge has not been ignited [52].

Variations of a pattern associated with a given branch from one bifurcation point to the other are illustrated by figure 2.2. Figures 2.2a and 2.2b show variations of the pattern with a central spot, associated with one of the branches of the first 2D mode. In the state a_1, which is a bifurcation point, the current density is the same at all points of the cathode surface. A weak variation of the current density over the cathode surface occurs in the vicinity of the bifurcation point (state c_1) and this variation is well described by the Bessel function $J_0(3.832\,r/R)$. Further away from the bifurcation point a_1 (state d_1), the current density at the cathode surface increases, except in the vicinity of the wall where it decreases. One can say that a current spot is being formed that occupies the whole surface of the cathode except the vicinity of the wall. The state e_1 represents a turning point of the branch being considered. The formation of the spot has already finished and the the spot starts shrinking. At states f_1 and g_1 the spot continues to shrink, while the current density inside the spot does not change much. From state h_1 the spot stops shrinking and the maximum current density inside the spot starts decreasing. There is still a well pronounced spot in state i_1. Further on, the spot becomes less pronounced. In the vicinity of the bifurcation point b_1 (state j_1), there is again only a weak variation of the current density along the cathode surface which is well described by the Bessel function $J_0(3.832\,r/R)$. The current density becomes constant along the cathode surface at the bifurcation point b_1. Note that the above-described numerical results conform to the analytical theory [79] as they should.

The above-described approximate constancy of current density inside the spot between states e_1 and h_1 is associated with the plateau of the CVC represented in figure 2.1a. These features are characteristic of the effect of normal current density. Hence, the section of the central-spot branch of the first 2D mode corresponding to the plateau of the CVC may be identified with the normal mode of the glow discharge.

Values of the current density inside the normal spot considerably exceed the current density at the minimum of the CVC of the fundamental mode, $j_{\min} \approx 325\,\mathrm{A\,m^{-2}}$, in contrast to what is sometimes believed. Rather, the current density inside the normal spot approximately corresponds to the current density which occurs on the abnormal mode at the same discharge voltage. For example, the value of discharge voltage in state f_1 is $U = 152.26\,\mathrm{V}$. At this U, the current density

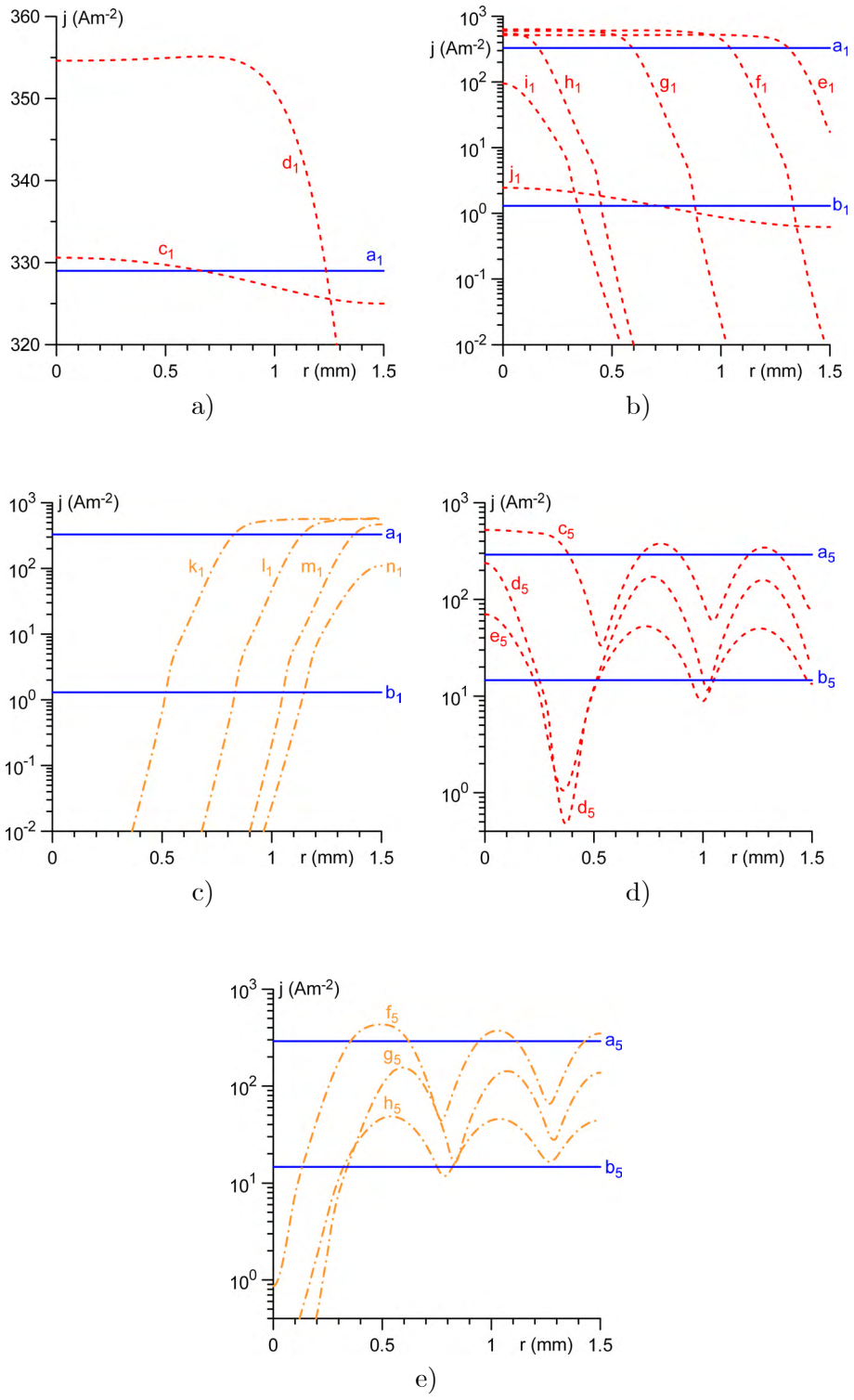

Figure 2.2: Distributions of current density over the cathode surface for the first and fifth 2D modes. $R = 1.5\,\mathrm{mm}$, neutralization neglected. (a), (b) The branch with a spot at the centre of the cathode; (c) the branch with a ring spot at the periphery of the cathode; (d) the branch with a spot at the centre of the cathode and two interior ring spots; (e) the branch with two interior ring spots and a ring spot at the periphery of the cathode. The states to which each of the lines correspond are indicated in figures 2.1 (a), (b), (d) and (e).

in the abnormal mode equals $610\,\mathrm{A\,m^{-2}}$, which is quite close to the maximum value of current density in state f_1, equal to $599\,\mathrm{A\,m^{-2}}$. Similarly, $U = 152.36\,\mathrm{V}$ in state g_1; the current density at this U in the abnormal mode equals $624\,\mathrm{A\,m^{-2}}$ and is quite close to the maximum value of current density in state g_1, which is $632\,\mathrm{A\,m^{-2}}$. Hence, one can view the effect of normal current density as a manifestation of coexistence of a hot phase, representing the abnormal mode, with a cold phase, representing a situation in which no discharge is present at the considered point of the cathode surface [79]. Note that the concept of coexistence of phases gives a hint as to why the discharge voltage is virtually constant in the normal mode: the coexistence of phases is usually possible at only one value of the control parameter, in this case, U. (This value is governed by a certain condition which follows from a treatment of an intermediate region that separates the phases and is known as Maxwell's construction; see, e.g., [80].)

A plateau is present also on the CVC of the branch of the first 2D mode associated with the ring spot on the periphery, as can be seen in figure 2.1a. The maximum of current density inside the spot between states k_1 and l_1 remains more or less constant, as is seen in figure 2.2c. The value of the discharge voltage U in state k_1 is 152.04 V and the value of the current density corresponding to this U in the abnormal mode is $566\,\mathrm{A\,m^{-2}}$, which exactly coincides with the maximum of current density in state k_1. For state l_1, U is 152.05 V. The value of the current density in the abnormal mode corresponding to this U is $576\,\mathrm{A\,m^{-2}}$, approximately equal to the maximum of current density in state l_1 which is $570\,\mathrm{A\,m^{-2}}$. One can conclude that the effect of normal current density is present also on the branch of the first 2D mode associated with the ring spot on the periphery, although it occurs in a current range substantially more narrow than on the branch with the central spot.

The effect of normal current density is manifested also by the second and subsequent 2D modes, however with increasing i it becomes less pronounced and occurs in a narrower range of the discharge currents and eventually disappears. The only feature of the fifth 2D mode (figures 2.2d and 2.2e) that reminds of this effect is a more or less constant current density inside the central spot in state c_5.

2.3.2 Effect of variation of the radius

Calculations for a discharge tube of the radius $R = 0.5\,\mathrm{mm}$ revealed only two 2D modes; see figure 2.3. Also shown in this figure is the fundamental mode (which is the same that the one found for $R = 1.5\,\mathrm{mm}$). Average current densities corresponding to the bifurcation points positioned on the first and second 2D modes are $\langle j\,(a_1)\rangle = 311\,\mathrm{A\,m^{-2}}$, $\langle j\,(b_1)\rangle = 7.7\,\mathrm{A\,m^{-2}}$, $\langle j\,(a_2)\rangle = 265\,\mathrm{A\,m^{-2}}$, and $\langle j\,(b_2)\rangle = 26\,\mathrm{A\,m^{-2}}$. Note that the similar values for $R = 1.5\,\mathrm{mm}$ are $\langle j\,(a_1)\rangle = 329\,\mathrm{A\,m^{-2}}$, $\langle j\,(b_1)\rangle = 1.3\,\mathrm{A\,m^{-2}}$, $\langle j\,(a_2)\rangle = 325\,\mathrm{A\,m^{-2}}$, and $\langle j\,(b_2)\rangle = 3.4\,\mathrm{A\,m^{-2}}$. One can conclude that a decrease of R causes a shift of the two bifurcation points belonging to each 2D mode in the directions towards each other. The range of existence of each of the 2D modes also shrinks with a decrease of R.

Calculations for intermediate R have shown that the third to eighth 2D modes disappear one by one with decreasing R, and the disappearance occurs through shrinking of their existence ranges. As an example, the disappearance of the third 2D spot mode is shown in figure 2.4 in the

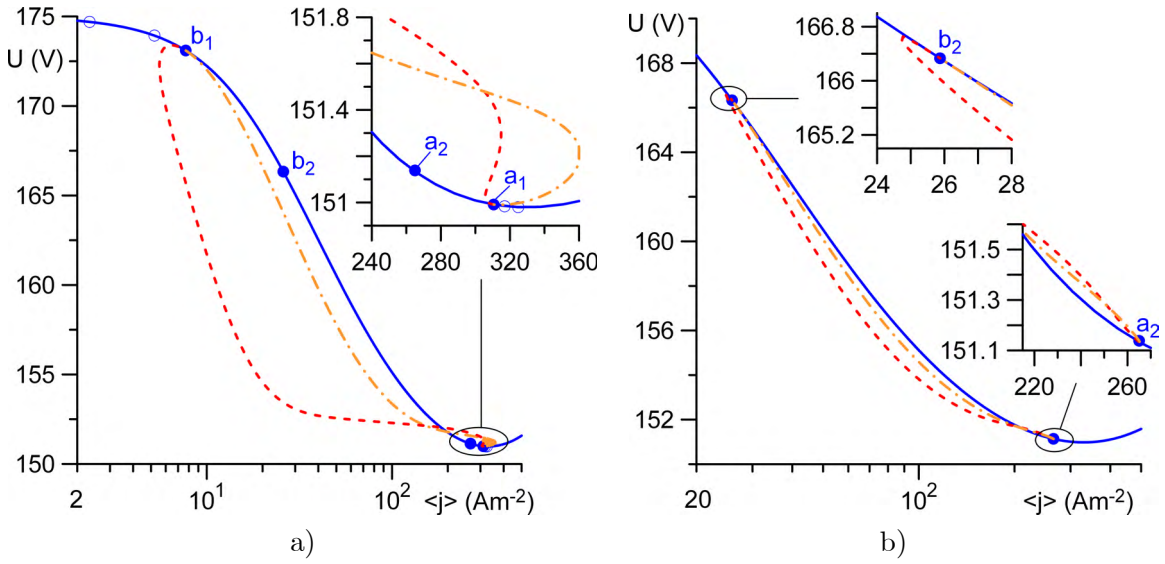

Figure 2.3: CVCs. $R = 0.5\,\mathrm{mm}$, neutralization neglected. Solid: the fundamental mode. Dashed: branches of 2D modes associated with patterns comprising a spot at the centre of the cathode. Dashed-dotted: branches of 2D modes associated with patterns without a central spot. (a) The first 2D mode and fundamental mode; (b) the second 2D mode and the fundamental mode.

plane $(j_c, \langle j \rangle)$. (Here j_c is the current density at the centre of the cathode; these coordinates have been chosen since the CVCs for the different values of R shown in figure 2.4 are nearly coincident.) As R decreases, the bifurcation points a_3 and b_3 move in the direction towards each other. There is only one bifurcation point at $R \approx 0.527\,\mathrm{mm}$. At $R \lesssim 0.527\,\mathrm{mm}$, the 2D spot mode is detached from the diffuse mode and its existence range continues to shrink. It is interesting to note that all states of the third 2D mode at $R \lesssim 0.527\,\mathrm{mm}$ possess a spot at the centre of the cathode and an interior ring spot. No steady states belonging to the third 2D mode have been found at $R \lesssim 0.520\,\mathrm{mm}$.

A more or less pronounced effect of normal current density is present at $R = 0.5\,\mathrm{mm}$ only on the first 2D mode, as evidenced by the CVCs shown in figure 2.3.

2.3.3 Role of diffusion of the charged particles

An interesting question is to what extent the above results are affected by diffusion of the charged particles. Results of calculation of the fundamental mode and the first 2D mode with the ion and electron diffusion coefficients reduced by a factor of two or four (or, equivalently, with the ion and electron temperatures reduced by a factor of two or four) in the vicinity of the minimum of the CVC of the fundamental mode are shown in figure 2.5. Also shown are results of calculations with the original values of D_i and D_e, as well as results of calculations without account of diffusion. The bifurcation points are represented by circles and the points of minimum of the CVC of the fundamental mode by triangles. The branch of 2D mode associated with a spot at the centre of the cathode in all the cases branches off into the range of low currents, although this can hardly be seen on the graph or cannot be seen at all. Note that the 2D mode in the case where the

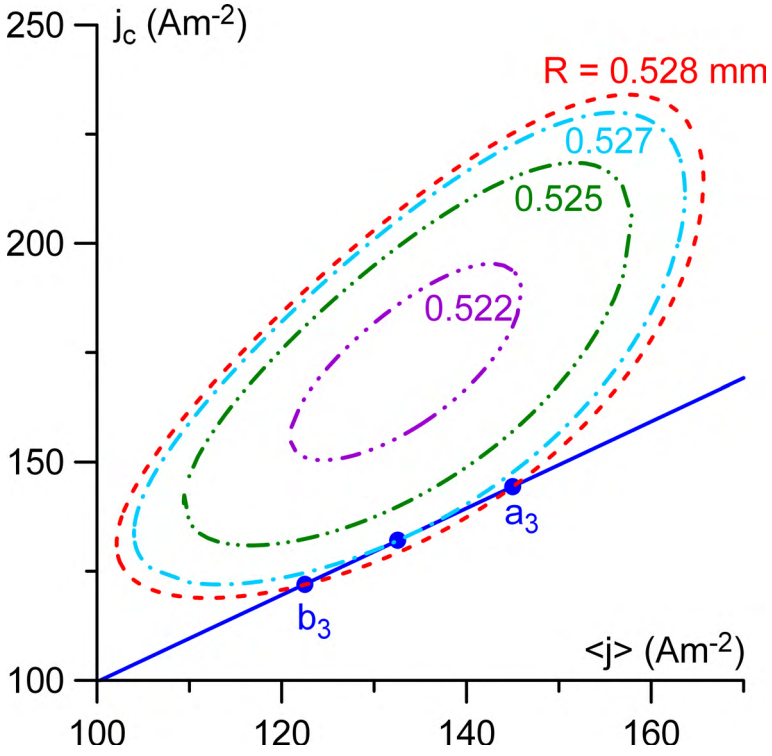

Figure 2.4: Electric current density at the centre of the cathode vs. average current density for the third 2D mode for discharge tubes of different radii. Neutralization neglected.

diffusion is neglected could only be calculated in the vicinity of the bifurcation point: the upper curve in figure 2.5 represents all the states where converged solutions have been obtained. (The width of this vicinity strongly depends on the numerical mesh; the results depicted in figure 2.5 have been calculated with the use of a non-uniform mesh with 18500 degrees of freedom.) The position of the bifurcation point in the case without diffusion conforms to the numerical accuracy to the one found in [54], as it should.

As the diffusion coefficients are reduced, the discharge voltage slightly increases. Two turning points visible on the branch of the 2D mode associated with a spot at the centre in the cases of the original and reduced diffusion coefficients disappear in the cases without diffusion. As the diffusion coefficients are reduced, the bifurcation point is shifted in the direction of higher currents and eventually crosses the point of minimum of the CVC of the fundamental mode and enters the rising section of the CVC. Thus, the present modelling confirms the conclusion [54] on the possibility of a bifurcation on a discharge mode with a positive differential resistance; a result very interesting theoretically.

One can conclude that the overall effect of diffusion is visible, but not very strong.

In figure 2.6, distributions of drift and diffusion components of radial projection of the ion current density in the cross section of the discharge at 0.06 mm from the cathode are shown for several states belonging to the normal discharge. The cross section $z = 0.06$ mm approximately corresponds to the point of maximum of the distribution of the density of space charge along the axis of the discharge and is positioned more or less in the middle of the cathodic space-charge sheath. Note that the maxima of both drift and diffusion currents are located at the edge of the

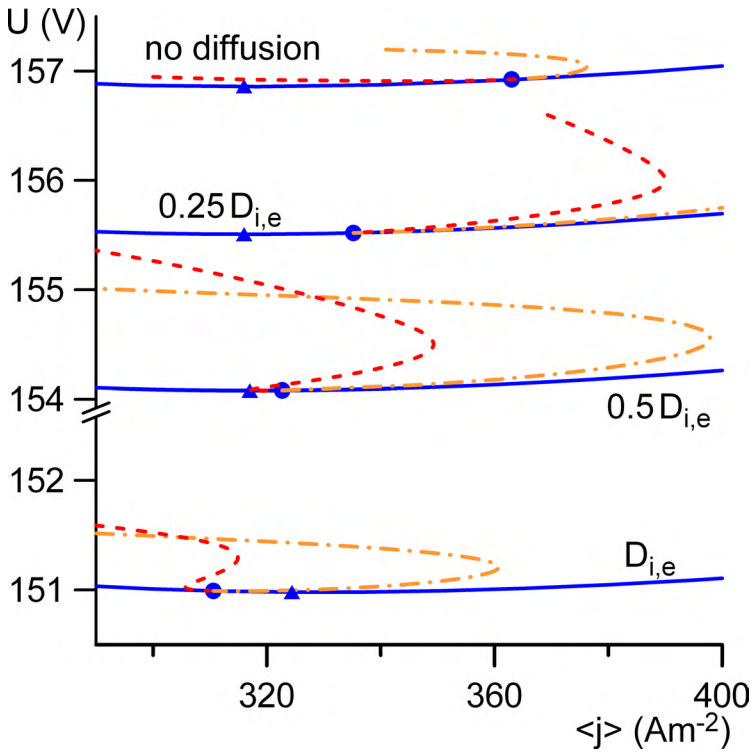

Figure 2.5: CVCs of the fundamental mode and of the first 2D mode for different diffusion coefficients near the minimum of the CVC of the fundamental mode. $R = 0.5$ mm, neutralization neglected. Solid: the fundamental mode. Dashed: branch with a spot at the centre of the cathode. Dashed-dotted: branch with a ring spot at the periphery of the cathode.

spot, as could be expected.

One can see from figure 2.6 that the drift current exceeds the diffusion current by three orders of magnitude. On the other hand, the diffusion still plays an important role, since the 2D mode without account of diffusion could only be calculated in the vicinity of the bifurcation point as mentioned above.

The question of the effect of diffusion of charged particles over the structure of normal spots is very interesting and has been raised in the literature more than once; see discussion in section 1.2.1 of Introduction. Leaving a detailed analysis beyond the scope of this work, we only note that a hypothetical explanation of the above results may be offered on the basis of analogy with the problem of calculation of shock waves in gas dynamics. It is well known that if dissipative processes are neglected, then shock waves appear (in the framework of the Euler equations) as discontinuities; if dissipative processes are taken into account, then shock waves may be resolved (in the framework of the Navier-Stokes equations). Similarly, one can hypothesize that the spot patterns in principle may appear without diffusion, due only to electrostatic effects and drift, however far away from the bifurcation points such patterns manifest abrupt transitions from spots to surrounding current-free region and are described by discontinuous solutions, which are difficult to calculate.

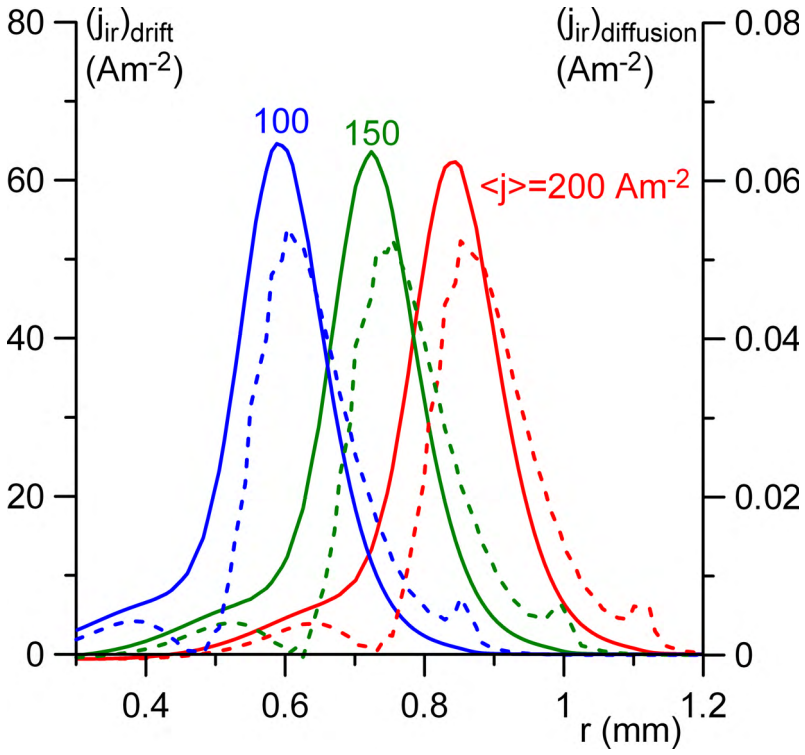

Figure 2.6: Distribution of components of radial projection of the ion current density in the cross section $z = 0.06\,\mathrm{mm}$. The first 2D mode, $R = 1.5\,\mathrm{mm}$, $z = 0.06\,\mathrm{mm}$, neutralization neglected. Solid: drift component. Dashed: diffusion component.

2.3.4 3D solutions

Calculations of 3D modes have been performed for a discharge tube of the radius $R = 0.5\,\mathrm{mm}$. Thirteen 3D modes exist under these conditions, in addition to two 2D modes discussed in section 2.3.2. The CVCs of the first, eighth and twelfth 3D modes are shown in figure 2.7. Also shown is the CVC of the fundamental mode. Each of the 3D modes exists in a limited range of values of the discharge current and branches off from (or joins) the fundamental mode at two points (bifurcation points): one at low currents and the other one in the vicinity of the point of minimum of the CVC of the fundamental mode. All the bifurcations involving the first and twelfth modes are subcritical (the CVC "turns back", as seen in the insert). Both bifurcations involving the eighth mode are supercritical.

Distributions of the current density over the surface of the cathode are shown in figures 2.8-2.10. Note that the states corresponding to $\langle j \rangle = 2.4,\ 382,\ 367,\ 339\,\mathrm{A\,m^{-2}}$ in figure 2.8 are positioned between the corresponding bifurcation and turning points, all the states shown in figure 2.10 are positioned between the corresponding turning points.

Distributions of discharge parameters along the cathode in the vicinity of bifurcation points are smooth (governed by the Bessel functions, in accordance with the theory [79]). Localized current spots are formed away from the vicinity of the bifurcation points. The first mode exhibits the normal current density effect: there is a large plateau in the corresponding CVC and the maximum current density on the cathode surface remains virtually unchanged in states on this plateau. In general, this pattern of self-organization corresponds to the theory [79] and is similar

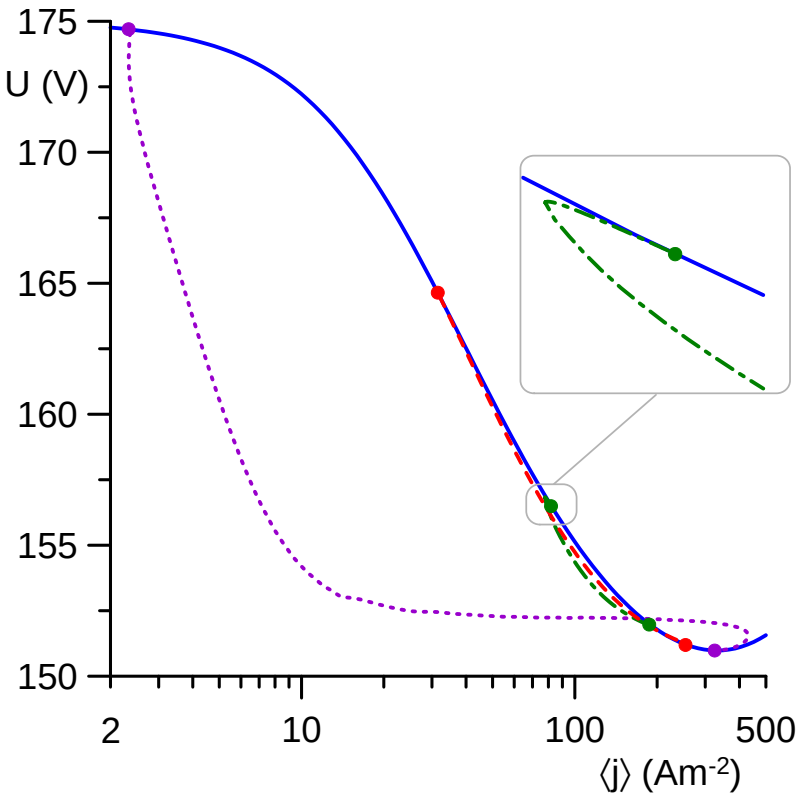

Figure 2.7: CVCs. $R = 0.5\,\mathrm{mm}$, neutralization neglected. Solid: the fundamental mode. Dotted: the first 3D mode. Dashed: the eight 3D mode. Dashed-dotted: the twelfth 3D mode. Circles: bifurcation points in which 3D modes branch off from the 1D mode.

to the pattern of self-organization of 2D modes without neutralization.

The effect of normal current density seen in figures 2.7 and 2.8 corresponds to the experimental observations and the spot patterns seen in figures 2.9 and 2.10 are qualitatively similar to those observed in microdischarges in xenon [5–11]. There is a minimum or, respectively, a maximum of the current density at the centre of the cathode in figures 2.9 and 2.10 . It should be stressed that there is no extreme point at the centre in the vicinity of bifurcation points involving 3D modes, where the distribution of parameters is governed by a Bessel function. On the other hand, both the patterns with and without spot at the centre have been observed in the experiment [5–11].

2.4 Solutions with neutralization of charged particles at the wall of the discharge vessel

The analysis in this section is limited to 2D modes. When neutralization of charged particles at the wall is taken into account, the fundamental mode is no longer 1D but rather becomes 2D. Furthermore, the non-fundamental 2D modes do not bifurcate from the fundamental mode. Under these circumstances it is not possible to rely on bifurcation analysis in order to obtain information on the range of existence of non-fundamental 2D modes or what these modes are like.

The procedure of finding these modes was as follows. Starting from a state belonging to a 2D mode without neutralization, the neutralization is gradually introduced for a fixed value of the

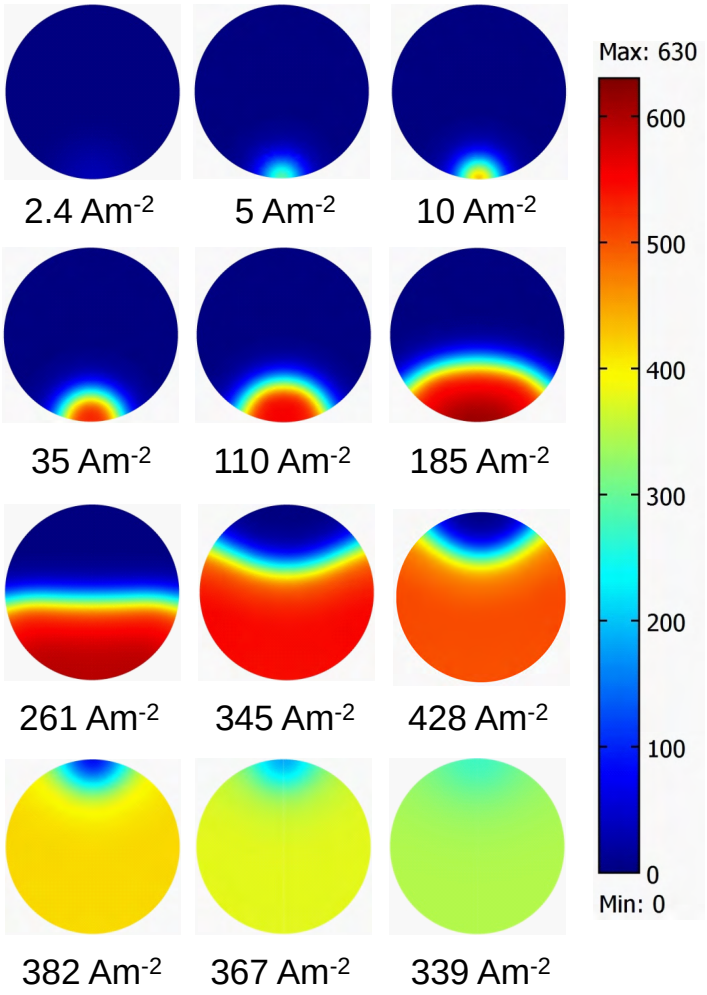

Figure 2.8: Distribution of current density over the cathode surface in states belonging to the first 3D mode. Color bar in $\mathrm{A\,m^{-2}}$.

input parameter (the discharge voltage or current). The boundary condition at the wall of the discharge tube for n_i and n_e is written in the form

$$s\, n_{i,e} + (1-s)\, R \frac{\partial\, n_{i,e}}{\partial\, r} = 0, \tag{2.8}$$

where s is a given parameter that was gradually varied from 0 to 1. $s = 0$ corresponds to a (totally) reflecting wall, or, in other words, to losses of the charged particles due to neutralization at the wall being neglected. $s = 1$ corresponds to an absorbing wall, or, in other words, to neutralization being taken into account.

Three 2D modes have been found for $R = 1.5\,\mathrm{mm}$ and $s = 0$. One of them exists at all current values, i.e., is fundamental, the other two modes exist only in limited current ranges. The CVCs of the three modes are shown in figure 2.11a. The CVCs of the two non-fundamental 2D modes are shown also in figure 2.11b. The modes are all disconnected from each other, although CVCs intersect at some values of the discharge current. The CVCs of the non-fundamental modes represent closed curves and each mode is constituted by two branches separated by two turning

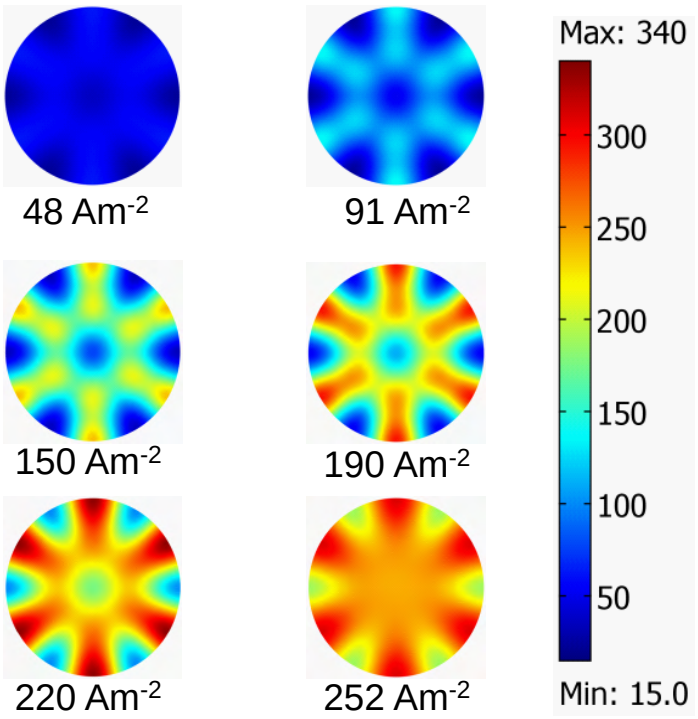

Figure 2.9: Distribution of current density over the cathode surface in states belonging to the eighth 3D mode. Color bar in $\mathrm{A\,m^{-2}}$.

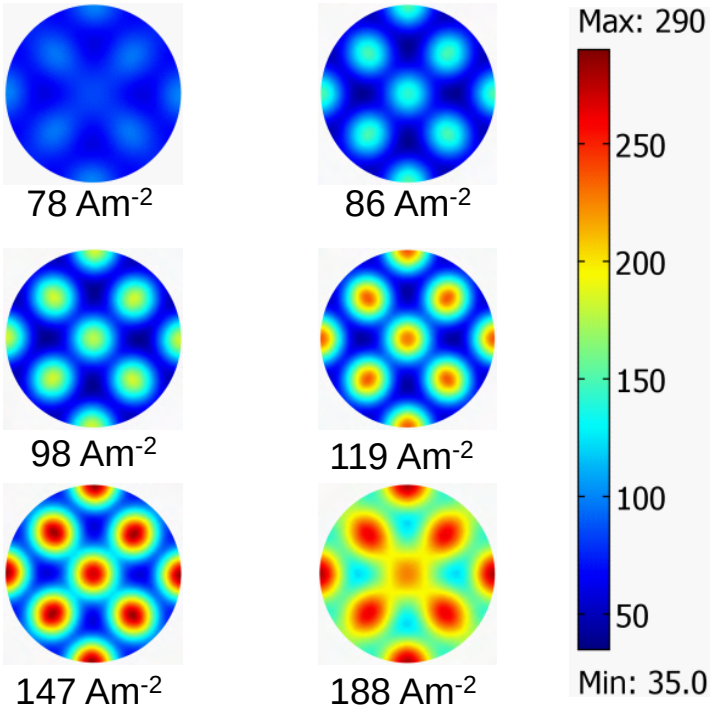

Figure 2.10: Distribution of current density over the cathode surface in states belonging to the twelfth 3D mode. Color bar in $\mathrm{A\,m^{-2}}$.

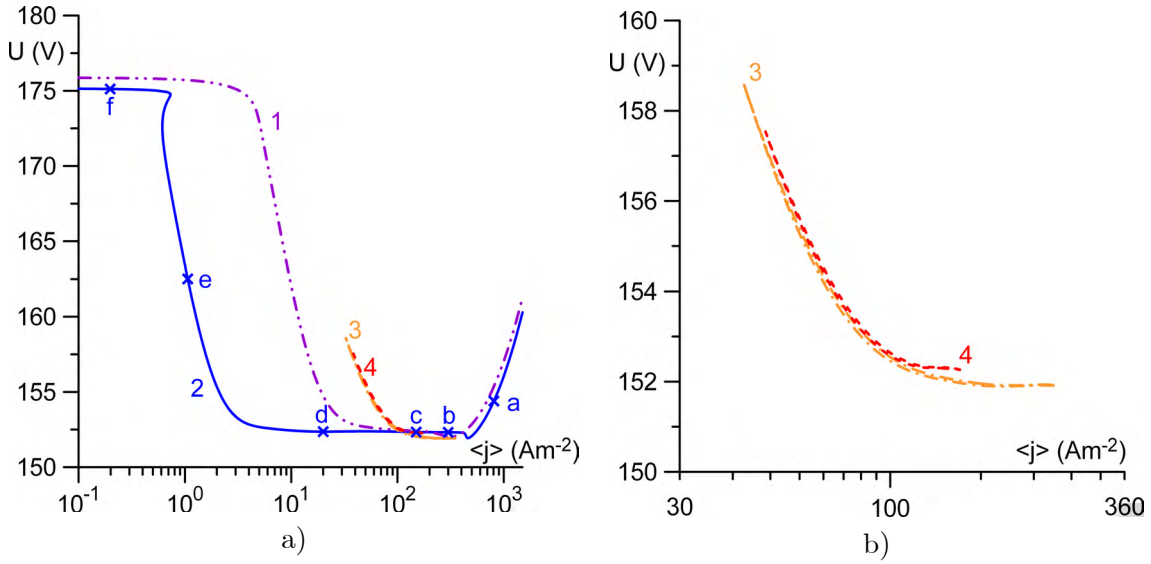

Figure 2.11: CVCs. Neutralization taken into account. 1: fundamental mode, $R = 0.5\,\mathrm{mm}$. 2: fundamental mode, $R = 1.5\,\mathrm{mm}$. 3: the first non-fundamental 2D mode, $R = 1.5\,\mathrm{mm}$. 4: the second non-fundamental 2D mode, $R = 1.5\,\mathrm{mm}$. (a) General view; (b) magnification of the first and second non-fundamental 2D modes.

points. The difference between values of the discharge voltage on different branches for the same value of $\langle j \rangle$ amounts to a few tens of mV and thus is hardly visible even in figure 2.11b. Also shown in figure 2.11a is the fundamental mode for $R = 0.5\,\mathrm{mm}$. No other 2D modes have been found for this value of R.

Distributions of current density over the cathode surface at several states belonging to the fundamental mode for $R = 1.5\,\mathrm{mm}$ are shown in figure 2.12. The current density in state a is constant over the most part of the cathode surface and sharply drops in the immediate vicinity of the wall. This distribution may be identified with the abnormal discharge. As the discharge current decreases, a normal spot at the centre of the cathode appears (states b, c, d). Somewhere between states d and e the spot stops shrinking and the maximum current density inside the spot starts decreasing; the subnormal discharge. Somewhere between states e and f the spot starts expanding, while the current density inside the spot continues to decrease. Eventually the Townsend discharge is formed with the radial dependence of current density described by the Bessel function $J_0\,(2.42\,r/R)$, in agreement with the theory [47] (state f).

In figure 2.13 maxima of numerically calculated distributions of the densities of charged particles along the axis of the discharge are shown as functions of $\langle j \rangle$. Also shown are analytical results (which are out of the scope of this thesis) for the limiting case of Townsend discharge obtained along the lines [47]. (Note that these results are independent of the radius of the tube.) One can see that the Townsend discharge occurs at $\langle j \rangle$ of the order of or below $1\,\mathrm{A\,m^{-2}}$, in agreement with what can be concluded from figure 2.11a.

Thus, the fundamental solution describes the abnormal discharge, the normal discharge, the subnormal discharge, and the Townsend discharge, and is similar to the solutions computed in [44–49].

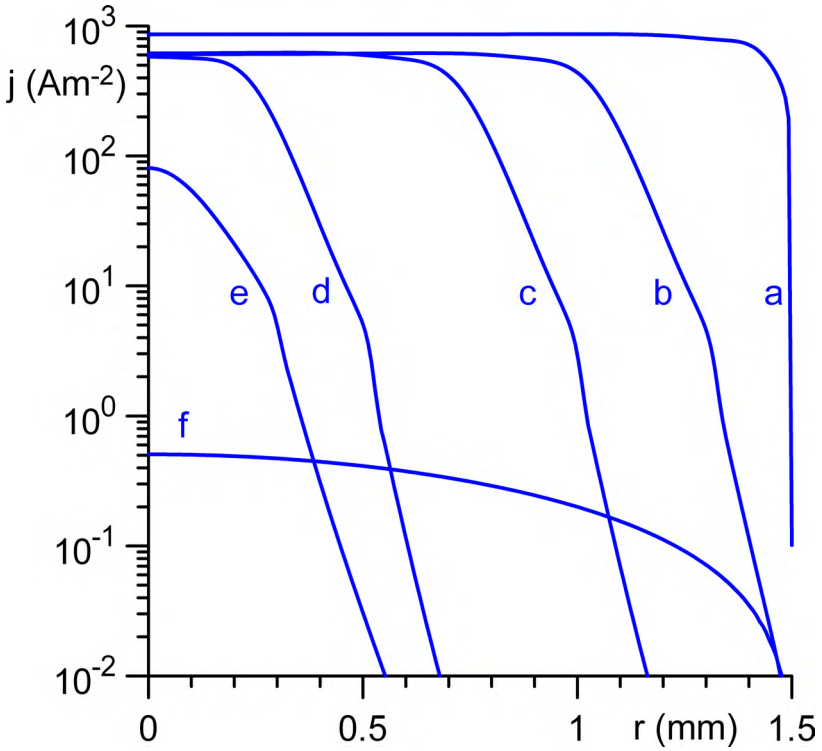

Figure 2.12: Distributions of current density over the cathode for the fundamental mode. $R = 1.5\,\mathrm{mm}$, neutralization taken into account. The states to which each of the lines correspond are indicated in figure 2.11.

The value of the discharge voltage U in state b is 152.32 V. At this U, the current density on the rising section of the CVC of the fundamental mode without neutralization is $610\,\mathrm{A\,m^{-2}}$, which exactly coincides with the maximum value of the current density over the cathode surface in state b. Similarly, $U = 152.34\,\mathrm{V}$ in state c; the current density at this U on the rising section of the CVC of the fundamental mode without neutralization is $614\,\mathrm{A\,m^{-2}}$ and is quite close to the maximum value of the current density over the cathode surface in state c, which equals $624\,\mathrm{A\,m^{-2}}$. Hence, the effect of normal current density in the glow discharge with neutralization can still be interpreted as a manifestation of coexistence of phases, provided that the hot phase is understood as the 1D abnormal discharge, i.e., the abnormal discharge without neutralization.

The ratio of the numerically computed electron current to the wall of the discharge tube to the discharge current is of the order of 10^{-3} or lower at all discharge currents. In other words, diffusion of the charged particles to the wall represents a weak effect. It is not surprising therefore that the distribution of current density over the cathode surface in states on the abnormal mode is virtually uniform except in a thin layer near the wall of the vessel, as shown by line a in figure 2.12. On the other hand, the Townsend discharge manifests a radial variation governed by the Bessel function as shown by line f in figure 2.12, i.e., is essentially nonuniform. A question arises how diffusion of the charged particles to the wall, which is a weak effect, can affect the discharge that significantly. Note that this question seems to have been discussed for the first time in the work [48].

The root cause of this effect is the linearity of process of multiplication of the charged particles

in the Townsend discharge. Consider an initial situation where a uniform flux of electrons is emitted from the cathode surface. Each electron produces on average $1/\gamma$ ions while travelling to the anode. The ions return to the cathode and are converted into one electron, and this completes the cycle. However, a part of the ions and the electrons produced inside a layer adjacent to the wall, as well as a part of the electrons emitted into this layer, will diffuse to the wall and will be absorbed there. A scale of thickness of this layer may be estimated as $L = v_{dif}\tau$, where $\tau = h^2/\mu_e U$ is a characteristic time of drift of electrons from the cathode to the anode and $v_{dif} = D_e/R$ is a characteristic speed of free diffusion of electrons to the wall of the vessel. One finds that L is of the order of 10^{-3} mm, i.e., much smaller than both h and R, in accordance with the above conclusion on smallness of the losses of the charged particles due to their diffusion towards the absorbing wall.

Thus, a near-wall layer of a thickness of the order L is depleted of charged particles after the first cycle. After the second cycle, the thickness of the depleted layer will double *etc.* The Bessel radial dependence in n_i and n_e appears after many cycles.

The distributions of current density over the cathode surface for several states belonging to the non-fundamental 2D modes and corresponding to different values of the discharge current are shown in figure 2.14. Both branches of the first non-fundamental 2D mode are associated with a ring spot inside the cathode, both branches of the second non-fundamental 2D mode are associated with a pattern comprising a spot at the centre of the cathode and an interior ring spot. Distributions of parameters in states belonging to different branches of the same mode and corresponding to the same discharge current are surprisingly close.

An example of distribution of parameters in the interelectrode gap is shown in figure 2.15. Arrows in figure 2.15c indicate local directions of the electric current and their length is proportional to the modulus of current density.

Two current filaments are seen, one in the form of a cylinder at the centre of the cathode and the other, which is not very well pronounced, in the form of a toroid. These filaments correspond to the central and, respectively, ring current spots on the cathode seen in figure 2.14b. The distribution of parameters inside the central part of the cylindrical filament is close to 1D. The densities of the charged particles and modulus of the current density drop by at least two orders of magnitude in the space between the filaments, the electric field here is more uniform. This picture again can be interpreted as the coexistence of hot and cold phases.

Let us proceed to the question posed in Introduction, section 1.2.1: how can the weak effect of loss of charged particles due to their diffusion to an absorbing wall produce the dramatic difference which exists between the 1D fundamental mode, that represents in essence the von Engel and Steenbeck solution, and the 2D fundamental mode, which includes the subnormal and normal regimes? The transition between states with and without neutralization was studied in order to answer this question.

As an example, the appearance of the fundamental mode and the first non-fundamental mode in a discharge tube with absorbing wall is illustrated by figure 2.16. The fundamental mode in the case $s = 0$ is 1D and is shown in figures 2.16 by the blue line. With the increase of s, a striking change occurs: the sections of the 1D (fundamental) mode at currents below $I(b_1)$ and above $I(a_1)$ join the branch of the first 2D mode associated with a spot at the centre of the

cathode. This new mode, which is shown by the solid line in figure 2.16a, plays now the role of fundamental mode. Schematics in figure 2.16a illustrate distributions of current over the cathode surface at states belonging to this mode. This new fundamental mode includes the Townsend discharge at low currents, the abnormal mode at high currents, and the subnormal and normal modes at intermediate currents.

Surprising changes occur also to the non-fundamental 2D modes. The branch of the first 2D mode for $s = 0$ without a spot in the centre of the cathode joins the branch of the second 2D mode for $s = 0$ without a spot in the centre of the cathode, the section of the 1D mode comprised between the bifurcation points b_1 and b_2, and the section of the 1D mode comprised between the bifurcation points a_1 and a_2; see the solid line in figure 2.16b. This is how the first non-fundamental 2D mode for $s > 0$ is formed. The branch of the second 2D mode for $s = 0$ with a spot in the centre of the cathode joins the branch of the third 2D mode for $s = 0$ with a spot in the centre of the cathode and the sections of the 1D mode comprised between the bifurcation points b_2 and b_3 and between the bifurcation points a_2 and a_3. This is how the second non-fundamental 2D mode for $s > 0$ is formed. The branch of the second 2D mode for $s = 0$ without a spot in the centre of the cathode joins the branch of the third 2D mode for $s = 0$ without a spot in the centre of the cathode and the sections of the 1D mode comprised between the bifurcation points b_3 and b_4 and between the bifurcation points a_3 and a_4; the third non-fundamental 2D mode for $s > 0$, and so on. The branch of the last 2D mode for $s = 0$ without a spot in the centre of the cathode joins the section of the 1D mode comprised between the bifurcation points of this last mode for $s = 0$; the last non-fundamental 2D mode for $s > 0$. A further increase of s causes a reduction of number of non-fundamental modes (from 8 at $s = 0.05$ to 2 at $s = 1$).

In summary, the change from reflecting to absorbing walls destroys bifurcations through which 2D modes branch off from the 1D mode, and this destruction is accompanied by the exchange of branches. In particular, this explains the difference between the fundamental mode in a tube with reflecting wall, which is described by a 1D solution similar to that of von Engel and Steenbeck, and the fundamental mode in a tube with absorbing wall, which is essentially 2D and includes the subnormal and normal regimes. We do not discuss here why are the bifurcations destroyed and branches exchanged; there are solid mathematical reasons for this which were revealed in [74].

2.5 Concluding remarks

Multiple steady-state solutions in the theory of DC glow discharge have been found for the first time. The modelling is performed in 2D and 3D in the framework of the basic model of glow discharge, comprising equations of conservation of a single ion species and the electrons, transport equations for the ions and the electrons written in the local approximation, and the Poisson equation. Modelling results are given for the plasma-producing gas being xenon at the pressure of 30 torr and the discharge tube being a cylinder of radius from 0.5 mm to 1.5 mm and of height 0.5 mm.

When neutralization of the ions and the electrons at the wall is neglected, one of the modes - namely, the fundamental mode, i.e., the one which exists at all values of the discharge current - is 1D and represents in essence the well-known solution of von Engel and Steenbeck. The other

modes are 2D (axially symmetric) or 3D and exist in limited ranges of the discharge currents. Each 2D mode is constituted by two branches, one associated with a pattern comprising a spot at the center of the cathode and the other with a pattern without a central spot. Each 3D mode represents in reality a continuum of 3D modes identical to the accuracy of a rotation. The first 3D mode and the branch with a spot at the center of the first 2D spot mode exhibit a well pronounced effect of normal current density. The latter may be interpreted as a manifestation of coexistence of a hot phase, representing the 1D abnormal mode, with a cold phase, which represents a situation where no discharge is present at the point of the cathode surface being considered. The second and higher 3D modes describe patterns similar to those observed in experiments [5–11]. Distributions of current density over the cathode surface associated with 3D modes develop extrema in the centre of the cathode which cannot be predicted by bifurcation theory and conform to observations.

With a decrease of the radius of the discharge tube, the number of existing 2D and 3D modes decreases.

When neutralization of the ions and the electrons at the wall is taken into account, the number of multiple solutions is significantly reduced: for example, the number of 2D modes existing in the case $R = 1.5\,\mathrm{mm}$ is reduced from eight to three. One of these 2D solutions describes the fundamental mode, comprising the Townsend, subnormal, normal and abnormal discharges. The first and second non-fundamental 2D modes are associated with patterns with an interior ring spot and, respectively, with a spot at the centre and an interior ring spot. Only one 2D mode (the fundamental mode) was found for $R = 0.5\,\mathrm{mm}$.

The above-described pattern of self-organization in DC glow discharges without neutralization is typical for bistable nonlinear dissipative systems; in fact, it has been predicted on these grounds [51]. In particular, there is a similarity with a classic problem of coexistence of fluid and vapor described by the van der Waals equation and Maxwell's rule: the von Engel and Steenbeck solution, which is 1D and exists at all currents, may be viewed as an analogue of the solution of the van der Waals equation, while the bifurcating 2D or 3D solution which describes the normal discharge and exists in a limited current range may be viewed as an analogue of a solution which describes states with coexisting fluid and vapor and is governed by Maxwell's rule.

An account of neutralization of the ions and the electrons at the wall causes a dramatic change of the pattern of self-organization: the bifurcations through which 2D modes branch off from the 1D mode are destroyed and this destruction is accompanied by the exchange of branches. In particular, the sections of the 1D (fundamental) mode at currents below $I(b_1)$ and above $I(a_1)$ join the branch of the first 2D mode associated with a spot at the centre of the cathode *etc.* The new fundamental mode, which has appeared, includes the Townsend discharge at low currents, the abnormal mode at high currents, and the subnormal and normal modes at intermediate currents.

The following question was formulated in section 1.2.1 of Introduction in connection with discussion of relation between the 1D von Engel and Steenbeck solution and 2D results [43–49]: where from have the subnormal and normal modes appeared and where to has the mode associated with the falling section of the von Engel and Steenbeck CVC gone? Now the answer to this question is clear: the subnormal and normal modes have not appeared, they exist also in the model without neutralization but belong to the other (non-fundamental) mode; the falling

section of the von Engel and Steenbeck CVC continues to exist in the model with neutralization but belongs to the other (non-fundamental) modes.

Obviously, this modelling represents just the first step; further work is required in order to make a meaningful quantitative comparison with the experiment [5–11] possible. It seems, however, that the computed 3D patterns with multiple spots are similar to those observed in [5–11]. Thus, the present modelling supports the hypothesis [52] that patterns with multiple spots may be described in the framework of basic mechanisms of glow discharge, so there is no need to introduce special mechanisms to this end.

Observations of axially symmetric self-organization patterns on cathodes of DC glow discharges have not been reported up to now. (Although axially symmetric patterns have been observed in gas discharges in other situations, e.g., on anode of glow discharge [81, 82] and in dielectric barrier discharge [21].) The results obtained in this work suggest that solutions describing axially symmetric self-organized patterns in DC glow discharges do exist. Some sections of these solutions are stable [83] and it would be interesting to look for these patterns in the experiment.

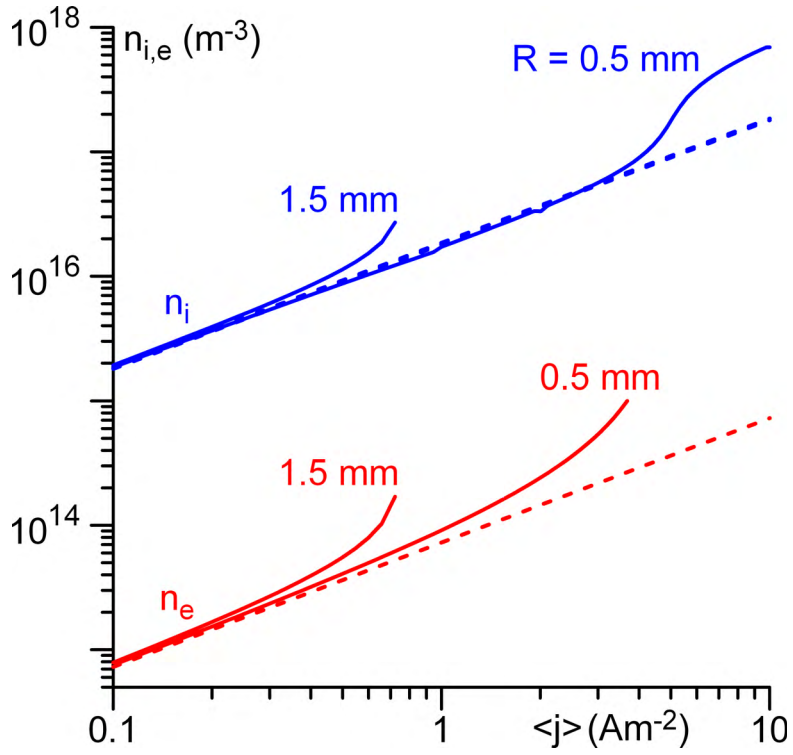

Figure 2.13: Maxima of densities of charged particles on the axis of the discharge. Neutralization taken into account. Solid: numerical results. Dashed: analytical results for the limiting case of Townsend discharge.

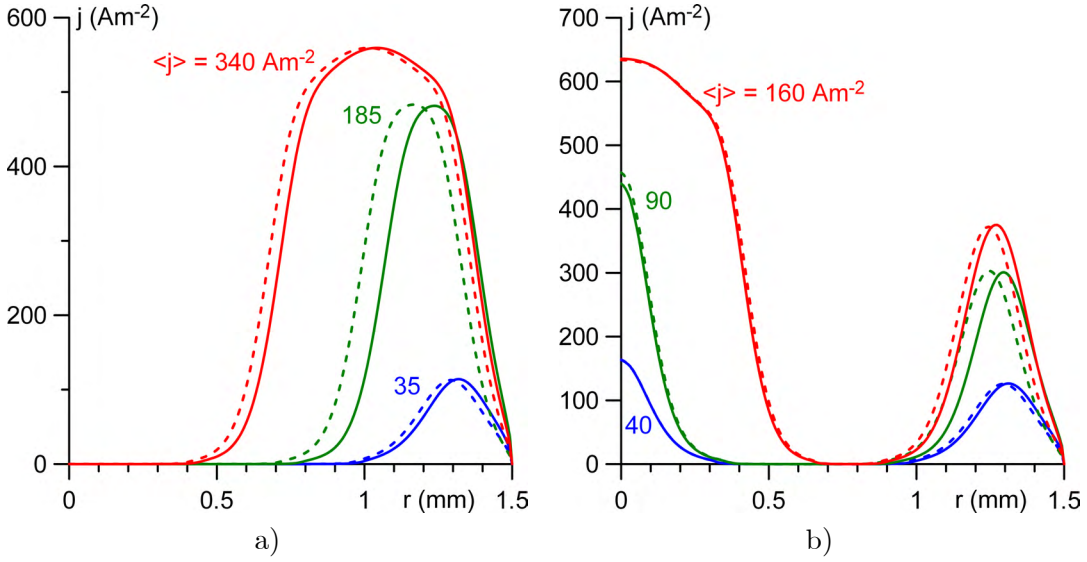

Figure 2.14: Distributions of current density over the cathode for the first (a) and second (b) non-fundamental 2D modes. $R = 1.5\,\mathrm{mm}$, neutralization taken into account. Solid/dashed: distributions corresponding to the branch with a lower/higher voltage.

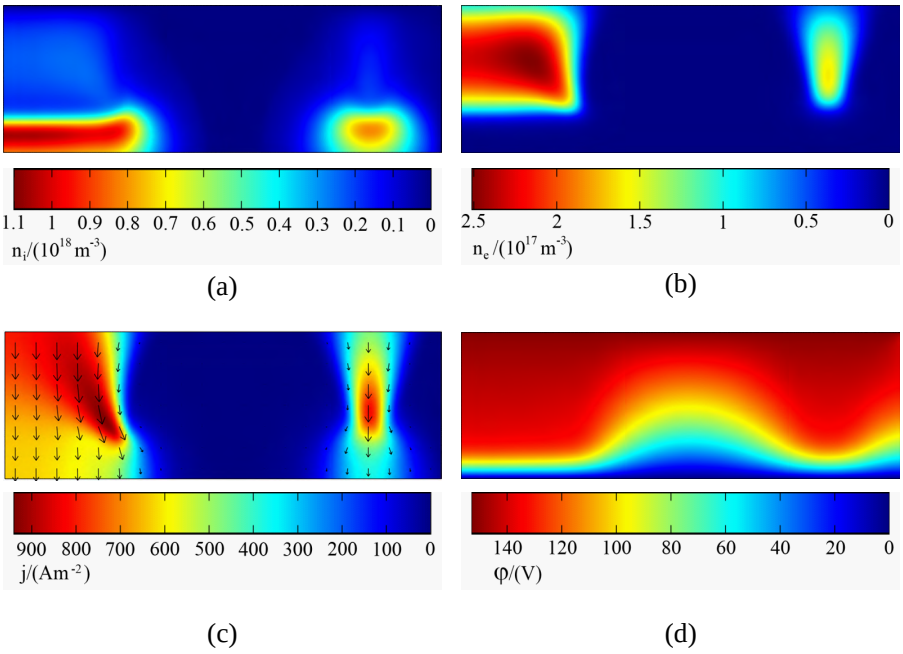

Figure 2.15: Distributions of parameters in the interelectrode gap. The second non-fundamental 2D mode, $\langle j \rangle = 170\,\mathrm{A\,m^{-2}}$, $R = 1.5\,\mathrm{mm}$, neutralization taken into account. (a) n_i, (b) n_e, (c) modulus of current density, (d) φ. Bottom: cathode, top: anode; left: axis of symmetry; right: wall of the discharge vessel.

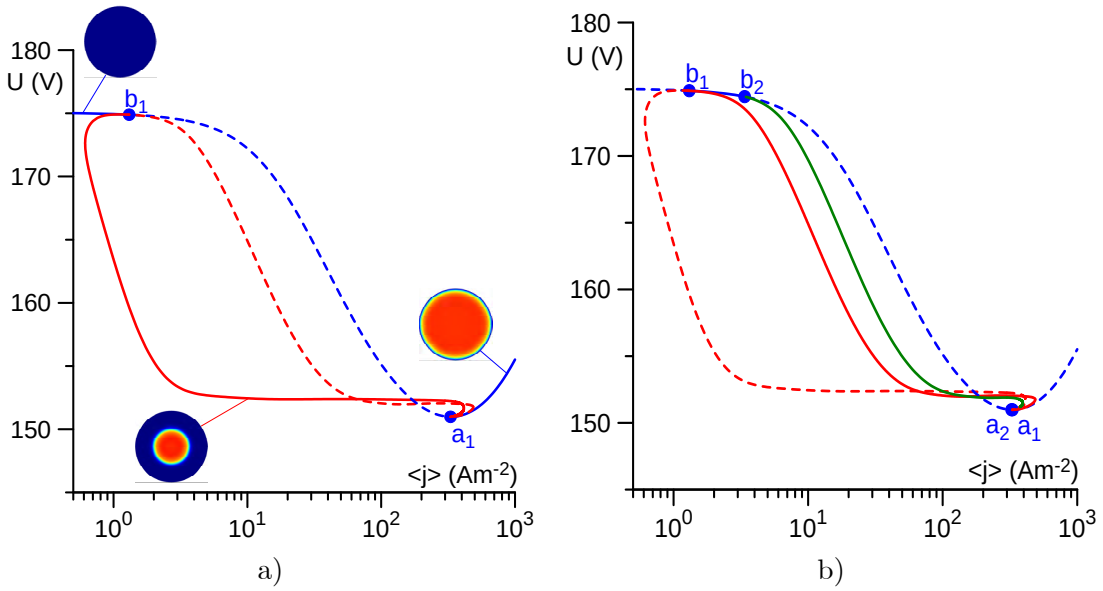

Figure 2.16: CVCs of different modes. $R = 1.5\,\mathrm{mm}$, $s = 0$. Blue: fundamental (1D) mode. Red: first non-fundamental mode. Green: second non-fundamental mode.

Chapter 3

Effect of kinetics over multiple modes of current transfer in DC glow discharges

3.1 Introduction

It was shown in chapter 2 that the basic model of glow discharges admits multiple solutions describing both the normal mode and modes with multiple spots similar to those observed in DC glow microdischarges [5–11]. The model comprised conservation equations for a single ionic species (molecular ions) and electrons and transport equations written in the local-field approximation, and the Poisson equation. A question arises whether these solutions exist in the framework of more realistic models of glow discharges, which take into account multiple ionic species, atomic excited states, excimers, and non-locality of electron transport and kinetic coefficients. Another question concerns reasons explaining why self-organized modes with multiple spots have been observed in xenon but not in argon [6, 12]. These questions are dealt with in this chapter.

The outline of this chapter is as follows. A model of glow discharge in xenon and argon, accounting for singly charged atomic ions, molecular ions, electrons, an effective species of excited atoms combining the most important resonance and metastable levels, excimers, and non-locality of the kinetic and transport coefficients of electrons (by means of differential equation of conservation of electron energy), is formulated on the basis of data available in the literature in section 3.2. The use of Comsol Multiphysics for modelling DC glow discharges in a wide current range is discussed in section 3.3 and some of its advantages and weaknesses are demonstrated. Results of calculation of multiple modes in xenon microdischarges are given in section 3.4. In section 3.5, results are given indicating that conditions of argon microdischarges are less favourable for the appearance of self-organization than the conditions of xenon microdischarges, which is due to lower cross sections of elastic collisions between electrons and atoms. Results from bifurcation theory for argon and helium indicate that it should be possible to observe formation of self-organized patterns also in these plasma-producing gases provided that the pressure is sufficiently high and the discharge radius is large enough. Finally, conclusions are summarized in section 3.6.

Results reported in this chapter have been partially presented at the 63rd Gaseous Electronics Conference (2010).

3.2 The model

Many works exist where detailed models of discharges are formulated, which include complex kinetic schemes and treatment of non-locality of electron transport and kinetics, e.g. [84–89]. The model employed in this work is more or less conventional, it is formulated using data available in the literature, and takes into account the following species: singly charged atomic ions, molecular ions, electrons, an effective species of excited atoms combining the most important resonance and metastable levels, and excimers. Non-local effects are taken into account by means of differential equation of conservation of electron energy.

3.2.1 Equations and boundary conditions

The model comprises conservation equations for all species, transport equations for all species written in the drift-diffusion approximation for the charged species and the diffusion approximation for excited atoms and excimers, the Poisson equation, and the equation of conservation of electron energy which is written in the form recommended in [76]:

$$\begin{aligned}
\nabla\cdot\mathbf{J}_{i1} &= S_{i1}, \quad \mathbf{J}_{i1} = -D_{i1}\,\nabla n_{i1} - n_{i1}\,\mu_{i1}\,\nabla\varphi,\\
\nabla\cdot\mathbf{J}_{i2} &= S_{i2}, \quad \mathbf{J}_{i2} = -D_{i2}\,\nabla n_{i2} - n_{i2}\,\mu_{i2}\,\nabla\varphi,\\
\nabla\cdot\mathbf{J}_{e} &= S_{e}, \quad \mathbf{J}_{e} = -D_{e}\,\nabla n_{e} + n_{e}\,\mu_{e}\,\nabla\varphi,\\
\nabla\cdot\mathbf{J}_{M1} &= S_{M1}, \quad \mathbf{J}_{M1} = -D_{M1}\,\nabla n_{M1},\\
\nabla\cdot\mathbf{J}_{M2} &= S_{M2}, \quad \mathbf{J}_{M2} = -D_{M2}\,\nabla n_{M2},\\
\varepsilon_0\nabla^2\varphi &= -e\left[n_{i1} + n_{i2} - n_e\right],\\
\nabla\cdot\mathbf{J}_{\varepsilon} &= F_{\varepsilon} - S_{\varepsilon}, \quad \mathbf{J}_{\varepsilon} = -D_{\varepsilon}\,\nabla n_{\varepsilon} + n_{\varepsilon}\,\mu_{\varepsilon}\,\nabla\varphi.
\end{aligned} \tag{3.1}$$

Here the indexes $i1$, $i2$, e, $M1$, $M2$ and ε represent atomic ions, molecular ions, electrons, atoms in excited states, excimers and average electron energy, respectively; n_α is number density of species α; the electron energy density is defined as $n_\varepsilon = n_e\overline{\varepsilon}$, where $\overline{\varepsilon}$ is the average electron energy, and coincides to the accuracy of a factor of 2/3 with electron pressure; φ is electric potential; S_α is the rate of production of particles of species α per unit time and unit volume; S_ε is the rate of loss of electron energy per unit time and unit volume due to collisions; $F_\varepsilon = -e\mathbf{J}_e\cdot\mathbf{E}$ is the rate of gain of electron energy per unit time and unit volume due to Joule heating; D_α is diffusion coefficient of species α in the gas of neutral atoms; D_ε is the so-called electron energy diffusion coefficient; μ_α is mobility of species α in the neutral gas of atoms; μ_ε is the so-called electron energy mobility; ε_0 is permittivity of free space and e is elementary charge.

Boundary conditions are written in a form similar to Eqs. (2.4)-(2.6). Diffusion fluxes of the attracted particles at the cathode and anode are neglected compared to drift. The normal flux of the electrons emitted by the cathode is related to the flux of incident ions in terms of the effective secondary emission coefficient γ, which is assumed to characterize all mechanisms

of electron emission (due to ion, photon, and excited atom bombardment) [2]. (In principle, several coefficients could be introduced characterizing secondary emission due to bombardment by different ionic and excited species; however, that is not done in this work.) Densities of ions vanish at the anode. Densities of excited atoms and excimers vanish at both electrodes. Electrostatic potentials of both electrodes are given. One boundary condition at the wall of the discharge vessel is the conventional condition of zero electric current density. Neutralization of charged particles at the wall is neglected. Deexcitation at the wall is also neglected. It is assumed that each electron emitted by the cathode possesses energy of $E_I - 2W$, where E_I is the ionization energy of atoms and W is the work function of the cathode surface; the boundary condition at the cathode for electron energy is the normal flux of emitted electrons multiplied by this energy. It is assumed that at the anode the normal flux of electron energy due to diffusion is negligible compared to the normal flux of electron energy due to drift, similarly to what is done with the boundary condition for electron density. The normal flux of electron energy at the wall is zero.

Let us consider a discharge vessel in the form of a right circular cylinder of a radius R and of a height h, and introduce cylindrical coordinates (r, ϕ, z) with the origin at the centre of the cathode and the z-axis coinciding with the axis of the vessel. Then the boundary conditions read

$$z = 0: \quad \frac{\partial n_{i1}}{\partial z} = \frac{\partial n_{i2}}{\partial z} = 0, \quad J_{ez} = -\gamma \left(J_{i1z} + J_{i2z} \right),$$
$$n_{M1} = n_{M2} = 0, \quad \varphi = 0, \quad J_{\varepsilon z} = (E_I - 2W) J_{ez};$$

$$z = h: \quad n_{i1} = n_{i2} = n_{M1} = n_{M2} = 0,$$
$$\frac{\partial n_e}{\partial z} = 0, \quad \frac{\partial n_\varepsilon}{\partial z} = 0, \quad \varphi = U;$$

$$r = R: \quad \frac{\partial n_{i1}}{\partial r} = \frac{\partial n_{i2}}{\partial r} = \frac{\partial n_e}{\partial r} = \frac{\partial n_{M1}}{\partial r} = \frac{\partial n_{M2}}{\partial r} = 0, \quad \frac{\partial n_\varepsilon}{\partial r} = 0, \tag{3.2}$$
$$J_{i1r} + J_{i2r} - J_{er} = 0.$$

Here U is the discharge voltage and the subscripts r and z denote radial and axial projections of corresponding vectors.

Calculations were performed using a steady-state solver of Comsol Multiphysics, similarly to chapter 2. The problem admits one 1D solution and several 2D solutions. The control parameter in calculations was discharge current I or discharge voltage U, depending on the slope of the CVC at the state being computed. The treatment is limited to the axially symmetric case.

3.2.2 Kinetic scheme

Calculations were performed for xenon and argon. The employed kinetic scheme was the same for both plasma-producing gases. Let us begin by describing the treatment of atomic excited states. The conventional approach to a description of excited states is to group states possessing values of binding energy not too far apart into a small number of representative states, rather than treating all excited states separately. Binding energies of representative states are calculated by averaging the energy of the grouped levels weighted by corresponding degeneracies. (Many examples of

$Xe + e^- \rightarrow Xe^+ + e^- + e^-$	BOLSIG+ [76], [90]
$Xe^* + e^- \rightarrow Xe^+ + e^- + e^-$	Eq. (3.3) [91]
$Xe_2^* + e^- \rightarrow Xe_2^+ + e^- + e^-$	$9.75 \times 10^{-8} T_e^{0.71} e^{-3.40/T_e}\ \mathrm{cm^3\,s^{-1}}$, T_e in eV [85]
$Xe + e^- \leftrightarrows Xe^* + e^-$	BOLSIG+ [76], [90]
$Xe^+ + Xe + Xe \rightarrow Xe_2^+ + Xe$	$2.5 \times 10^{-31}\ \mathrm{cm^6\,s^{-1}}$ [85]
$Xe^* + Xe^* \rightarrow Xe^+ + Xe + e^-$	$5 \times 10^{-10}\ \mathrm{cm^3\,s^{-1}}$ [85]
$Xe_2^+ + e^- \rightarrow Xe^* + Xe$	$3.7 \times 10^{-8} T_e^{-0.5}\ \mathrm{cm^3\,s^{-1}}$, T_e in eV [85]
$Xe^* \rightarrow Xe + \phi$	$9 \times 10^7\ \mathrm{s^{-1}}$ [84]
$Xe_2^* \rightarrow 2Xe + \phi$	$7.22 \times 10^7\ \mathrm{s^{-1}}$ [85]
$Xe^* + Xe + Xe \rightarrow Xe_2^* + Xe$	$5 \times 10^{-32}\ \mathrm{cm^6\,s^{-1}}$ [85]

Table 3.1: Kinetic scheme for xenon and data used to describe each process.

$Ar + e^- \rightarrow Ar^+ + e^- + e^-$	BOLSIG+ [76], [92]
$Ar^* + e^- \rightarrow Ar^+ + e^- + e^-$	Eq. (3.3) [91]
$Ar_2^* + e^- \rightarrow Ar_2^+ + e^- + e^-$	$9 \times 10^{-8} T_e^{0.7} e^{-3.66/T_e}\ \mathrm{cm^3\,s^{-1}}$, T_e in eV [85]
$Ar + e^- \leftrightarrows Ar^* + e^-$	BOLSIG+ [76], [92]
$Ar^+ + Ar + Ar \rightarrow Ar_2^+ + Ar$	$2.5 \times 10^{-31}\ \mathrm{cm^6\,s^{-1}}$ [85]
$Ar^* + Ar^* \rightarrow Ar^+ + Ar + e^-$	$10^{-9}\ \mathrm{cm^3\,s^{-1}}$ [85]
$Ar_2^+ + e^- \rightarrow Ar^* + Ar$	$5.38 \times 10^{-8} T_e^{-0.66}\ \mathrm{cm^3\,s^{-1}}$ [85]
$Ar^* \rightarrow Ar + \phi$	$7.00 \times 10^8\ \mathrm{s^{-1}}$ [93]
$Ar_2^* \rightarrow 2Ar + \phi$	$3.5 \times 10^5\ \mathrm{s^{-1}}$ [93]
$Ar^* + Ar + Ar \rightarrow Ar_2^* + Ar$	$1.0 \times 10^{-32}\ \mathrm{cm^6\,s^{-1}}$ [93]

Table 3.2: Kinetic scheme for argon and data used to describe each process.

this treatment exist in the literature, e.g. [84–89].) Strictly speaking, this approach is justified if transitions between nearby states through excitation and deexcitation by electron impact are the dominant processes or, in other words, if a characteristic time of transition to a nearby level by electron impact is much smaller than characteristic times of other processes involving atoms in the grouped excited state.

In this work only one representative excited state is considered in the model for each gas. For xenon, the representative excited state is denoted Xe^* and includes all excited states in the $6s$ manifold. The representative excited state for argon is denoted Ar^* and includes all excited states in the $4s$ manifold.

The system of reactions, data necessary for calculations and corresponding references are summarized in tables 3.1 and 3.2. Electron temperature is defined as $T_e = 2\overline{\varepsilon}/3$. Reaction rates for processes of electron impact ionization and excitation from the ground state were calculated using BOLSIG+ [76] and following recommendations by Hayashi in the electron cross section data compilations [90, 92]. Excited states of higher energy than the $6s$ and $4s$ manifolds for xenon and argon, respectively, were assumed to decay instantly into the representative states Xe^* and Ar^*. In other words, the total rate of excitation into higher excited states, which was computed with BOLSIG+, was included in the source term of species Xe^* and Ar^*.

Much data necessary to describe the processes considered in the model were taken from [85], where an extensive compilation is made with the purpose of modelling the breakdown in a metal halide HID lamp. Rate coefficients of ionization from states Xe^* and Ar^* were found using the formula given in [91]:

$$I_{M1} = \frac{9.56 \times 10^{-6} \, (T_e)^{-1.5} \exp\left(-\epsilon_{M1I}\right)}{\epsilon_{M1I}^{2.33} + 4.38\epsilon_{M1I}^{1.72} + 1.32\epsilon_{M1I}} \, \mathrm{cm}^3 \, \mathrm{s}^{-1}, \tag{3.3}$$

where

$$\epsilon_{M1I} = \frac{E_{M1I}}{T_e},$$

T_e is the electron temperature in eV and $E_{M1I} = E_I - E_{M1}$, in eV, is the energy difference between ionized states Xe^+ or Ar^+ and representative excited states Xe^* or Ar^*, respectively.

Results reported in this chapter refer to discharges in xenon and argon with radius and inter-electrode gap of 0.5 mm and under the pressure of 30 torr, unless otherwise stated. The mobilities and diffusion coefficients of atomic ions Xe^+ and Ar^+ were evaluated as functions of the reduced electric field E/p by means of the two-temperature displaced-distribution theory [94]. Mobilities and diffusion coefficients of molecular ions Xe_2^+ and Ar_2^+ were evaluated by means of the formula $\mu_{i2} = b/n_n$, where b takes the values 2.1×10^{21} $\mathrm{m}^{-1}\,\mathrm{V}^{-1}\,\mathrm{s}^{-1}$ for Xe_2^+ and 7.1×10^{21} $\mathrm{m}^{-1}\,\mathrm{V}^{-1}\,\mathrm{s}^{-1}$ Ar_2^+ (here n_n is the density of the neutral gas), which is an approximation of the measurements [75]. Diffusion coefficients of molecular ions were found by means of Einstein relation, $D_{i2} = k\,T\,\mu_{i2}\,/e$. Mobility and diffusion coefficient of electrons as well as electron energy mobility and electron energy diffusion coefficient were found using BOLSIG+ [76] and cross sections recommended in [90, 92]. Diffusion coefficients of excited states and excimers were set equal to $10^{-2}\,\mathrm{m}^2\,\mathrm{s}^{-1}$ following [84]. This value is an estimate and has little influence on results, which is in accordance with [84]. The effective secondary emission coefficient γ was set equal to 0.03. The work function of the cathode surface was set equal to 4 eV.

It is important to mention the reason why heating of the neutral gas is not taken into account in the modelling: estimates reveal that the characteristic length scale of heat conduction in the neutral gas under the considered conditions is much larger than the dimensions of the discharge vessel.

3.3 Modelling DC glow discharges in a wide range of currents with Comsol Multiphysics. New results, fortes and weaknesses

The description of modelling of multiple modes existing in the framework of the basic model of DC glow discharges given in chapter 2 paints Comsol Multiphysics as a nearly flawless modelling tool. One of very strong points of Comsol Multiphysics is the possibility of practical and reasonably straightforward modelling of complex systems, which gas discharges definitely are. Another forte is the possibility of using powerful steady state solvers, which are indispensable for a systematic study of multiple modes; see discussion in section 2.2. Another forte is the possibility to specify the discharge current as a control parameter, without the need to introduce an external circuit, and to switch seamlessly between discharge current and voltage, a feature which is indispensable for calculation of the most of multiple modes since they possess turning points and their CVCs possess extrema.

The fact that Comsol Multiphysics has allowed finding a new and important class of solutions in the classical model by itself attests to its power. Furthermore, when Comsol Multiphysics is applied to more complex models, then new and surprising results can be obtained even setting aside the multiple solutions: the glow discharge can manifest complex behaviour in apparently simple situations. This complex behaviour does not seem to have been detected in previous works. On the other hand, weaknesses of Comsol Multiphysics become visible, which in some cases restrict applicability of the software and are hard to overcome since, as opposed to home-made codes and despite the flexibility of the software, there is not much room for adjustment of routines included in Comsol Multiphysics. Some examples of complex behaviour of glow discharge will be shown and weaknesses of Comsol Multiphysics illustrated in the current section prior to the main subject of this chapter, which is the effect of kinetics over multiple modes.

The first example of complex behaviour is the 1D mode found in the framework of the model described in section 3.2 and accounting for multiple ion species, multiple ionization channels, diffusion of excited states, and non-locality of the kinetic and transport coefficients of electrons. The solid line in figure 3.1 depicts the CDVC of the 1D glow discharge in xenon. This mode exists at all discharge currents and in terms of chapter 2 represents the fundamental mode. The CDVC is qualitatively similar to that given by the von Engel and Steenbeck solution and also to that calculated in the framework of the basic model (cf. figure 2.1), except for the S-shaped section in the range $200\,\mathrm{A\,m^{-2}} \lesssim j \lesssim 300\,\mathrm{A\,m^{-2}}$. The existence of this S-shape in the CDVC of the 1D mode is a surprising result. Also shown in figure 3.1 is the CDVC of the 1D mode calculated without account of stepwise ionization (dashed line). It can be seen that the S-shape disappears when stepwise ionization is neglected.

Figure 3.1 is a clear illustration of the above mentioned fortes of Comsol Multiphysics. The whole CDVC was found, including the whole of the S-shape. It is unclear whether if the use of a nonstationary solver would allow to calculate the S-shape; apparently similar S-shapes have not been reported before.

Complex behaviour similar to that depicted in figure 3.1 may be present not only in situations where detailed kinetics is included in the model. In figure 3.2, the CVC is shown of the fundamental (2D) mode of a cathode boundary layer discharge calculated in the framework of the basic model described in chapter 2. The discharge configuration is the same as shown in figure 1.4, the radius of the opening in the anode and the dielectric is 0.5 mm, thickness of the dielectric is 0.5 mm. Neutralization of charged particles at the dielectric surface is taken into account, i.e., the boundary condition ii) in Eq. (2.6) is employed.

Surprisingly, the CVC of the fundamental mode exhibits a loop. (In fact, there is no major difference between this loop and the S-shape seen in figure 3.1: what matters is that in both cases the fundamental mode possesses a retrograde section limited by two turning points.) The fundamental mode is associated with a pattern comprising a ring spot in the range of discharge currents below the loop and a central spot in the range of currents above the loop. Note that neither spot is normal, i.e., the effect of normal current density is absent. The loop is associated with a transition from the pattern with a ring spot to the pattern with a central spot. This transition is smooth and occurs as follows: the inner radius of the ring spot decreases and then turns zero (i.e., the ring spot becomes a circle) and the outer radius is somewhat reduced. Note

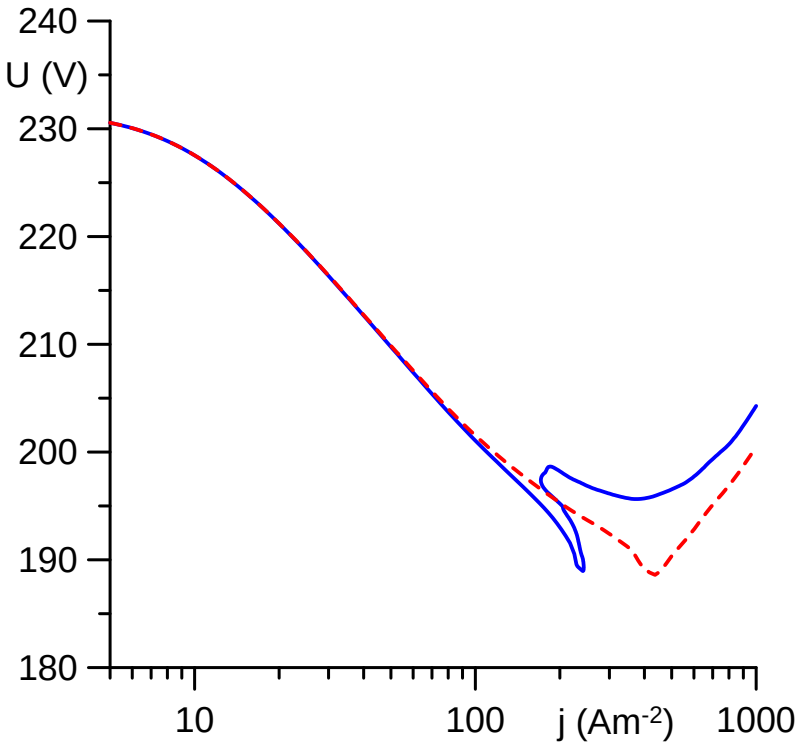

Figure 3.1: CDVC of the 1D mode. Xenon, $p = 30\,\mathrm{torr}$, $h = 0.5\,\mathrm{mm}$. Solid: detailed model. Dashed: stepwise ionization neglected.

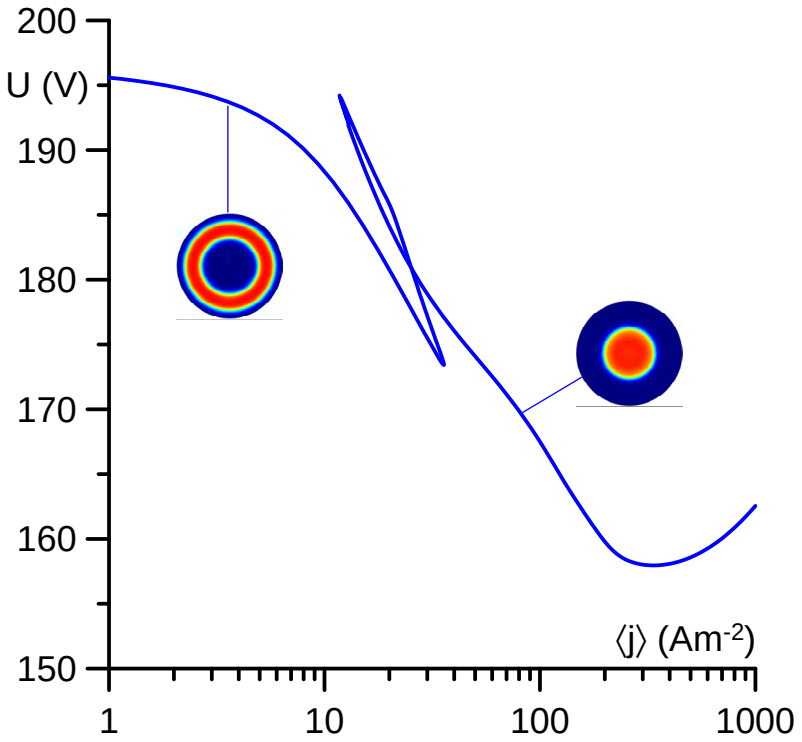

Figure 3.2: CVC of the 2D fundamental mode. Cathode boundary layer discharge configuration. Xenon, $p = 30\,\mathrm{torr}$, $R = h = 0.5\,\mathrm{mm}$.

that although methods of numerical simulations of microdischarges are generally well developed, e.g. [86, 88, 95–97], no retrograde sections have apparently been reported. It is unclear whether the complex behaviour exhibited in figure 3.2 could be noticed if a time-dependent solver is employed. On the other hand, it is easy to calculate it with Comsol Multiphysics due to the possibility of seamless switching between discharge current and discharge voltage as the control parameter.

Both the S-shape seen in figure 3.1 and the loop seen in figure 3.2 are scientifically very interesting. One could think of further numerical work on these effects, and also of experiments.

Let us give a few examples of limitations revealed by Comsol Multiphysics when applied to the model described in section 3.2 and contemplating multiple ion species, multiple ionization channels, diffusion of excited states, and non-locality of the kinetic and transport coefficients of electrons, even in the simplest parallel-plane geometry. In figure 3.3, CDVCs are shown of the 1D mode calculated in different ways in the framework of this model: in the 1D geometry with the use of the same mesh as in figure 3.1 (solid line; these are the same data that are shown by the solid line in figure 3.1); in the 1D geometry with the use of a numerical mesh with half as many elements (every other node was removed; dotted line); in the 2D geometry with the discharge radius of 0.5 mm (dashed line); in the same 2D geometry with the use of a numerical mesh with half as many elements in each direction (every other node in each direction was removed; dashed-dotted line). The parts of the CDVCs manifesting the S-shape are shown in figure 3.4.

The effect of the mesh on 1D calculations is hardly visible and this attests to reliability of the results. The effect of the mesh on 2D calculations cannot be seen in figure 3.3 but can be seen in figure 3.4: the calculation of the whole range of existence of the 1D mode in the 2D geometry with the coarser mesh was not possible. There is a visible difference between the CDVCs calculated in the 1D and 2D geometries. The difference decreases as the discharge current increases, but it does not decrease with a refinement of the numerical mesh.

It should be stressed that the trend exhibited by CDVCs calculated in 1D and 2D is the same, even in the range $200\,\mathrm{A\,m^{-2}} \lesssim j \lesssim 300\,\mathrm{A\,m^{-2}}$ where the S-shape occurs, and the numerical difference is not large. Therefore, this difference can hardly discredit the above results. On the other hand, the fact that the difference between the 1D and 2D calculations of the 1D mode does not decrease with a refinement of the numerical mesh is difficult to understand and therefore worrying.

Figures 3.1, 3.3 and 3.4 refer to the case of reflecting lateral wall. An attempt to introduce an account of neutralization of charged particles at the lateral wall into calculations of the fundamental mode in the framework of the detailed model was undertaken with the use of a boundary condition which is similar to the one employed in chapter 2, Eq. (2.8), and ensure a transition from zero-derivative conditions, Eq. (3.2), at $s = 0$ to conditions characterizing an absorbing wall at $s = 1$. Several variants of the latter conditions have been tested, including those indicated in the user manual of the Plasma Module of Comsol Multiphysics. (The latter is a recently released simulation tool specifically designed for modelling of gas discharges. It allows users to build glow discharge models with complex kinetic schemes and an equation of conservation of electron energy.) However, the transition was not possible since the iterations did not converge for values of s larger than approximately 0.98.

A limitation has been encountered also in calculations of multiple modes in the framework of

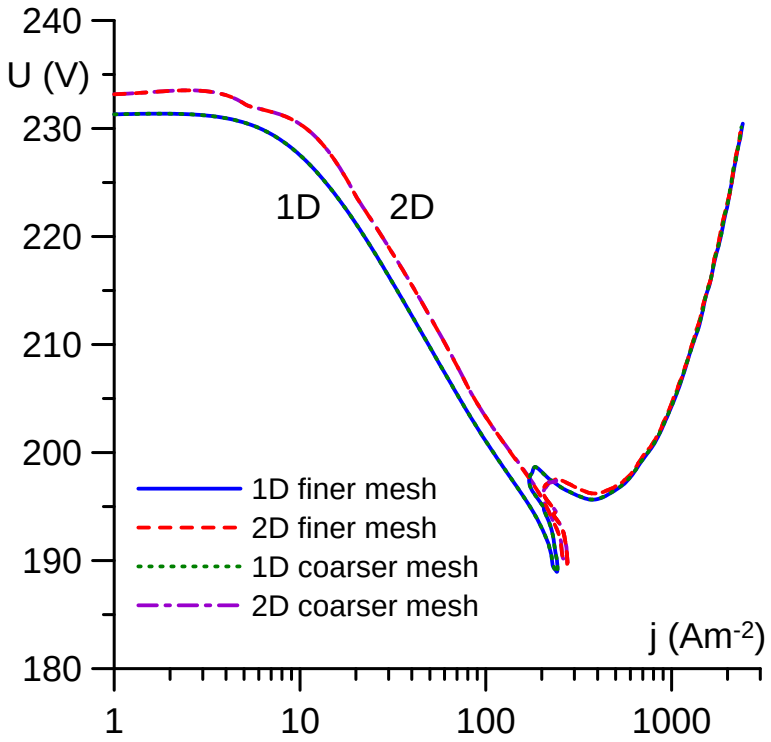

Figure 3.3: CDVCs of the 1D mode calculated on different meshes. Xenon, $p = 30\,\text{torr}$, $h = 0.5\,\text{mm}$.

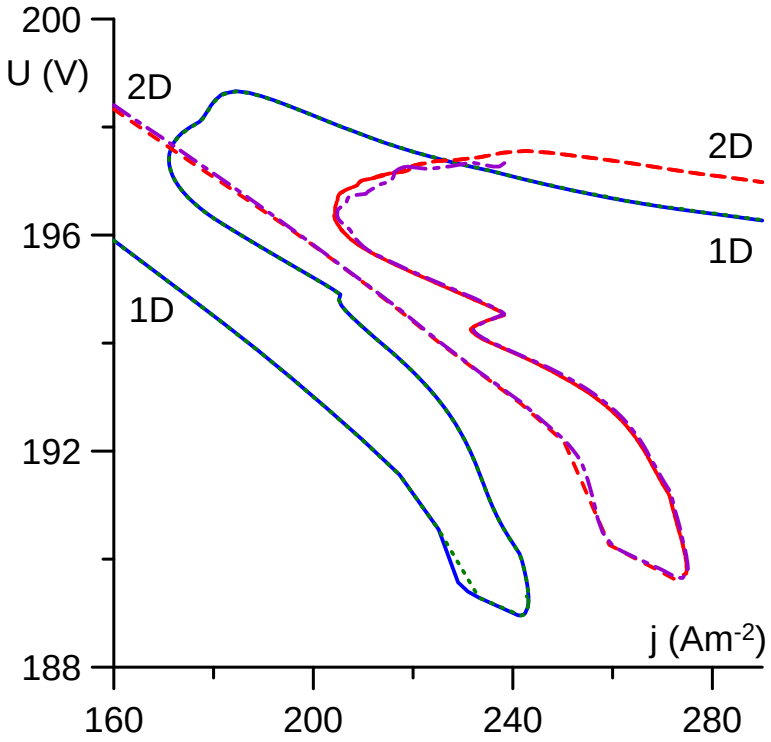

Figure 3.4: CDVCs of the 1D mode calculated on different meshes, details of the S-shape. Same as figure 3.3.

the detailed model described in section 3.2: as will be discussed in the next section, it is possible to find 2D modes in some current ranges but not in the whole region of their existence.

Results not shown here indicate that these difficulties are likely to originate in the equation of conservation of electron energy. Note that the Plasma Module of Comsol Multiphysics employs an equation of conservation of electron energy written in the same form as Eq. (3.1), and test calculations performed with the Plasma Module showed that no problems arise from accounting for absorption at the wall. The reason behind this may be that the Plasma Module contains some built-in optimization to cope with the equation of conservation of electron energy. Unfortunately, the current version (version 4.1) of Plasma Module does not support steady-state solvers; although this is not expressly indicated in the user manual, it has been confirmed by the support team. Therefore, this tool cannot be used for a detailed and systematic study of multiple solutions, nor can it be used to describe complex behaviour with S-shapes or loops. Nevertheless, the fact that the Plasma Module can deal with the equation of conservation of electron energy suggests that the problem has a solution.

It is interesting to note that a similar difficulty has been encountered in calculations for the cathode boundary layer configuration in the framework of the basic model with the use of versions 3.5a and older of Comsol Multiphysics: it was impossible to calculate the fundamental mode in the whole range of its existence. This weakness disappeared with the release of version 4.0.

3.4 Xenon: multiple solutions

Calculations of microdischarges in xenon in the framework of the detailed model described in section 3.2 revealed, in addition to the 1D (fundamental) mode described in the preceding section, three different 2D modes. Although these modes have not been calculated in the whole range of their existence due to numerical difficulties described in the preceding section, enough information has been obtained to characterize these modes in some detail.

We recall the pattern of 1D and 2D modes found in the framework of the basic model without account of neutralization, section 2.3. The 1D mode exists at all discharge currents and 2D modes bifurcate from it. Each 2D mode exists in a limited range of discharge currents and is constituted by two branches separated by two bifurcation points. One of the branches is associated with a spot pattern containing one central spot and possibly ring spot(s), while the other branch is associated with a pattern comprising ring spot(s) and no central spot.

The results obtained in the framework of the detailed model described in section 3.2 fit the same pattern. Calculated sections of the CVCs of the three detected 2D modes are shown in figure 3.5. The solid line depicting the CVC of the fundamental (1D) mode was calculated on a 2D mesh (it represents the same data that the dashed line in figure 3.4). The bifurcation points, which are marked in figure 3.5 by circles, were not evaluated independently (in contrast to what was done in section 2.3, where the bifurcation points have been evaluated by means of bifurcation analysis); they were assumed to coincide with states of 2D modes where variations of discharge parameters in the radial direction are negligible. Schematics in figure 3.5a illustrate distribution of current density over the cathode surface corresponding to each branch of the 2D modes.

One bifurcation point, b_1, was found for the first mode and one bifurcation point, b_2, was

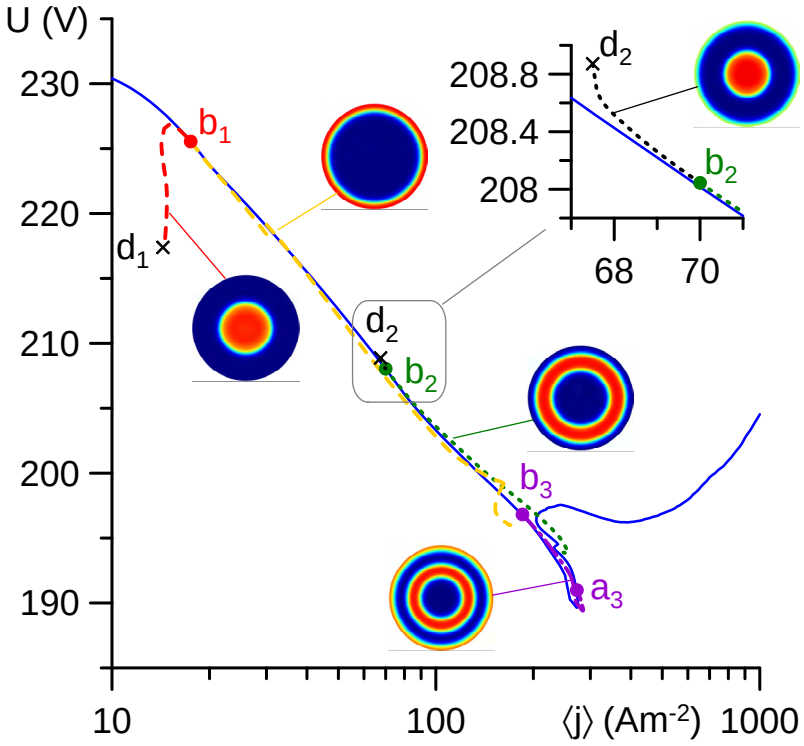

a)

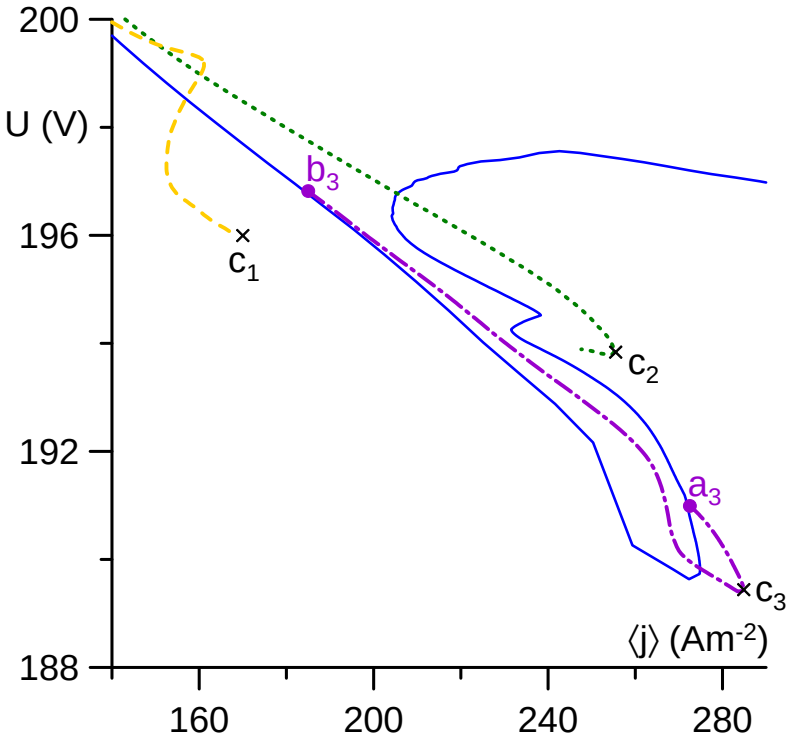

b)

Figure 3.5: CVCs. Xenon, $R = h = 0.5\,\text{mm}$, $p = 30\,\text{torr}$. Solid: the fundamental (1D) mode. Dashed: the first 2D mode. Dotted: the second 2D mode. Dashed-dotted: the third 2D mode. (a) General view. (b) Details in the vicinity of the S-shaped section of the fundamental mode.

found for the second mode. Two bifurcation points, a_3 and b_3, were found for the third mode: a_3 designates the bifurcation point positioned at higher currents and b_3 designates the bifurcation point positioned at lower currents.

Of the first 2D mode, the branch that bifurcates into the current range below $I(b_1)$[1] was computed up to the state designated d_1. This branch is associated with a pattern comprising a spot at the centre of the cathode. The branch that bifurcates into the current range above $I(b_1)$ was computed up to the state designated c_1 and is associated with a pattern comprising a ring spot at the periphery of the cathode.

Of the second 2D mode, a small section of the branch that bifurcates into the current range below $I(b_2)$ was computed (up to the state d_2). This branch is associated with a pattern comprising a spot in the centre and a ring spot at the periphery. The branch that bifurcates into the current range above $I(b_2)$ was computed a little beyond the state c_2 and is associated with a pattern comprising a ring spot inside the cathode. Note that the latter pattern becomes more diffuse from state c_2 onwards; an indication that the bifurcation point a_2 should be nearby and that the branch was computed in almost the whole range of existence.

Only one branch of the third 2D mode was computed. In both bifurcation points a_3 and b_3, this branch bifurcates into the current range above $I(a_3)$ or $I(b_3)$, respectively. This branch is associated with a pattern comprising a ring spot inside the cathode and a ring spot at the periphery.

All the above features, including the type of pattern associated with each branch and the direction of bifurcations of all branches, coincide with those found in the framework of the basic model in section 2.3. There is, however, a very interesting difference. Only two axially symmetric modes exist for the same conditions in the framework of the basic model; it was necessary to increase the discharge radius beyond 0.52 mm in order that the third 2D mode appears; cf. figure 2.4. On the other hand, at least three axially symmetric modes exist in the framework of the detailed model. One can conclude that the presence of different ion and excited species, different ionization channels, and non-locality of electron kinetic and transport coefficients favour appearance of multiple modes.

The branch with the central spot of the first mode computed in the framework of the basic model and shown in figure 2.3a manifests a well-pronounced effect of normal current density. In the framework of the detailed model treated in the current chapter this branch was not computed beyond the initial section of the subnormal discharge, so one cannot say anything about the effect of normal current density.

Examples of distributions of densities of atomic ions, molecular ions, electrons, atoms in excited states, excimers and mean electron energy are shown in figures 3.6 - 3.10. States to which these distributions correspond were chosen in a way to ensure that corresponding spot patterns are as well developed as possible; these states are marked with crosses in figure 3.5. The density of molecular ions is well below the density of atomic ions. The maximum of mean electron energy is localized inside the cathode layer, as it should. Results not shown here reveal the presence of field reversal at the edge of the cathode layer for all modes.

[1] Here, as in chapter 2, $I(b_i)$ represents the value of discharge current corresponding to state b_i.

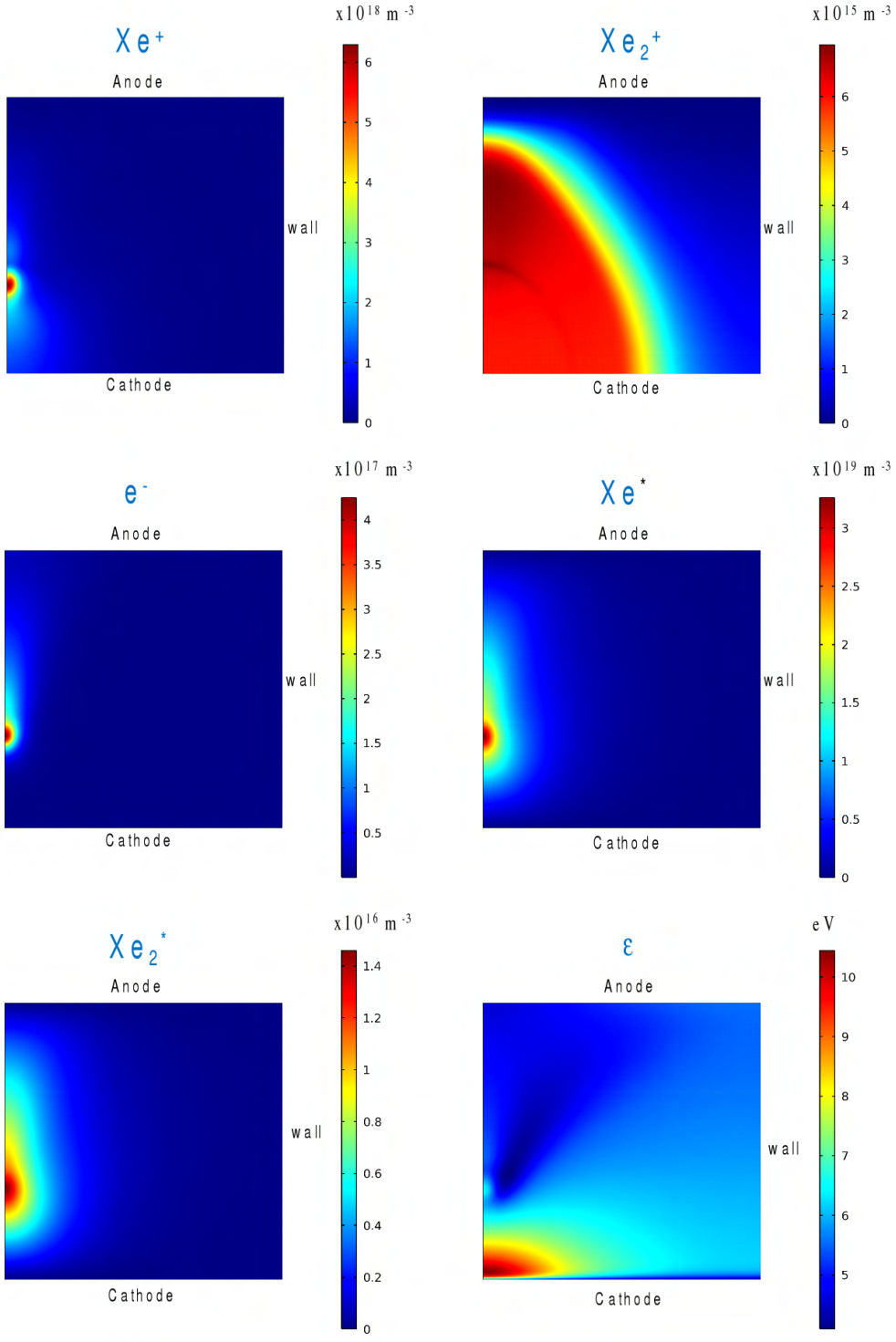

Figure 3.6: Distributions of parameters in the interelectrode gap. Xenon, $p = 30\,\text{torr}$, $R = h = 0.5\,\text{mm}$. State d_1 of the branch of the first 2D mode comprising a spot at the centre of the cathode.

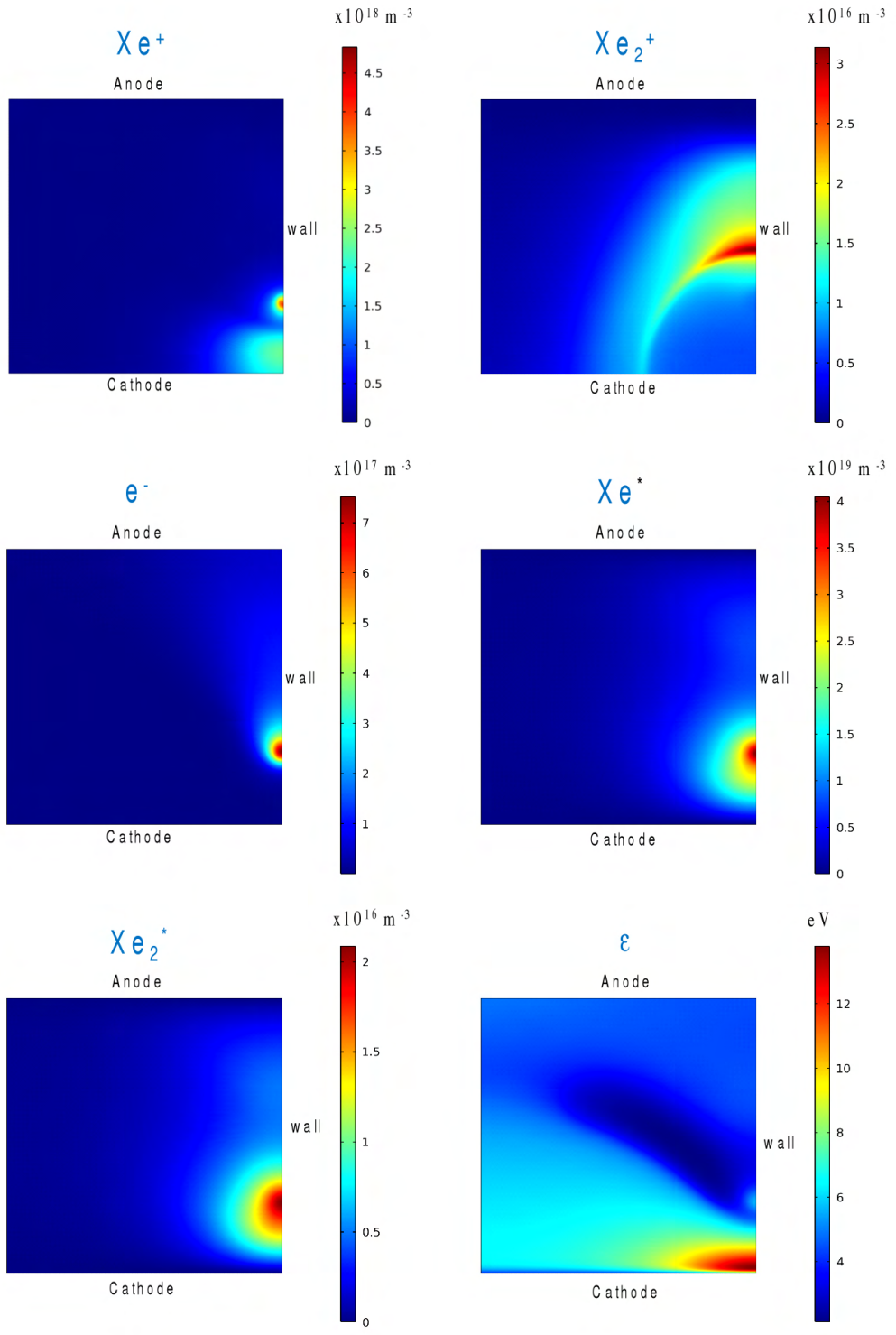

Figure 3.7: Distributions of parameters in the interelectrode gap. Xenon, $p = 30\,\text{torr}$, $R = h = 0.5\,\text{mm}$. State c_1 of the branch of the first 2D mode comprising a ring spot at the periphery of the cathode.

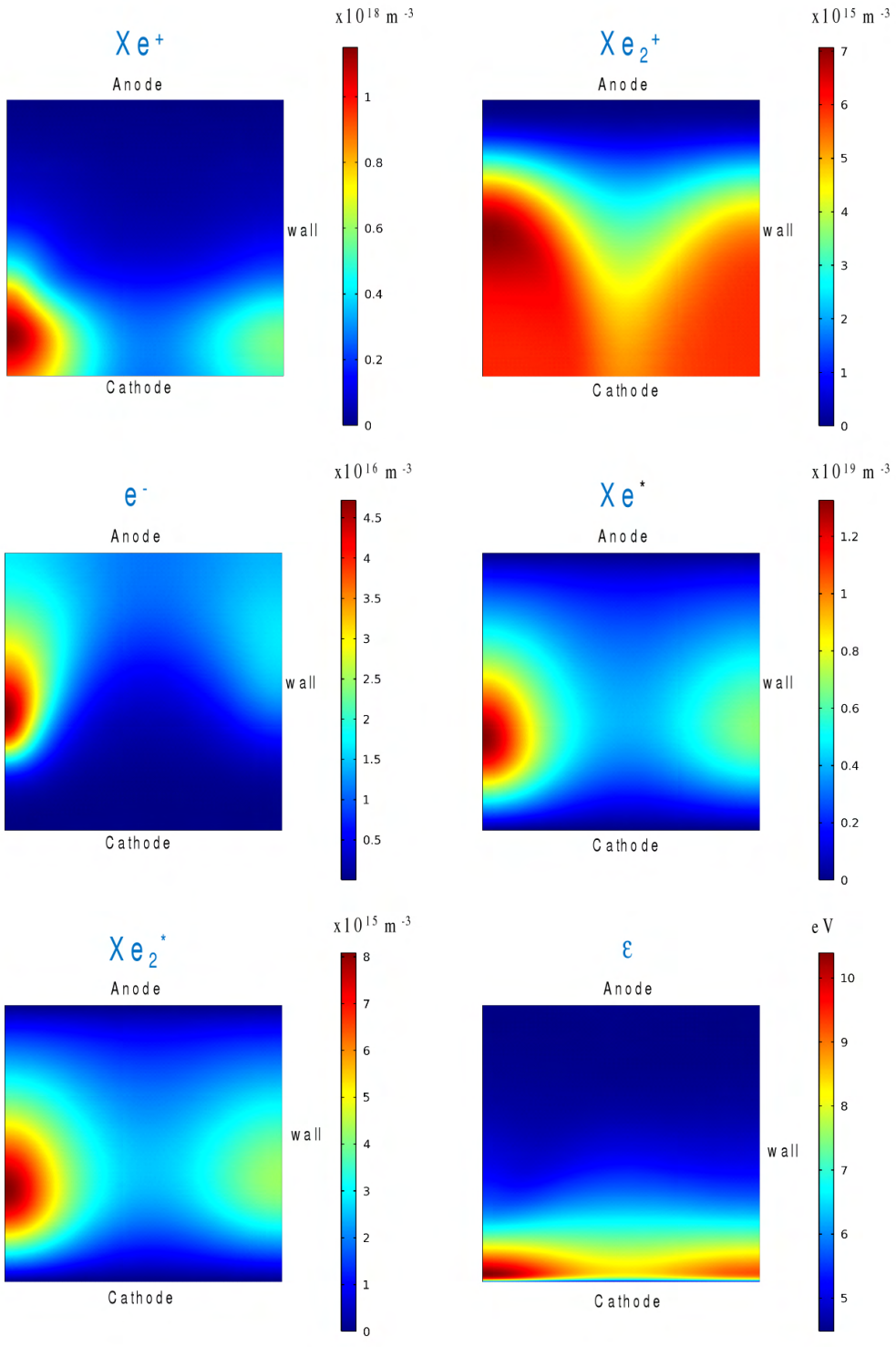

Figure 3.8: Distributions of parameters in the interelectrode gap. Xenon, $p = 30\,\text{torr}$, $R = h = 0.5\,\text{mm}$. State d_2 of the branch of the second 2D mode comprising a spot at the centre and a ring spot at the periphery of the cathode.

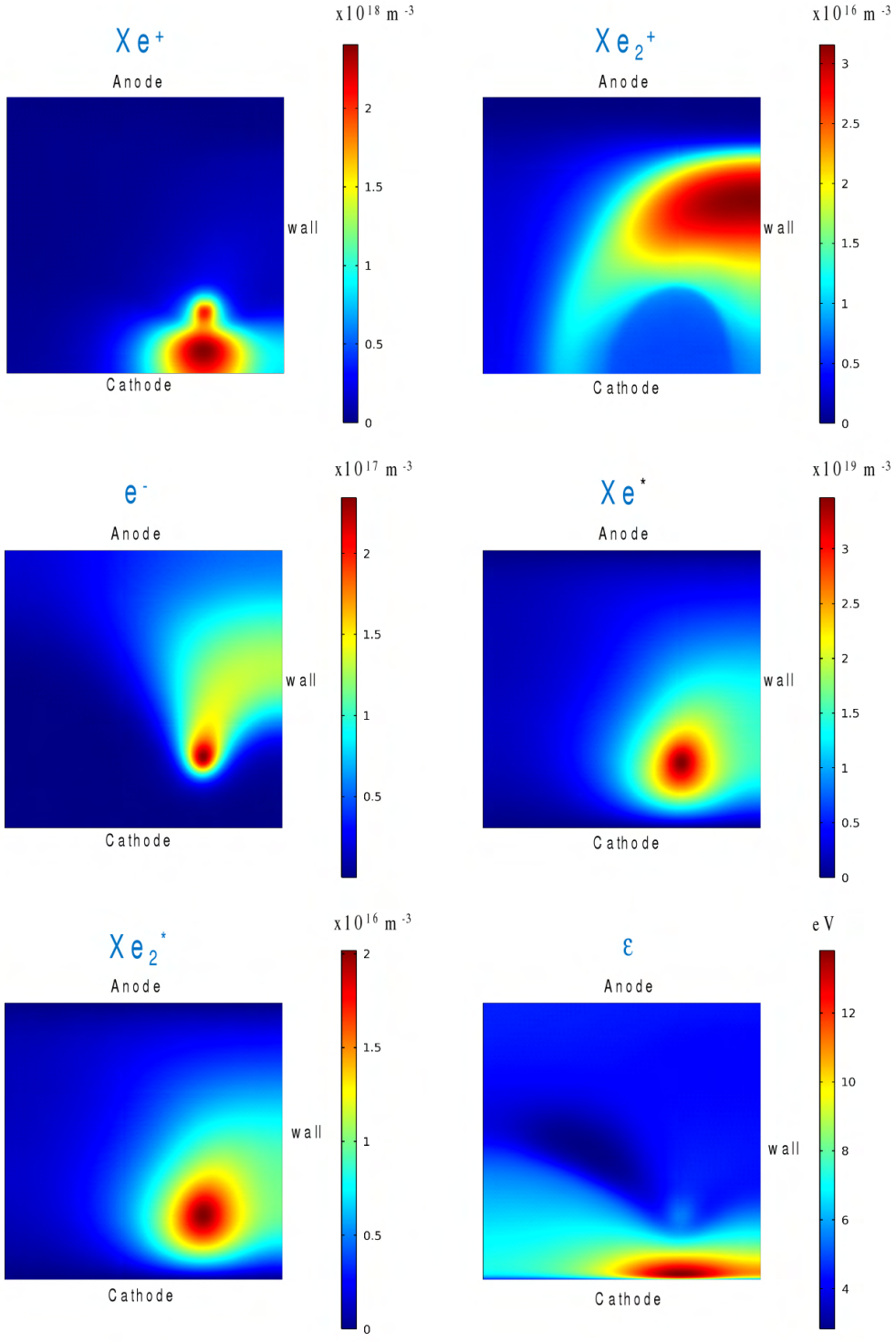

Figure 3.9: Distributions of parameters in the interelectrode gap. Xenon, $p = 30\,\text{torr}$, $R = h = 0.5\,\text{mm}$. State c_2 of the branch of the sencond 2D mode comprising a ring spot inside the cathode.

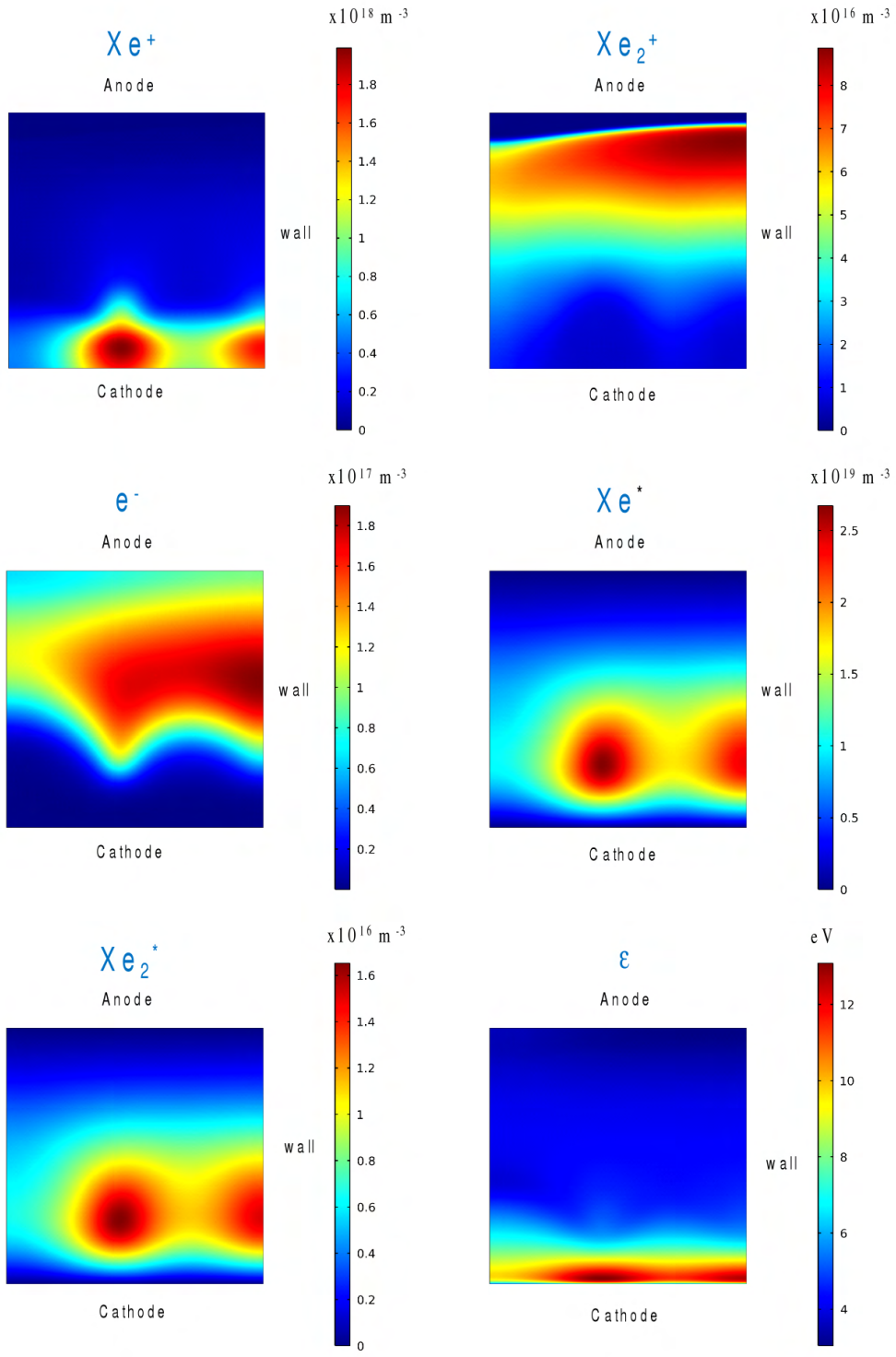

Figure 3.10: Distributions of parameters in the interelectrode gap. Xenon, $p = 30\,\text{torr}$, $R = h = 0.5\,\text{mm}$. State c_3 of the branch of the third 2D mode comprising a ring spot inside the cathode and a ring spot at the periphery.

Patterns seen in distributions of densities of atomic ions, electrons, excited atoms and excimers in the states belonging to the first 2D mode (figures 3.6 and 3.7) are similar, although the patterns seen in the distribution of excimers are somewhat more diffuse than those of the other species. The patterns seen in distributions of molecular ions are much less localized. The same is generally true for the states belonging to the second and third 2D modes (figures 3.8-3.10), however the degree of similarity of distributions of densities of atomic ions, electrons, excited atoms, and excimers decreases.

In summary, inclusion of detailed kinetics and non-locality of electron energy in the model does not prevent existence of multiple solutions describing different modes of current transfer to cathodes of DC glow discharges and is in fact favourable. It does not affect qualitatively results obtained in the framework of the basic model of chapter 2: multiple solutions fit the same pattern. The latter is not surprising, since self-organization is governed by the same trends in different systems, in particular in glow and arc cathodes [74].

3.5 Other plasma-producing gases

A very interesting question is why modes with multiple self-organized spots have been observed in DC glow microdischarges in xenon [5–11], but not argon [6, 12]. In this section, simple 1D calculations are reported that provide a possible explanation.

The CDVC of the 1D mode of a microdischarge in argon computed by means of the detailed model described in section 3.2 is shown in figure 3.11 for the same pressure (30 torr) and interelectrode gap (0.5 mm) as in the computations for xenon described in the preceding sections.

Also shown is the CDVC obtained in the framework of the basic model described in chapter 2. The Townsend ionization coefficient was evaluated by means of Eq. (2.7) with $C = 2.92 \times 10^3\,\mathrm{m^{-1}\,torr^{-1}}$ and $D = 2.66 \times 10^2\,\mathrm{V^{1/2}\,(m\,torr)^{-1/2}}$ [2]. The rate coefficient of dissociative recombination was set equal to $5.38 \times 10^{-14}\,\mathrm{m^3\,s^{-1}}$ [85]. Electron mobility was estimated using the formula $\mu_e = 10^{24}/n_n\,\mathrm{m^{-1}\,V^{-1}\,s^{-1}}$ (n_n is the density of the neutral gas), which represents an approximation of mobility data calculated using BOLSIG+ [76]. Mobility of ions is estimated by means of the formula $\mu_i = 7.1 \times 10^{21}/n_n\,\mathrm{m^{-1}\,V^{-1}\,s^{-1}}$, which represents an approximation of measurements [75]. The diffusion coefficients of the ions and the electrons were evaluated with the use of Einstein's relation with the gas and electron temperatures equal to 300 K and 1 eV, respectively.

The CDVC obtained in the framework of the basic model is similar to the one obtained in the framework of the detailed model. Both CDVCs exhibit the same trend: a falling section is absent; a feature characteristic of an obstructed discharge.

The absence of a falling section of the CDVC suggests that there are no multidimensional modes bifurcating from the 1D mode. It has been confirmed by bifurcation analysis performed in the framework of the basic model that this is indeed the case. We remind that modelling for xenon in the framework of the basic model under the same pressure and for the same radius and interelectrode gap revealed two 2D modes and thirteen 3D modes; at least three 2D modes exist in the framework of the detailed model. These results represent a quite clear indication that conditions of argon microdischarges are not as favourable for the appearance of modes with spot

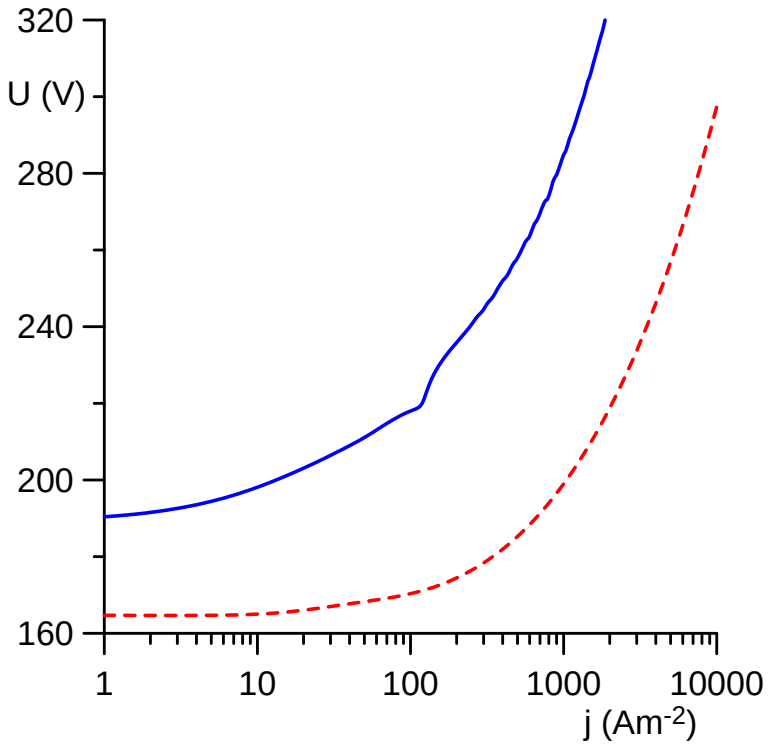

Figure 3.11: CDVCs of the 1D mode. Argon, $p = 30\,\text{torr}$, $h = 0.5\,\text{mm}$. Solid: detailed model. Dashed: basic model.

patterns as conditions of microdischarges in xenon.

The difference between CVDCs of the 1D mode for xenon and argon can be understood by comparing cross sections of elastic collisions between electrons and the atoms. These cross sections are shown in figure 3.12 for the values of average electron energy of interest. (Data from [90, 92, 98].) Also shown are cross sections of elastic collisions between electrons and helium atoms. The fact that the cross section of elastic collisions between electrons and atoms is larger for xenon than for argon is the reason why the discharge in argon is obstructed under the conditions considered: since the mean free path of electrons in argon is higher, the ionization coefficient of argon saturates at discharge currents lower than in xenon for the same product of pressure and interelectrode gap and the discharge in argon operates on the left-hand side of the Paschen curve. This effect should be even more pronounced for helium, since the corresponding cross sections are even lower than those of argon. (Note that the average electron energy in a helium glow discharge should be higher than in xenon and argon due to a higher ionization energy.)

If product of pressure and interelectrode gap is increased sufficiently, a falling section of the CDVC will appear. An illustration is given in figure 3.13. In this figure the calculated CDVC of the 1D mode in the framework of the basic model for argon is shown for a pressure of 75 torr and for the same interelectrode gap of 0.5 mm. The pressure was chosen in a way such that the falling section of the CDVC decreases by about 15% of the breakdown voltage, as it does in baseline calculations for xenon at a pressure of 30 torr and the same interelectrode gap of 0.5 mm.

Also shown in figure 3.13 is a CDVC calculated in the framework of the basic model for helium for the same interelectrode gap. The Townsend ionization coefficient in helium was evaluated by

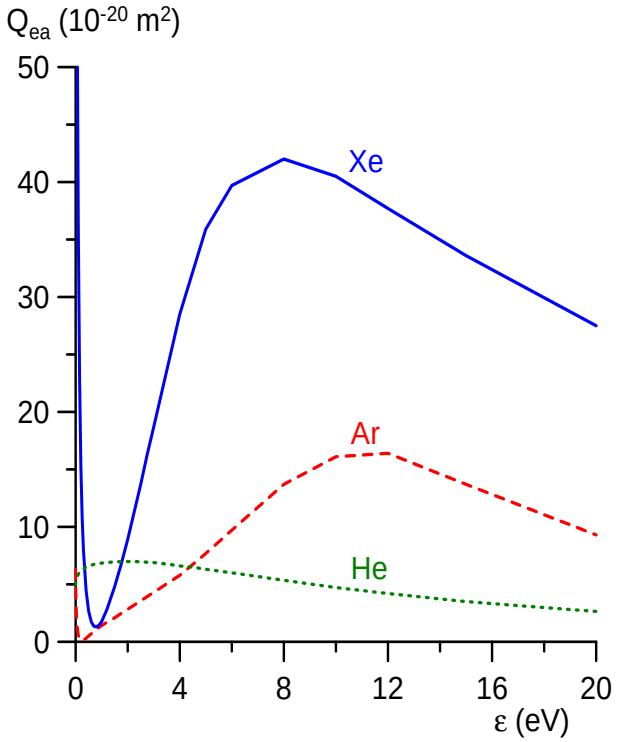

Figure 3.12: Cross sections of elastic collisions between electrons and neutrals as a function of electron energy.

means of Eq. (2.7) with $C = 4.4\times10^2\,\mathrm{m^{-1}\,torr^{-1}}$ and $D = 1.4\times10^2\,\mathrm{V^{1/2}\,(m\,torr)^{-1/2}}$ [2]. The rate coefficient of dissociative recombination was set equal to $3.75\times10^{-17}\,\mathrm{m^3\,s^{-1}}$ [99]. Electron mobility was estimated using the formula $\mu_e = 2.25\times10^{24}/n_n\,\mathrm{m^{-1}\,V^{-1}\,s^{-1}}$, which is an approximation of mobility calculated using BOLSIG+ [76]. Mobility of ions is estimated by means of the formula $\mu_i = 5.5\times10^{22}/n_n\,\mathrm{m^{-1}\,V^{-1}\,s^{-1}}$, which is an approximation of the measurements [75]. The diffusion coefficients of the ions and the electrons were evaluated with the use of Einstein's relation with the gas and electron temperatures set equal to 300 K and 1 eV, respectively. The pressure is set equal to 530 torr; a falling section of the 1D CDVC is present for this pressure with a decrease of about 15% of the breakdown voltage.

Bifurcation analysis has shown that at least five multidimensional modes exist for each plasma-producing gas (argon and helium) in the conditions of figure 3.13. Bifurcation points where the first two 3D modes (the one with a spot at the periphery and the one with two spots at the periphery opposite each other) branch off, or join, the 1D mode are shown in figure 3.13. One can see that modes with spot patterns can occur in plasma-producing gases other than xenon provided that the conditions are right.

The above-mentioned calculations were performed neglecting neutralization of the charged particles at the lateral wall of the discharge vessel. When neutralization at the wall is taken into account, a diffusion flux will appear in radial direction which tends to smooth out perturbations, in accordance with numerical results reported in chapter 2. Increased values of diffusion coefficients enhance this stabilizing effect. Therefore, the effect of reduction of the number of non-fundamental modes when neutralization at the wall is taken into account should be more significant in argon

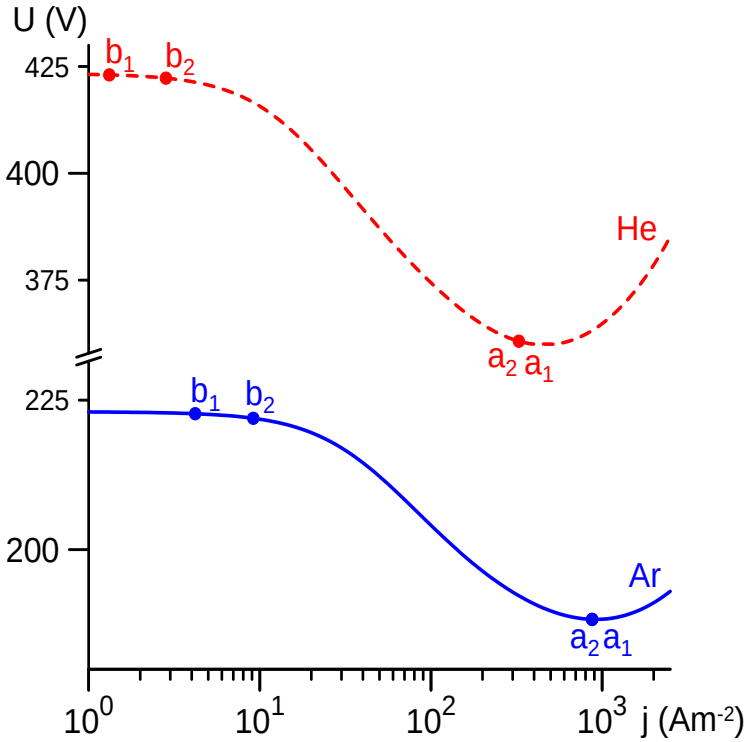

Figure 3.13: CDVCs of the 1D mode. $h = 0.5\,\mathrm{mm}$, basic model. Solid: argon, $p = 75\,\mathrm{torr}$. Dashed: helium, $p = 530\,\mathrm{torr}$. Circles: bifurcation points of the first (a_1, b_1) and second (a_2, b_2) 3D modes for $R = 0.5\,\mathrm{mm}$.

than in xenon and still more significant in helium. In accordance with results in section 2.4, the effect of increase of diffusion coefficients can be compensated with an increase of the radius of the discharge vessel.

The results and discussion given in this section indicate that the formation of self-organized patterns of spots should not be exclusive of discharges in xenon. Given the right conditions, it should be possible to observe self-organization in discharges in other gases, for example argon and helium. It would be interesting to try to observe self-organization in experiments with argon microdischarges with a larger radius and higher pressure than in [6, 12].

3.6 Conclusions

Complex behaviour of the fundamental mode was found using a steady state solver of Comsol Multiphysics in two different situations. This behaviour is manifested through a retrograde section limited by two turning points. In the case of the fundamental (1D) mode calculated in the framework of a detailed model of discharge in xenon between parallel-plane electrodes, this behaviour manifests itself in the plane (I, U) as an S-shaped section of the CDVC and is associated with stepwise ionization. In the case of the fundamental (2D) mode calculated in the framework of a basic model of a cathode boundary layer discharge in xenon, this behaviour manifests itself in the plane (I, U) as a loop in the CVC. The effect is a consequence of the geometry of the discharge: the loop is associated with a smooth transition of the pattern between one with a ring

spot inside the cathode at low currents and a pattern with a central spot at high currents. Both the S-shape and the loop are scientifically very interesting. One could think of further numerical work on these effects and also of experiments.

Complex behaviour has emerged as a consequence of consideration of either a more detailed kinetic scheme, or a discharge geometry other than parallel-plane electrodes. These results give the impression that complex behaviour in DC glow microdischarges is a rule rather than an exception.

Comsol Multiphysics is a very powerful tool which allows, for example, prediction of complex behaviour which may be present even in apparently simple situations; this behaviour can hardly be noticed if time-dependent solvers were used. Like other rapidly developing simulation tools, it has unfortunate drawbacks which manifest themselves under certain conditions. However, past experience shows that new versions of Comsol Multiphysics usually offer significant improvements and add flexibility. One can hope that the weaknesses revealed in this work will be overcome in the near future.

The inclusion in the model of detailed kinetics (multiple ionic species, atomic excited states, excimers) and non-locality of electron transport and kinetic coefficients does not prevent existence of multiple solutions describing different modes of current transfer to cathodes of DC glow discharges and is in fact favourable: three 2D modes were found, in addition to the fundamental (1D) mode, for xenon in the framework of the detailed model where only two 2D modes exist in the framework of the basic model under the same conditions. Account of the detailed kinetics and non-locality of electron transport and kinetic coefficients does not affect the results qualitatively: the multiple solutions fit the same pattern that those found in the framework of the basic model. The latter is not surprising, since self-organization is governed by the same trends in different systems, in particular on glow and arc cathodes [74].

Numerical results for argon, obtained in the framework of the detailed and basic models, and those for helium, obtained in the framework of the basic model, give a clear indication that the conditions of argon and helium microdischarges are less favourable for self-organization than those in xenon. This is a consequence of the difference between cross sections of elastic collisions between electrons and atoms of these gases. However, it should be possible to observe self-organization also in argon and helium microdischarges provided that the pressure is sufficiently high and the discharge radius is sufficiently large.

Chapter 4

Transient spot modes on thermionic cathodes and their prevention

4.1 Introduction

The appearance of spots on cathodes of HID lamps represents a major problem for designers, in the first place, due to the blackening of burner's walls which accompanies the appearance of spots. At present, the physics of spots on thermionic arc cathodes is understood relatively well. They appear as a result of a thermal instability for which the role of positive feedback is played by the growing dependence $q\,(T_w)$, where q is the density of the energy flux from the plasma to the cathode surface and T_w is the local temperature of the surface. This positive feedback is opposed by heat conduction in the cathode body, which tends to smooth out perturbations, i.e., produces a stabilizing effect. A competition of these two mechanisms results in appearance, or not, of spots on thermionic arc cathodes.

The stabilizing effect of heat conduction is enhanced by a reduction of cathode dimensions. Therefore, DC cathodes may be forced into the spotless, or diffuse, mode by reducing their dimensions. (The same idea may be expressed in other words which are well familiar to designers of arc devices: if a cathode is small, it is easier to heat it up to temperatures necessary for the diffuse operation [15].) Besides, prevention of spots on DC cathodes may be facilitated by an intelligent choice of the cathode shape.

The situation is more complex as far as AC arcs are concerned: transient spots may be provoked even on small cathodes by rapid variations of the arc current. Typically, spots appear on electrodes of AC HID lamps at the beginning of the cathodic phase immediately after current zero, when the cathode on the whole is not yet hot enough to efficiently transfer current from the arc. After operating in the spot mode for some time, the cathode on the whole usually gets hot enough, the arc attachment switches into the diffuse mode and remains diffuse during the rest of the cathode phase.

It seems natural to try to prevent formation of transient spots on cathodes of AC HID lamps by means of an intelligent choice of the current waveform. Such choice can be guided by numerical modelling, which has at present attained an advanced stage and is capable of providing a reasonably accurate description of most aspects of operation of thermionic arc cathodes.

In this chapter, formation of transient spots on thermionic cathodes is studied experimentally. The obtained results also shed light over the mechanism of blackening of walls of burners of HID lamps which accompanies the appearance of transient spots: the cathode material gets into the gas phase most probably due to evaporation from the spot rather than due to sputtering that could occur during the voltage spikes after current zero.

The experiments have been performed on COST-529 standard HID lamps. Spots are induced by a current step: after a few seconds at a constant current, the arc current is instantly increased to a higher value which is maintained constant until the transition process terminates. This way of inducing transient cathodic spots has been described in the literature [100, 101]; it is convenient for methodical purposes while being adequate for reproducing the scenario of spot formation on cathodes of AC HID lamps after current zero.

The outline of the chapter is as follows. In section 4.2, a general pattern of appearance of stationary and transient spots on thermionic cathodes and the effect of the cathode shape and material are analyzed with the use of numerical results. (As mentioned in section 1.3 of the Introduction, these results were obtained not by the author of the thesis, however they are relevant for completeness and clarity. These results are cited here according to the paper [66].) The experimental setup is described in section 4.3. In section 4.4, a comparison between the experimental and simulation results is given. Prevention of transient spots is considered in section 4.5. Conclusions of the work are summarized in section 4.6.

Results reported in this chapter were published in [66, 67].

4.2 General pattern of appearance of transient spots

Formation of transient spots on thermionic arc cathodes induced by current steps was studied numerically in [100, 101]. An important question which has not been dealt with in these works is a relation between transient spots and steady-state modes of current transfer and their stability. This question is studied in the present section.

Let us consider the following conditions which are convenient for the purposes of illustration and not very different from those treated in [100]: a rod cathode of radius $R = 0.5\,\mathrm{mm}$ and a height of $h = 12\,\mathrm{mm}$, with a flat front surface, with all the lateral surface active (i.e., without electrically and/or thermally insulated sections), the temperature at the base of the cathode T_c is 1000 K, the arc is operated in argon under the pressure of 2 bar.

According to results of the linear stability theory [31, 32], the only steady-state modes of current transfer that can be stable are the diffuse mode and the first spot mode (the mode with a spot at the edge of the front surface of the cathode). The diffuse mode is associated with axially symmetric temperature distributions in the cathode, the first spot mode is associated with 3D distributions. Current-voltage characteristics of these modes for the above conditions are shown in figure 4.1. In agreement with the general pattern established in [56], the steady-state spot mode is composed of two branches separated by a turning point and exists in a limited current range $I \leq I_t$, where I_t is the arc current corresponding to the turning point; $I_t \approx 1.95\,\mathrm{A}$ in this case. According to results [31, 32], the diffuse mode is stable under the considered conditions, the branch of the spot mode which manifests higher values of U in the vicinity of the turning point

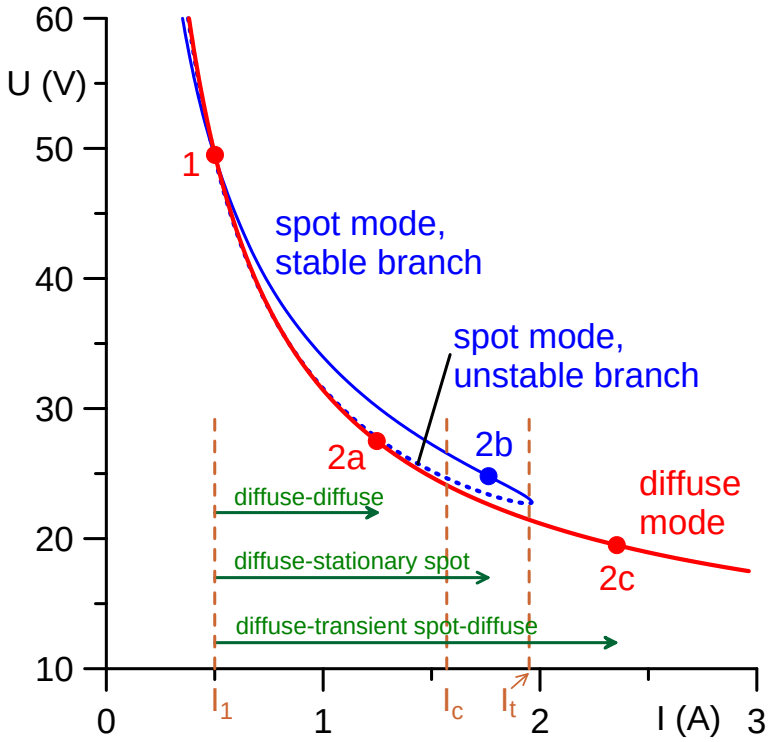

Figure 4.1: Current-voltage characteristics of steady-state modes of current transfer and scenarios of non-stationary transitions. Cathode with a flat front surface in argon plasma.

(and is represented in figure 4.1 by the solid line) is also stable, and the branch of the spot mode which manifests lower values of U in the vicinity of the turning point (and is represented by the dotted line) is unstable.

Let us assume that the cathode initially operates in the steady-state diffuse mode at a certain current $I = I_1$. The corresponding initial state is represented in figure 4.1 by a circle marked 1. At a certain moment the current starts rapidly growing and swiftly attains a target value $I = I_2$, after which it remains constant. (It was assumed that the arc current grows from I_1 to I_2 in 1 μs linearly with time in the modelling reported in this section.) The temperature distribution in the cathode body and the near-cathode voltage drop will undergo a transition process and finally a new steady state will be reached. One could think of three scenarios of such transition.

According to results of the linear stability theory [31, 32], the diffuse mode of current transfer is stable against small perturbations. It should be stable also against finite perturbations unless their amplitude exceeds a certain threshold. Therefore, one can expect that the diffuse mode is maintained during the whole transition process if the target current I_2 does not exceed a certain threshold value I_c; if $I_2 > I_c$, the diffuse mode gives way to the spot mode. This threshold value depends on conditions and also on the initial current I_1.

Thus, the first possible scenario occurs in the case $I_2 < I_c$: the diffuse mode is maintained during the whole transition process and the final steady state is diffuse as well. In other words, this is a transition between two stable diffuse states with intermediate states being diffuse as well. This scenario is schematically shown in figure 4.1 by the horizontal arrow marked "diffuse-diffuse" and the final steady state is depicted by the circle marked 2a.

Now let us consider the case $I_2 > I_c$. If the target current is within the range of existence of the steady-state spot mode, i.e., $I_c < I_2 < I_t$, then the final steady state may belong either to the diffuse mode or to one of the two branches of the spot mode. The first possibility does not look very probable: a spot, once having started to form, will tend to persist whenever possible. The branch of the spot mode that is shown in figure 4.1 by the dotted line is unstable. Hence, one should expect that the final steady state will belong to the branch of the spot mode which is depicted in figure 4.1 by the solid line. This state is represented by the circle marked 2b. Thus, the second possible scenario occurs in the target current range $I_c < I_2 < I_t$: the diffuse mode during the transition process gives way to the spot mode and the latter is maintained indefinitely. In other words, this is a transition from a stable diffuse state to a stable state with a stationary spot. This scenario is schematically shown in figure 4.1 by the horizontal arrow marked "diffuse-stationary spot". Obviously, this scenario is possible provided that $I_c < I_t$.

If the target current is beyond the range of existence of the steady-state mode, $I_2 > I_t$, then the final state can only belong to the diffuse mode as represented by the circle marked 2c since no other stationary states are possible at $I = I_2$. One can say that a transient spot, which has appeared at the initial stage of the transition process, is destroyed by heat conduction at a later stage. This is the third possible scenario: in the target current range $I_2 > I_t$, the diffuse mode during the transition process gives way to the spot mode, which later gives way to the diffuse mode again. In other words, this is a transition between two stable diffuse states which occurs through intermediate states with a transient spot. This scenario is schematically shown in figure 4.1 by the horizontal arrow marked "diffuse-transient spot-diffuse".

The above scenarios are confirmed by the numerical modelling. Let us consider, as an example, results for the initial current $I_1 = 0.5\,\mathrm{A}$. The temperature distribution in the cathode is axially symmetric in the initial state. If the target current is below approximately 1.57 A, then the temperature distribution in the cathode remains axially symmetric during the transition process and the electric current distribution along the front surface of the cathode remains more or or less uniform. If the target current exceeds approximately 1.57 A, the axial symmetry breaks down during the transition process and a current distribution with a narrow maximum at the edge of the front surface of the cathode occurs: a hot cathode spot appears. This non-stationary spot either evolves into a stationary spot belonging to the branch of the spot mode which is depicted in figure 4.1 by the solid line, or disappears giving way to a diffuse steady state, depending on whether the target current is in the range $1.57\,\mathrm{A} \lesssim I_2 \lesssim 1.95\,\mathrm{A}$ or above this range.

Numerically calculated temporal variation of the maximum temperature of the cathode surface and near-cathode voltage drop for the initial current $I_1 = 0.5\,\mathrm{A}$ and three values of the target current are shown in figure 4.2. (It is assumed that the current starts growing at the moment $t = 100\,\mu\mathrm{s}$.) In the case $I_2 = 1.5\,\mathrm{A}$, the temperature distribution during the whole transition process remains axially symmetric, the maximum temperature of the cathode surface remains around 3000 K. The near-cathode voltage drop gradually decreases after the initial spike. One can say that the transition process in this case occurs in the diffuse mode.

In the case $I_2 = 1.8\,\mathrm{A}$, the axial symmetry breaks down during the transition process and a hot spot is formed, with a maximum temperature of the cathode surface being around 4500 K. The formation of the spot is accompanied by a sharp fall of the near-cathode voltage. Once having

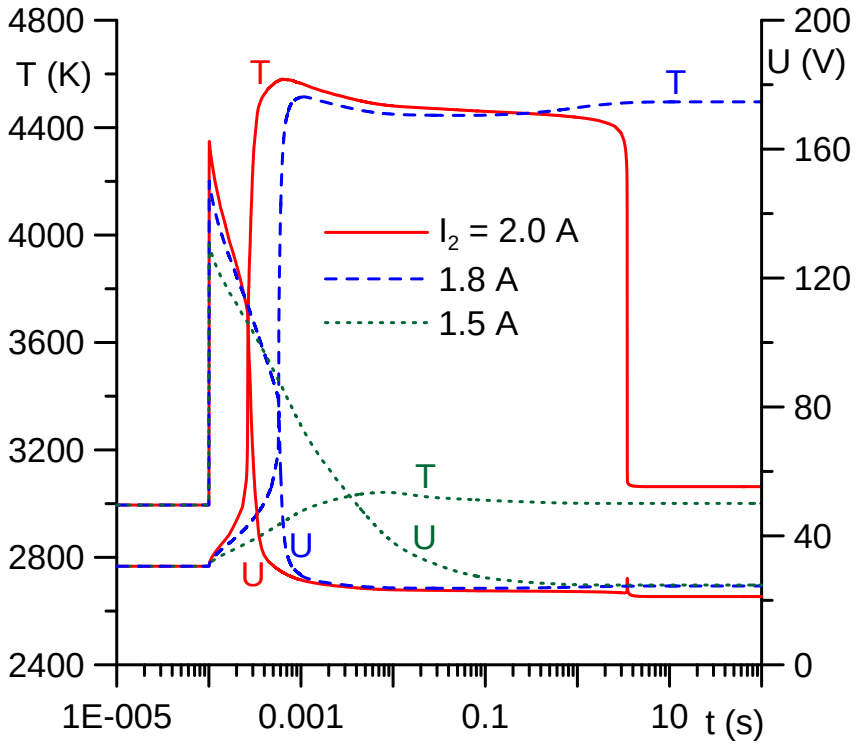

Figure 4.2: Maximum temperature of the cathode surface and near-cathode voltage drop for different current jumps. Cathode with a flat front surface in argon plasma. $I_1 = 0.5\,\mathrm{A}$.

been formed, the spot continues to exist indefinitely. In other words, the final steady state belongs to a spot mode. A more detailed investigation shows that this state belongs to the branch of the first spot mode which is depicted in figure 4.1 by the solid line, thus confirming conclusions on stability obtained in [31, 32] by means of a linear stability analysis.

A spot is formed also in the case $I_2 = 2.0\,\mathrm{A}$, however in this case it does not exist at all times but rather disappears around $t = 3\,\mathrm{s}$, its disappearance being accompanied by a small voltage peak. In other words, the spot is transient in this case and the final steady state in this case belongs to the diffuse mode.

Obviously, these numerical results fully conform to the above qualitative considerations and $I_c \approx 1.57\,\mathrm{A}$ for this case. These results also qualitatively conform to numerical results reported in [100], however with an important exception: the second above-described scenario, a transition from a stable diffuse state to a stable state with a stationary spot, was not detected in [100].

An essential question is how sensitive is appearance of transient spots with respect to variations of the cathode shape and material properties. This point is illustrated by figure 4.3. Solid lines in this figure represent calculated maximum temperature of the cathode surface and near-cathode voltage drop for the same conditions as above at $I_1 = 0.5\,\mathrm{A}$, $I_2 = 2.0\,\mathrm{A}$. (These lines are the same that the corresponding lines on figure 4.2). Dashed lines represent simulation results for the same conditions but for a cathode with a rounded edge of the front surface, with a rounding of the radius of $100\,\mu\mathrm{m}$. One can see that the spot on a rounded cathode is formed considerably later, is considerably less hot and lives much less, than the spot on a cathode with the flat front surface. This difference can be interpreted as a consequence of better cooling conditions on a

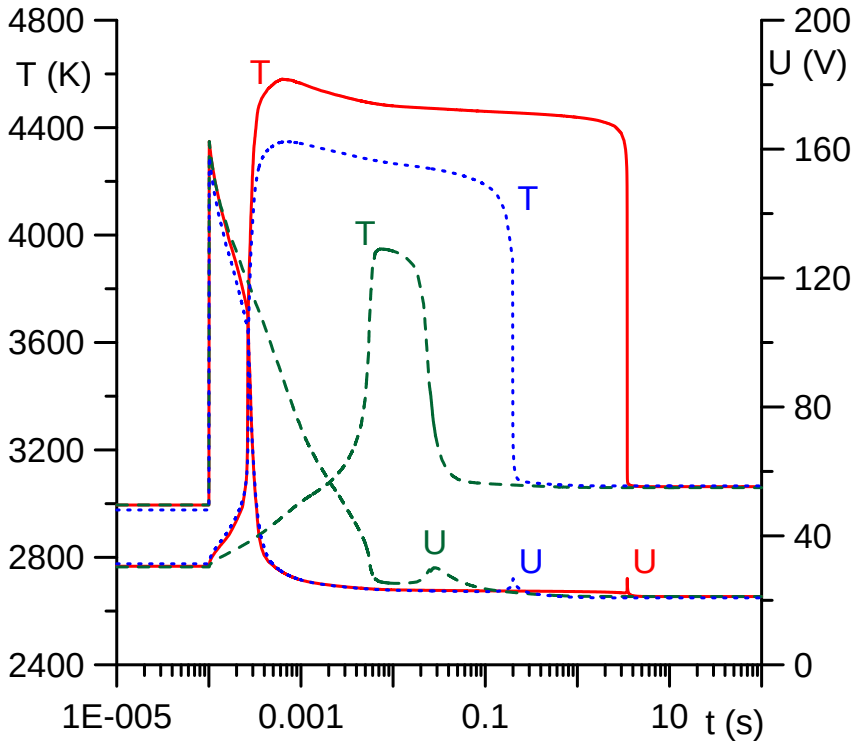

Figure 4.3: Maximum temperature of the cathode surface and near-cathode voltage drop. argon plasma, $I_1 = 0.5\,\mathrm{A}$, $I_2 = 2.0\,\mathrm{A}$. Solid: cathode with a flat front surface. Dashed: cathode with a rounded edge at the front surface. Dotted: cathode with a flat front surface, thermal conductivity of tungsten from [102].

rounded edge.

Dotted lines in figure 4.3 represent results of simulations performed for a cathode with a flat front surface for the same conditions as above but with the use of data on thermal conductivity of tungsten given in [102]. The latter data seem to refer to thoriated tungsten but have also been used for modelling cathodes made of pure tungsten [61, 100, 101, 103]. At moderate temperatures these data are nearly the same that the data given in [104] and used to obtain results given in the present work, however at higher temperatures the thermal conductivity from [102] appreciably exceeds that from [104]. One can see from figure 4.3 that the replacement of the data [104] by those from [102] results in an appreciable decrease both in the temperature and lifetime of the spot, while the time of formation of the spot remains virtually unchanged. Again, this effect can be interpreted as a consequence of better cooling conditions for a spot due to higher thermal conductivity at high temperatures.

4.3 Experimental setup

Experiments were performed on COST-529 standard lamps, which are experimental HID lamps produced by Philips in the framework of action 529 of programme COST of the EU. The lamps have quartz walls and a quartz envelope [65]; lamps used in this work were an especially produced version which had no coils around the electrodes.

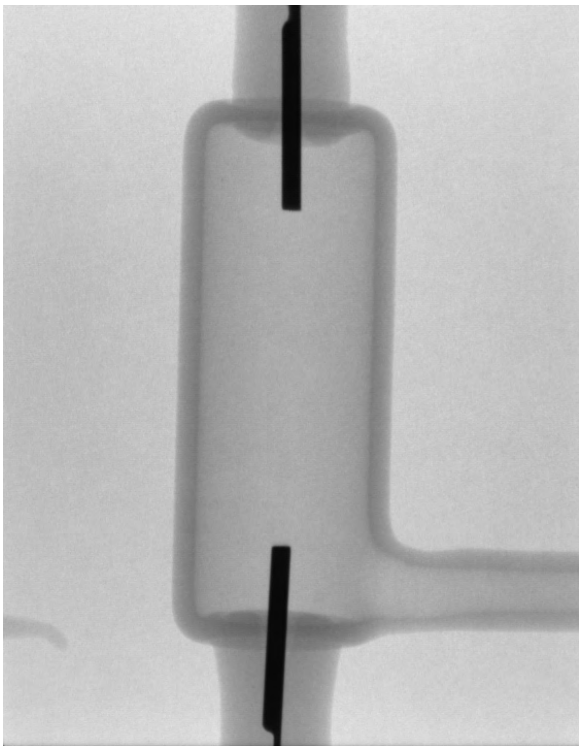

Figure 4.4: X-ray photograph of the burner of a type 2 lamp.

The lamps used were filled with 5 mg of mercury, apart from about 300 mbar argon filling (at room temperature) as the starter gas, which resulted in an operating pressure of about 4 bar. The lamps were equipped with pure tungsten rod electrodes shown in figure 4.4. Some of the lamps had electrodes of radius $R = 250\,\mu$m and of height (the total length of the rod from one tip to another) $h = 9$ mm, and the others had electrodes with $R = 350\,\mu$m and $h = 11$ mm. In the following, these lamps will be referred to as lamps of type 1 or 2, respectively. X-ray photographs show that the part of the electrode which is inside the burner slightly varies from one lamp to another. For lamps of type 1 the average length of the electrodes inside the burner is 1.9 mm with an average dispersion of 0.1 mm, while for lamps of type 2 the average length of the electrodes inside the burner is 3.7 mm with an average dispersion of 0.29 mm. The X-ray photographs show also a rounded edge at the front surface of the electrodes with 25 μm radius in average.

The power was supplied to the lamps by means of a voltage-driven power amplifier FM 1295 DCU/I 750 developed and supplied by MedTech Engineering, which functioned as a current source controlled by an arbitrary waveform generator Agilent 33220A. This power supply allows for rapid variations of the discharge current (on a time scale of the order of the μs); a feature which is very important for the present experiments. Note that ensuring this feature is not difficult at low power output, however is non-trivial at high power output typical for HID lamps.

During warm up, the lamps were operated for about 5 minutes at a 100 Hz square wave, at the power level of 70 W. Current jumps necessary to induce the spots were generated by superimposing a square wave of 0.1 Hz over a DC current. In other words, the cathode operated for 5 s at a (constant) current $I = I_1$ and then for 5 s at a higher current $I = I_2$, after which the current was again reduced to I_1 and the cycle was repeated. The transition time between the two

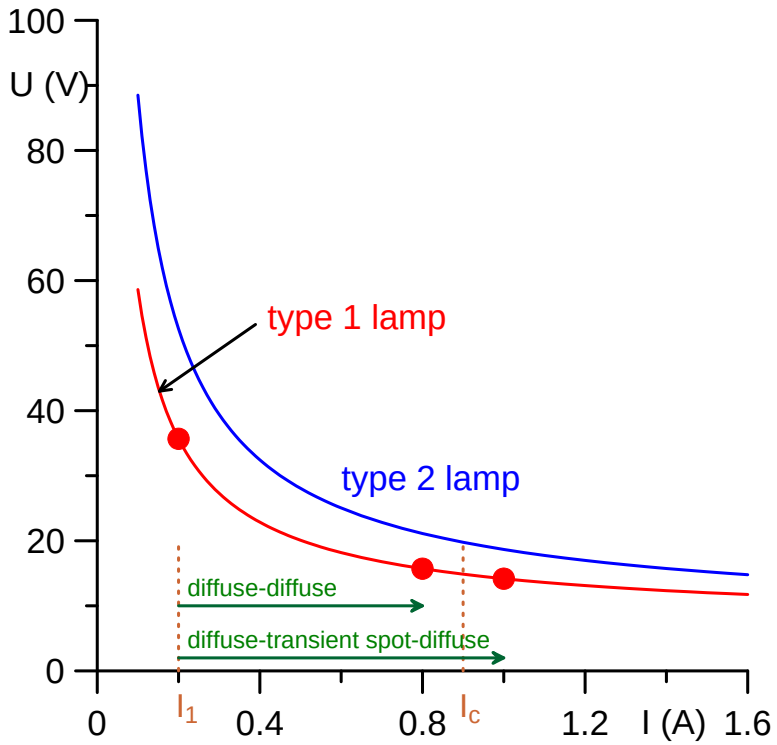

Figure 4.5: Calculated current-voltage characteristics of the steady-state diffuse mode and scenarios of non-stationary transitions. Cathodes of COST-529 standard lamps.

current values was within 5 μs.

The lamps were operated in vertical position. The electrode at the bottom of the burner was operated as the cathode. The image of the cathode and the near-cathode region was magnified 10 times and focused on a screen. The mode of arc attachment to the cathode was diagnosed by photodiodes placed on the screen in front of the cathode's image. Measurements were registered by a digital oscilloscope Yokogawa DL 1640 with sampling rate of 200 MS s^{-1}.

4.4 Results and discussion

Let us apply the above-established pattern to conditions of the experiments with COST-529 standard lamps. Current-voltage characteristics of the diffuse mode of current transfer calculated for cathodes of type 1 and 2 are shown in figure 4.5. Stationary spots for these conditions exist at very low currents and very high voltages and the corresponding current-voltage characteristics cannot be shown on the graph. In terms of the preceding section, the value I_t is very low, hence the second above-described scenario does not take place in these conditions and only diffuse-diffuse and diffuse-transient spot-diffuse transitions are possible, as is schematically shown in figure 4.5 for the lamps of type 1.

This conclusion is confirmed by the numerical modelling. (It was assumed that the arc current grows from I_1 to I_2 linearly with time in 5 μs in the modelling of COST-529 lamps.) For a cathode of type 1 and $I_1 = 0.2$ A, a diffuse-diffuse transition occurs for $I_2 < 0.96$ A and a diffuse-transient spot-diffuse transition occurs for $I_2 \geq 0.96$ A; in other words, $I_c \approx 0.96$ A in this case. For a

cathode of type 2 and $I_1 = 0.3\,\mathrm{A}$, a diffuse-diffuse transition occurs for $I_2 < 1.27\,\mathrm{A}$ and a diffuse-transient spot-diffuse transition occurs for $I_2 \geq 1.27\,\mathrm{A}$; $I_c \approx 1.27\,\mathrm{A}$. Typical calculation results on evolution of the maximum temperature of the cathode surface and near-cathode voltage drop for conditions of COST-529 standard lamps are shown in figure 4.7b and are similar to those discussed in the preceding section.

An essential point in the experiment is an appropriate choice of the initial current I_1 of the current jump. This current must be not too small in order to minimize sputtering that occurs at low currents where the near-cathode voltage drop is high, while at the same time it must be not too high in order that the limit I_c of appearance of transient spots correspond to the lamp power not much more than 100 W. It is seen from figure 4.5 that the difference in the near-cathode voltage drop between type 1 and type 2 cathodes at $I = 0.2\,\mathrm{A}$ is of about 17 V. One can expect therefore that sputtering for a type 2 lamp at 0.2 A should be significantly increased compared to a type 1 lamp operating at the same current and this indeed was observed in the experiment: operation of a type 2 lamp with an initial current of 0.2 A resulted in a very fast blackening of the burner. Therefore, the initial current I_1 of the current jump was set equal to 0.2 A for type 1 lamps and to 0.3 A for type 2 lamps.

Typical photos of formation and disappearance of transient spots are shown in figure 4.6a. In figure 4.6b, the details of the process are shown as seen via modelling. At the initial state, the temperature distribution in the cathode is axially symmetric, which is characteristic of the diffuse mode. After the current jump, axial symmetry breaks down and a current distribution with a narrow maximum at the edge of the front surface of the cathode occurs: a hot cathode spot appears. Once having been formed, the spot exists during a certain time and then disappears; axial symmetry is restored.

Typical measurements results can be seen in figure 4.7a, where the lamp voltage and the intensity $L.I.$ of light emitted by the near-cathode region are shown. Modelling results (maximum temperature of the cathode surface and near-cathode voltage drop) for the same conditions are shown in figure 4.7b. For $I_2 = 0.8\,\mathrm{A}$, the light intensity increases before it stabilizes about 0.1 s after the jump. This is an expected behavior: the cathode and arc temperatures are higher at higher currents. There is a sharp peak in the lamp voltage just after the jump, which afterwards undergoes a smooth decrease down to a constant voltage of about 80 V. For $I_2 = 1.0\,\mathrm{A}$, there is a steep increase of the intensity of light emitted by the near-cathode region at about 0.7 ms which is accompanied by a steep decrease of the lamp voltage at the same instant; a hot cathode spot is being formed. After about 50 ms, the light intensity steeply decreases and then remains constant, this decrease being accompanied by a small peak in the lamp voltage; the spot has decayed.

The experimental results on the lamp voltage conform to trends observed in [100], however the measured light intensity does not. A spot formation in the experiments [100] was indicated by triangle-shaped peaks in the intensity of light emitted by the near-cathode region, which are accompanied by a steep decrease of the lamp voltage drop at the same instant. In the experiments of the present work such peaks have not been observed and what indicates a spot formation is a change of slope of the temporal dependence of the light intensity accompanied by a steep decrease of the lamp voltage drop at the same instant. Furthermore, the light intensity signal observed in the present work is rectangular and not triangular as in [100].

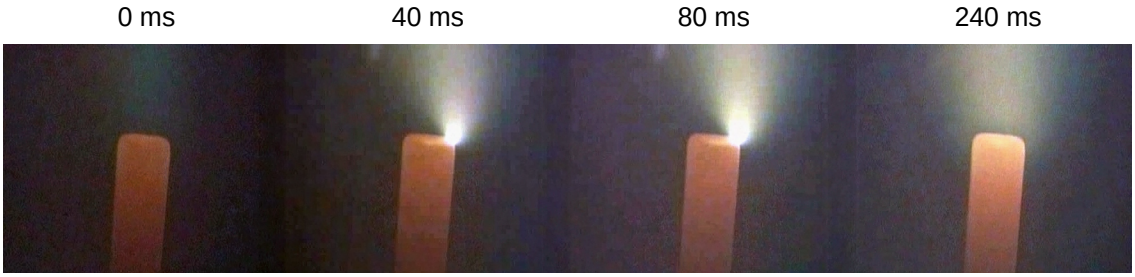

(a)

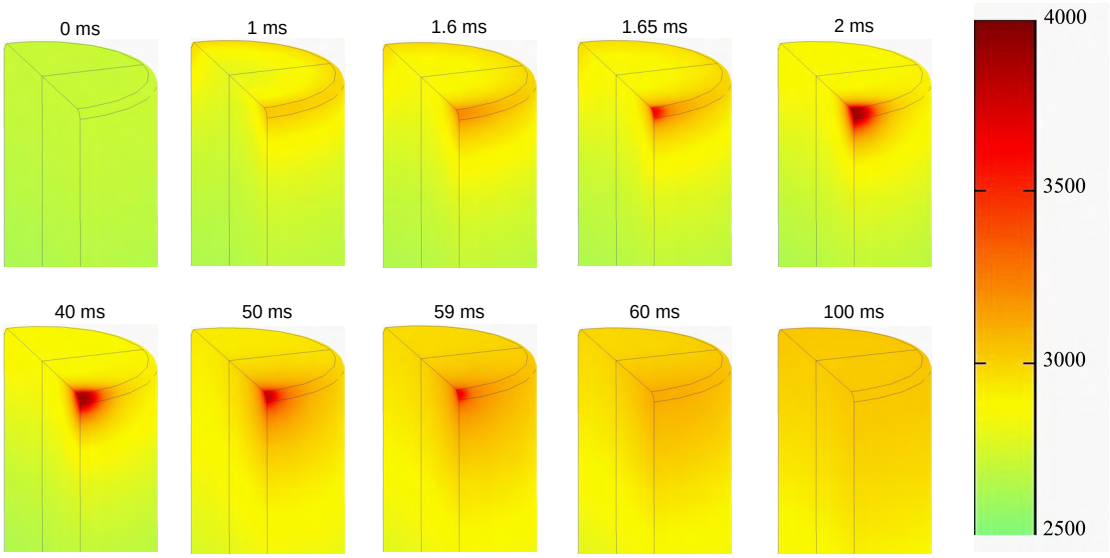

(b)

Figure 4.6: Transient spot on the cathode of a type 2 lamp, $I_1 = 0.3\,\mathrm{A}$, $I_2 = 1.3\,\mathrm{A}$. (a) Photos taken in the experiment. (b) Computed distribution of temperature along the surface of the cathode (the bar is in kelvin).

Comparing figures 4.7a and 4.7b, one can see that, although computed quantities are not the same that those measured (the lamp voltage V and the intensity $L.I.$ of light emitted by the near-cathode plasma vs. the near-cathode voltage drop $U$and the maximum temperature T of the cathode surface), a good qualitative agreement exists between the simulations and the experiments. In particular, the diffuse-diffuse transition occurs in the case $I_2 = 0.8\,\mathrm{A}$ and a diffuse-transient spot-diffuse transition occurs in the case $I_2 = 1.0\,\mathrm{A}$ both in the modelling and in the experiment, a rectangular peak in the light intensity observed in the case $I_2 = 1.0\,\mathrm{A}$ conforms to numerical results for the maximum cathode temperature for this case. The spot formation time in the modelling for the case $I_2 = 1.0\,\mathrm{A}$ was 0.52 ms, while the average spot formation time for type 1 lamps and $I_2 = 1.0\,\mathrm{A}$ in the experiment was 0.55 ms with an average dispersion of 0.15 ms. Note that the spot formation time was defined in the modelling and in the experiment as the time interval between the current jump and the rapid decrease of the near-cathode or, respectively, lamp voltage; since the latter decrease occurs very rapidly (within $10\,\mu$s both in the modelling and in the experiment), such definition is unambiguous.

However, there is a significant difference in the lifetime of transient spots: for example, the average lifetime in the experiment for type 1 lamps and $I_2 = 1.0\,\mathrm{A}$ was 58 ms with an average dispersion of 3 ms, while the lifetime in the modelling was 12 ms. In other words, the model predicts a much earlier decay of transient spots than the one observed in the experiment.

A good qualitative agreement between the experiment and the modelling occurs also for type 2 lamps, as is shown by an example depicted in figure 4.8. The average spot formation time in the experiment for the case $I_2 = 1.3\,\mathrm{A}$ was 3.27 ms with an average dispersion of 0.37 ms, while the spot formation time in the modelling for this case was 1.64 ms; an agreement not so good as for type 1 lamps, but still within the factor of 2. Again, there is a significant difference in the lifetime of transient spots: the average lifetime in the experiment for type 2 lamps and $I_2 = 1.3\,\mathrm{A}$ was 245 ms with an average dispersion of 15 ms, while the lifetime in the modelling was 57 ms.

It is unclear what is the reason of the latter discrepancy. It can hardly be attributed to the effect of parameters such as cathode radius, portion of the cathode inside the burner, rounding of the cathode edge and temperature of the base of the cathode: this effect has been numerically investigated and found to be not strong enough. For example, an increase of the calculated spot lifetime by a factor of 3.3 is attained by an increase of 20% in the cathode radius, however the latter increase is far above the accuracy of characterization of the electrodes.

4.5 Prevention of transient spots

The formation of a spot induced by a current jump can be interpreted as a result of the cathode failure to undergo a uniform heating, as a response to the increase of current. Educated guesswork would lead one to expect that a brief reduction of the current shortly after the current jump could aid the cathode to be heated up uniformly, thus preventing the appearance of a spot. This applies to both stationary and transient spots, however only prevention of transient spots is considered in this work since no stationary spots exist under conditions of the present experiment.

The experiments have confirmed the above idea: transient spots indeed do not appear provided that the timing, duration, and magnitude of the current reduction are right. An example is shown

in figure 4.9a, which refers to a 0.2 A − 1.0 A current jump on a type 1 cathode. 0.4 ms after the jump, the current was for 0.3 ms reduced to 0.3 A. The shape of temporal variations of the light intensity and of the lamp voltage indicate that the transient spot is indeed prevented. Note that the intensity of light emitted by the near-cathode region sharply decreases when the current is lowered to 0.3 A and again increases as soon as the current grows back to 1.0 A, however variations in the light intensity on such short time scale are not perceivable by the human eye. The corresponding modelling results are shown in figure 4.9b. The maximum temperature of the cathode surface is below 3200 K: appearance of a spot is indeed prevented. There is excellent agreement between the experimental and modelling results.

An example of experimental and modelling results on spot prevention on type 2 cathodes is given in figure 4.10, which refers to the 0.3 A − 1.3 A current jump. Here, spots are prevented with a reduction of the current to 0.4 A which starts 0.3 ms after the current jump and lasts for 0.5 ms.

The mechanism of prevention of spots as seen via computer simulation is illustrated by figure 4.11. The appearance of a spot identical to the one seen in figure 4.6b is prevented by a reduction of current to 0.4 A which starts 0.3 ms after the current jump and lasts for 0.5 ms.

It is well known that transient spots appearing in the beginning of the cathodic phase on electrodes of AC HID lamps cause a rapid blackening of walls of the burner. One could think of two principal mechanisms leading to this blackening: sputtering of the cathode material, which can accompany near-cathode voltage spikes occurring after the current zero, and evaporation of cathode material from the spot. In the conditions being considered in the present work, the current reduction aimed at preventing spots occurs some time after the current jump, thus the near-cathode voltage spike that occurs immediately after the jump is not affected by the current reduction. This allows one to separate effects caused by the two above-mentioned mechanisms.

In this connection, the following experiment was performed. Two lamps of the type 1 were operated during one hour with a square-wave arc current between 0.2 A and 1.0 A with the frequency of 0.1 Hz. Transient spots were prevented in one of the lamps by means of the above-described current reduction, while no measures were taken to control the arc attachment to the cathode of the second lamp. Blackening of the burner around the cathode turned out to be much more pronounced in the second lamp. Since the voltage spike immediately after the jump was the same in both lamps and, consequently, the sputtering also is likely to be the same, one can conclude that the increased blackening of the burner occurring in the second lamp is a result of evaporation of tungsten from the cathode rather than sputtering. Of course, this experiment also demonstrates that the prevention of transient spots may considerably increase the lifetime of a lamp.

Obviously, a brief reduction of current proposed in this work does not represent the only way to prevent appearance of transient spots: modelling has revealed that this could be achieved, e.g., by controlling the portion of the cathode inside the burner of the lamp. However, this can require a considerable change in the design: for example, for a 0.2 A − 1.0 A current jump on a type 1 cathode the transient spot may be prevented by a reduction in the length of the portion of the cathode inside the burner of the lamp of about 50%.

It is interesting to note that short rectangular current pulses have already been used for controlling the spot mode of arc attachment in ultra-high pressure lamps [105, 106]. However, the

pulses employed in [105, 106] were used to add current to the electrode and took place at the end of the anodic phase, i.e., were substantially different from those employed in the present work, and served a different objective, namely, to facilitate appearance of a protrusion on the electrode surface. On the other hand, this attests to the technical viability of the spot prevention method proposed in this work.

4.6 Conclusions

Formation of transient spots on thermionic cathodes was studied experimentally. The experiments have been performed on COST-529 standard HID lamps. The experimental setup includes a power supply which allows for rapid variations of the discharge current (on a time scale of the order of $1\,\mu$s) while maintaining high power output; a feature which is important for these experiments. The experiments have been performed in parallel and coordinated with numerical modelling.

The intensity of light emitted by the near-cathode region and the lamp voltage were measured as functions of time and found to be in a good qualitative agreement with the near-cathode voltage drop and maximum temperature of the cathode surface computed for conditions of the experiments. There is a good agreement also on the threshold current and time of formation of transient spots, although not on their lifetime.

A possibility of prevention of appearance of transient spots by means of a brief reduction of the arc current shortly after the initial current increase is proposed and justified. Experiments on identical HID lamps performed with and without prevention of transient spots allow one to separate effects produced by sputtering by voltage spikes and evaporation of the cathode material on blackening of burners of HID lamps that accompanies appearance of transient cathode spots. The conclusion is that the main mechanism is evaporation and not sputtering.

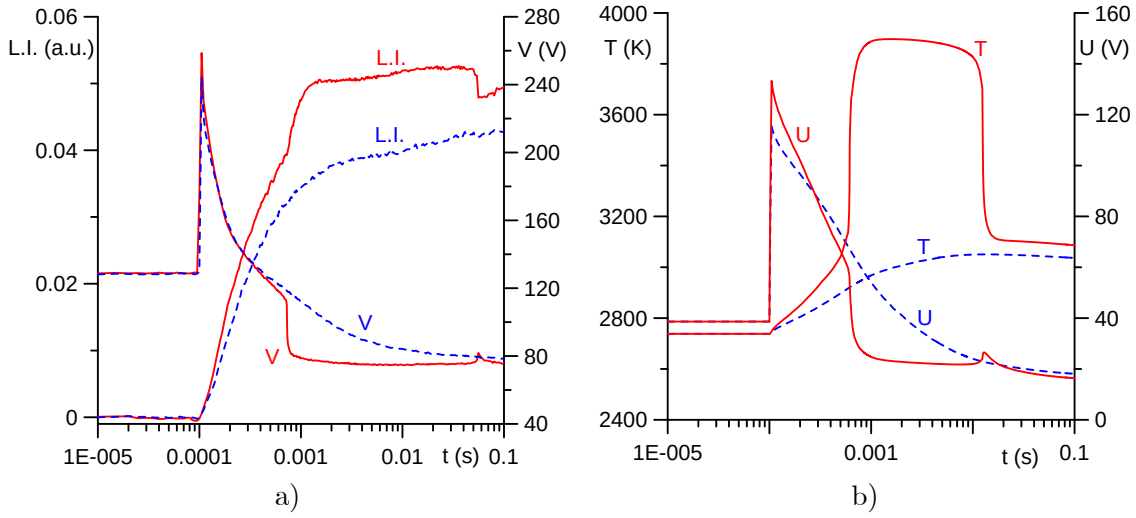

Figure 4.7: Diffuse transition and transient spots on cathodes of type 1 lamps. $I_1 = 0.2\,\mathrm{A}$. Solid: $I_2 = 1.0\,\mathrm{A}$. Dashed: $I_2 = 0.8\,\mathrm{A}$. (a) Measured intensity of light emitted by the near-cathode region and lamp voltage. (b) Calculated maximum temperature of the cathode surface and near-cathode voltage drop.

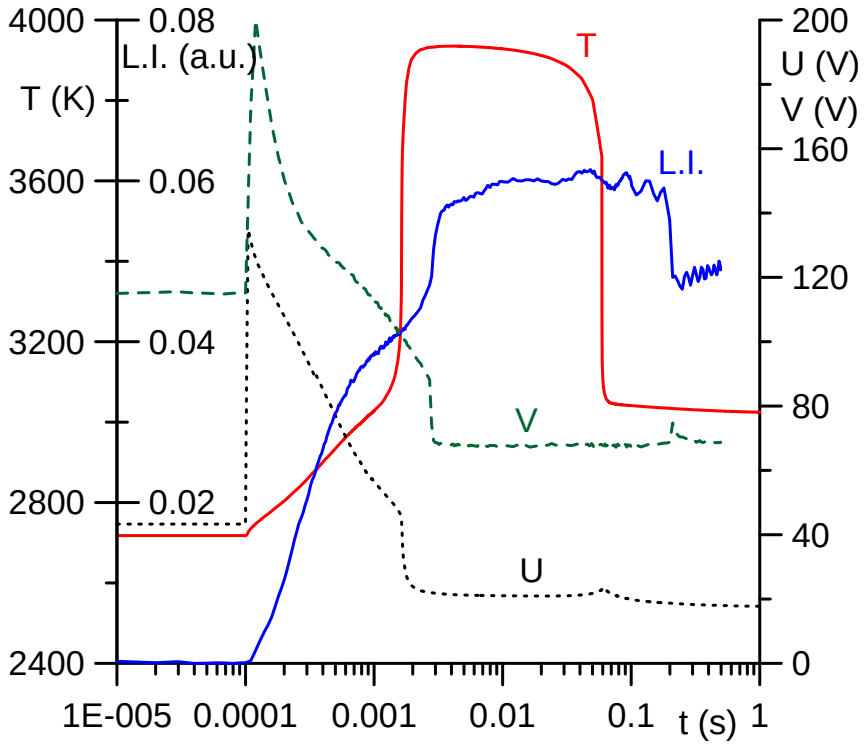

Figure 4.8: Measured intensity of light emitted by the near-cathode region and lamp voltage and calculated maximum temperature of the cathode surface and near-cathode voltage drop. Type 2 lamps, $I_1 = 0.3\,\mathrm{A}$, $I_2 = 1.3\,\mathrm{A}$.

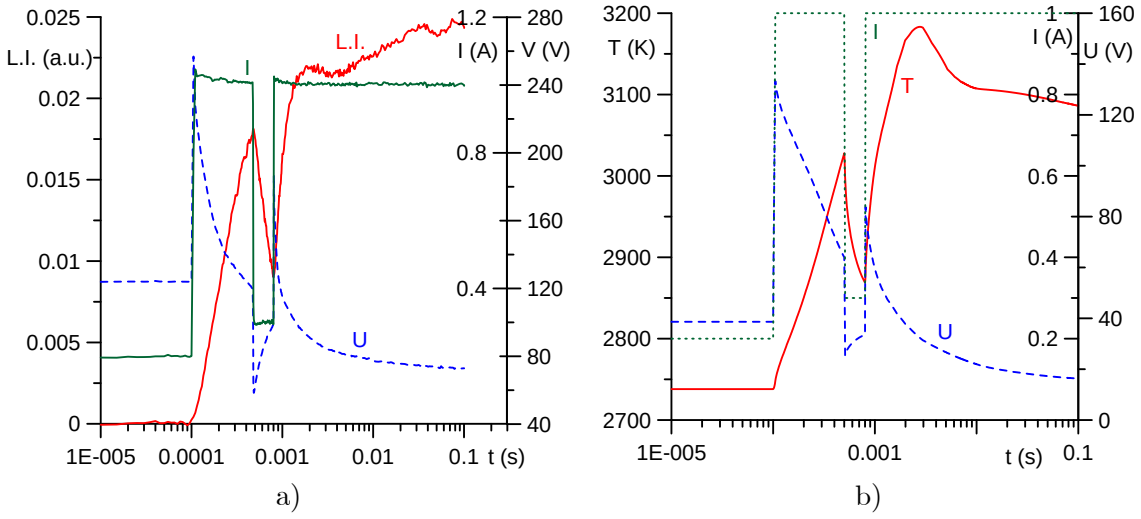

Figure 4.9: Prevention of transient spots on cathodes of type 1 lamps, 0.2 A – 1.0 A current jump. (a) Measured intensity of light emitted by the near-cathode region and lamp voltage. (b) Calculated maximum temperature of the cathode surface and near-cathode voltage drop.

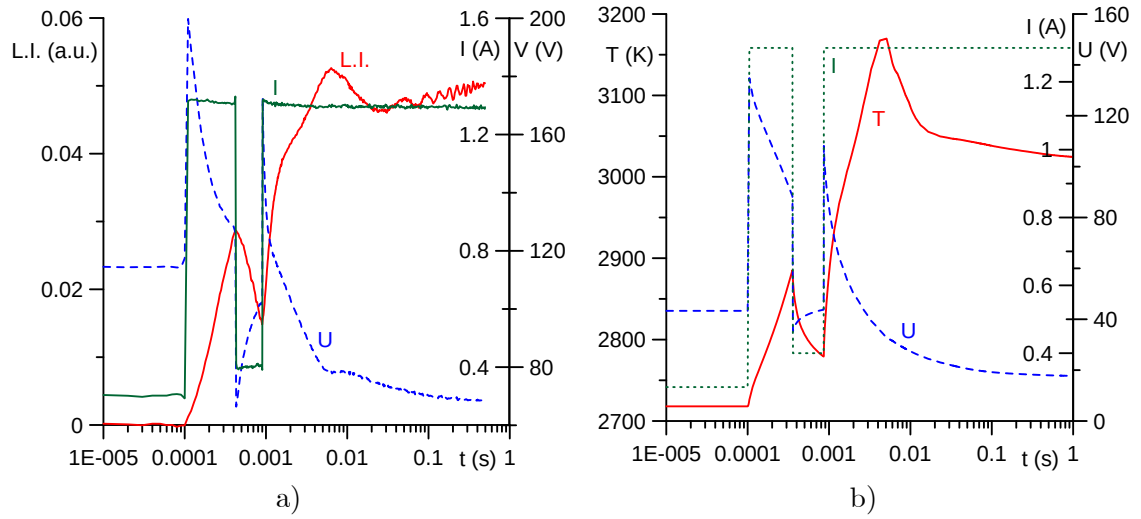

Figure 4.10: Prevention of transient spots on cathodes of type 2 lamps, 0.3 A – 1.3 A current jump. (a) Measured intensity of light emitted by the near-cathode region and lamp voltage. (b) Calculated maximum temperature of the cathode surface and near-cathode voltage drop.

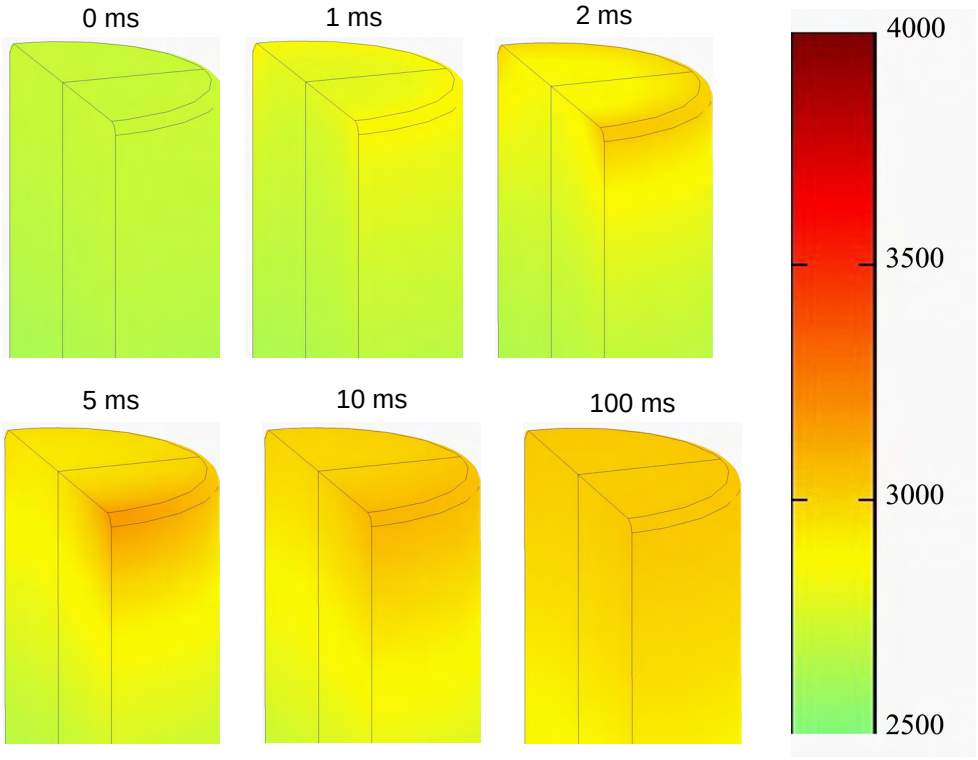

Figure 4.11: Prevention of transient spots under conditions of figure 4.6. At $t = 0$, current rises from 0.3 A within 5 μs to 1.3 A. At $t = 0.3$ ms the current is reduced to 0.4 A. At $t = 0.8$ ms the current again rises to 1.3 A (the bar is in kelvin).

Chapter 5

Conclusions of the thesis

Multiple steady-state solutions in the theory of DC glow discharge have been found for the first time. The modelling was performed in the framework of the basic model of glow discharge, comprising equations of conservation of a single ion species and the electrons, transport equations for the ions and the electrons written in the local approximation, and the Poisson equation, and in the framework of a detailed model which takes into account atomic and molecular ions, atomic excited states, excimers, and non-locality of electron energy.

In the case where neutralization of the ions and the electrons at the wall is neglected, one of the solutions existing in the framework of the basic model of glow discharge is 1D and represents an analogue of the classical solution of von Engel and Steenbeck. This solution describes the fundamental mode, i.e., the one which exists at all values of the discharge current. The other modes are 2D (axially symmetric) or 3D and exist in limited ranges of the discharge currents. Each 2D mode is constituted by two branches, one associated with a pattern comprising a spot at the center of the cathode and the other with a pattern without a central spot. Each 3D mode represents in reality a continuum of modes identical to the accuracy of a rotation. The first 3D mode and the branch with a spot at the center of the first 2D spot mode exhibit a well pronounced effect of normal current density. The second and higher 3D modes describe patterns similar to those observed in experiments [5–11].

An account of neutralization of the ions and the electrons at the wall causes a dramatic change of the pattern of self-organization: the bifurcations through which 2D modes branch off from the 1D mode are destroyed and this destruction is accompanied by the exchange of branches. The new fundamental mode, which has appeared in this way, includes the Townsend discharge at low currents, the abnormal mode at high currents, and the subnormal and normal modes at intermediate currents. The question where from have the subnormal and normal modes appeared and where to has gone the mode associated with the falling section of the von Engel and Steenbeck CDVC has now a clear answer: the subnormal and normal modes have not appeared, they exist also in the model without neutralization but belong to the other (non-fundamental) mode; the falling section of the von Engel and Steenbeck CDVC continues to exist in the model with neutralization but belongs to the other (non-fundamental) modes.

The inclusion in the model of detailed kinetics (multiple ionic species, atomic excited states, excimers) and an account of non-locality of electron transport and kinetic coefficients (by means

of a differential equation of conservation of electron mean energy) does not prevent existence of multiple solutions describing different modes of current transfer to cathodes of DC glow discharges and is in fact favourable: three 2D modes were found, in addition to the fundamental (1D) mode, for xenon in the framework of the detailed model where only two 2D modes exist in the framework of the basic model under the same conditions. Account of the detailed kinetics and non-locality of electron transport and kinetic coefficients does not affect the results qualitatively: the multiple solutions fit the same pattern that those found in the framework of the basic model. The latter is not surprising, since self-organization is governed by the same trends in different systems, in particular in glow and arc cathodes [74].

Numerical results for argon, obtained in the framework of the detailed and basic models, and those for helium, obtained in the framework of the basic model, give a clear indication that the conditions of argon and helium microdischarges are less favourable for self-organization than those in xenon. This is a consequence of the difference between cross sections of elastic collisions between electrons and atoms of these gases. However, it should be possible to observe self-organization also in argon and helium microdischarges provided that the pressure is sufficiently high and the discharge radius is sufficiently large.

The modelling revealed the existence of complex behaviour of the fundamental mode in two different situations. This behaviour is manifested through a retrograde section limited by two turning points. In the case of the fundamental (1D) mode calculated in the framework of the detailed model of discharge in xenon between parallel-plane electrodes, this behaviour manifests itself in the plane (j, U) as an S-shaped section of the CDVC and is associated with stepwise ionization. In the case of the fundamental (2D) mode calculated in the framework of a basic model of a cathode boundary layer discharge in xenon, this behaviour manifests itself in the plane (I, U) as a loop in the CVC. The effect is a consequence of the geometry of the discharge: the loop is associated with a smooth transition between the pattern with a ring spot inside the cathode at low currents and a pattern with a central spot at high currents.

Formation of transient spots on thermionic cathodes was studied experimentally on COST-529 standard HID lamps. The experimental setup includes a power supply which allows for rapid variations of the discharge current (on a time scale of the order of the μs) while maintaining high power output; a feature which is important for these experiments. The experiments have been performed in parallel and coordinated with numerical modelling.

The intensity of light emitted by the near-cathode region and the lamp voltage were measured as functions of time and found to be in a good qualitative agreement with the near-cathode voltage drop and maximum temperature of the cathode surface computed for conditions of the experiments. There is a good agreement also on the threshold current and time of formation of transient spots, although not on their lifetime.

A possibility of prevention of appearance of transient spots by means of a brief reduction of the arc current shortly after the initial current increase is proposed and justified. The main mechanism of blackening of burners of HID lamps that accompanies appearance of transient cathode spots is evaporation of the cathode material and not sputtering.

In the future, one could think of studying 3D modes with multiple spots in xenon and argon with account of the effect of neutralization of charged particles at the wall of the discharge vessel.

This could offer a guide for experiments with the aim of detecting self-organization in argon microdischarges.

Another question which deserves attention in future work concerns the above-described complex behaviour detected in modelling of DC glow microdischarges. Both the S-shape and the loop are scientifically very interesting. Regarding the S-shape, future work includes computing the fundamental 2D mode with account of neutralization of the charged particles at the wall in the framework of the detailed model and determining if a retrograde section will be present. (This implies attempting to overcome the weaknesses of Comsol Multiphysics which were revealed in this work. This could be achieved by conveying the usefulness of steady-state solvers to the developers of the Plasma Module and/or by rewriting the equation of conservation of electron energy and the associated boundary condition in a form suitable for modelling with steady-state solvers of Comsol Multiphysics.) Regarding the section with the loop, future work includes determining how does the fundamental mode change from the form reported in section 2.4 into the form reported in section 3.3. It will be interesting also to determine if similar complex behaviour exists also in discharges in other plasma-producing gases, e.g. argon.

Recently, experiments with microhollow cathode discharge systems in argon, e.g. [107, 108] revealed existence of oscillations and sections of the measured CVC possessing both positive and negative differential resistivities. The oscillations have been detected also in the modelling by means of a non-stationary solver; e.g., [96]. It would be very interesting to model these experiments also by means of steady state solvers of Comsol Multiphysics, in order to check for the possible complex behaviour similar to that found in this work for a cathode boundary layer discharge configuration.

Bibliography

[1] A. von Engel, *Ionized Gases* (American Institute of Physics, New York, 1965).

[2] Yu. P. Raizer, *Gas Discharge Physics* (Springer, Berlin, 1991).

[3] D. Staack, B. Farouk, A. Gutsol, and A. Fridman, Plasma Sources Sci. Technol. **17**, 025013 (13pp) (2008).

[4] K. H. Becker, K. H. Schoenbach, and J. G. Eden, J. Phys. D: Appl. Phys. **39**, R55 (2006).

[5] K. H. Schoenbach, M. Moselhy, and W. Shi, Plasma Sources Sci. Technol. **13**, 177 (2004).

[6] M. Moselhy and K. H. Schoenbach, J. Appl. Phys. **95**, 1642 (2004).

[7] N. Takano and K. H. Schoenbach, Plasma Sources Sci. Technol. **15**, S109 (2006).

[8] N. Takano and K. H. Schoenbach, in *Abstracts of the 2006 IEEE International Conference on Plasma Science* (IEEE, Traverse City, MI, USA, 2006) p. 247.

[9] B.-J. Lee, H. Rahaman, K. Frank, L. Mares, and D.-L. Biborosch, in *Proc. 28th ICPIG (Prague, July 2007)*, edited by J. Schmidt, M. Šimek, S. Pekárek, and V. Prukner (Institute of Plasma Physics AS CR, ISBN 978-80-87026-01-4, Prague, 2007) pp. 900–902.

[10] W. Zhu, N. Takano, K. H. Schoenbach, D. Guru, J. McLaren, J. Heberlein, R. May, and J. R. Cooper, J. Phys. D: Appl. Phys. **40**, 3896 (2007).

[11] B.-J. Lee, D.-L. Biborosch, K. Frank, and L. Mares, J. Optoelectron. Adv. Mater. **10**, 1972 (2008).

[12] M. Moselhy, I. Petzenhauser, K. Frank, and K. H. Schoenbach, J. Phys. D: Appl. Phys. **36**, 2922 (2003).

[13] W. Thouret, W. Weizel, and P. Günther, Z. Physik **130**, 621 (1951).

[14] H. N. Olsen, J. Quant. Spectrosc. Radiat. Transfer **3**, 305 (1963).

[15] M. S. Benilov, J. Phys. D: Appl. Phys. **41**, 144001 (30pp) (2008).

[16] M. S. Benilov, M. D. Cunha, and M. J. Faria, J. Phys. D: Appl. Phys. **42**, 145205 (17pp) (2009).

[17] S. Lichtenberg, D. Nandelstädt, L. Dabringhausen, M. Redwitz, J. Luhmann, and J. Mentel, J. Phys. D: Appl. Phys. **35**, 1648 (2002).

[18] H.-G. Purwins, H. U. Bödeker, and S. Amiranashvili, Adv. Phys. **59**, 485 (2010).

[19] W. Breazeal, K. M. Flynn, and E. G. Gwinn, Phys. Rev. E **52**, 1503 (1995).

[20] A. L. Zanin, A. W. Liehr, A. S. Moskalenko, and H.-G. Purwins, Appl. Phys. Lett. **81**, 3338 (2002).

[21] E. L. Gurevich, A. L. Zanin, A. S. Moskalenko, and H.-G. Purwins, Phys. Rev. Lett. **91**, 154501(4) (2003).

[22] L. Stollenwerk, Sh. Amiranashvili, J.-P. Boeuf, and H.-G. Purwins, Phys. Rev. Lett. **96**, 255001 (2006).

[23] C. Strümpel, Yu. A. Astrov, and H.-G. Purwins, Phys. Rev. E **62**, 4889 (2000).

[24] C. Strümpel, H.-G. Purwins, and Yu. A. Astrov, Phys. Rev. E **63**, 026409(7) (2001).

[25] E. L. Gurevich, Yu. A. Astrov, and H.-G. Purwins, J. Phys. D: Appl. Phys. **38**, 468 (2005).

[26] D. Malik, K. Orlov, I. Miroshnikov, and A. Smirnov, Tech. Phys. Lett. **31**, 500 (2005), 10.1134/1.1969779.

[27] Yu. D. Korolev, V. G. Rabotkin, and A. G. Filonov, High Temp. **17**, 181 (1979).

[28] S. A. Bystrov, A. M. Lushchikova, D. A. Mazalov, A. F. Pal, A. N. Starostin, M. D. Taran, T. V. Taran, and A. V. Filippov, J. Phys. D: Appl. Phys. **27**, 273 (1994).

[29] V. Arkhipenko, A. Kirillov, T. Callegari, Y. Safronau, and L. Simonchik, IEEE Trans. Plasma. Sci. **37**, 740 (2009).

[30] A. von Engel and M. Steenbeck, *Elektrische Gasentladungen. Ihre Physik und Technik*, Vol. Vol II (Springer-Verlag, Berlin, 1934).

[31] M. S. Benilov, J. Phys. D: Appl. Phys. **40**, 1376 (2007).

[32] M. S. Benilov and M. J. Faria, J. Phys. D: Appl. Phys. **40**, 5083 (2007).

[33] M. Steenbeck, Physikalische Zeitschrift **XXXIII**, 809 (1932).

[34] M. S. Benilov and G. V. Naidis, J. Phys. D: Appl. Phys. **43**, 175204 (9pp) (2010).

[35] Yu. P. Raizer, High Temp. **24**, 984 (1986).

[36] Th. Peters, Z. Physik A **144**, 612 (1956).

[37] V. N. Melekhin and N. Yu. Naumov, Sov. Tech. Phys. Lett. **12**, 41 (1986).

[38] V. Yu. Baranov, A. A. Vedenov, and V. G. Niz'ev, Teplofiz. Vys. Temp. **10**, 1039 (1972).

[39] A. V. Engel, K. G. Emeleus, and M. Kennedy, Phys. Lett. A **42**, 191 (1972).

[40] A. L. Ward, Phys. Rev. **112**, 1852 (1958).

[41] A. L. Ward, J. Appl. Phys. **33**, 2789 (1962).

[42] G. G. Gladush and A. A. Samokhin, J. Appl. Mech. Tech. Phys. **22**, 608 (1981).

[43] Yu. P. Raizer and S. T. Surgikov, Sov. Tech. Phys. Lett. **13**, 186 (1987).

[44] Yu. P. Raizer and S. T. Surgikov, High Temp. **26**, 428 (1988).

[45] J.-P. Boeuf, J. Appl. Phys. **63**, 1342 (1988).

[46] A. Fiala, L. C. Pitchford, and J. P. Boeuf, Phys. Rev. E **49**, 5607 (1994).

[47] V. I. Kolobov and A. Fiala, Phys. Rev. E **50**, 3018 (1994).

[48] R. R. Arslanbekov and V. I. Kolobov, J. Phys. D: Appl. Phys. **36**, 2986 (2003).

[49] S. T. Surzhikov, High Temp. **43**, 825 (2005).

[50] H. C. Kim, F. Iza, S. S. Yang, M. Radmilovic-Radjenovic, and J. K. Lee, J. Phys. D: Appl. Phys. **38**, R283 (2005).

[51] M. S. Benilov, Sov. Phys. - Tech. Phys. **33**, 1267 (1988).

[52] M. S. Benilov, Plasma Sources Sci. Technol. **16**, 422 (2007).

[53] I. R. Rafatov, D. D. Šijačić, and U. Ebert, Phys. Rev. E **76**, 036206(18) (2007).

[54] M. S. Benilov, Phys. Rev. E **77**, 036408 (2008).

[55] http://www.arc_cathode.uma.pt.

[56] M. S. Benilov, M. Carpaij, and M. D. Cunha, J. Phys. D: Appl. Phys. **39**, 2124 (2006).

[57] W. L. Bade and J. M. Yos, *Theoretical and Experimental Investigation of Arc Plasma-Generation Technology. Part II, Vol. 1: A Theoretical and Experimental Study of Thermionic Arc Cathodes. Technical Report No. ASD-TDR-62-729* (Avco Corporation, Wilmington, Mass., USA, 1963).

[58] W. Neumann, *The Mechanism of the Thermoemitting Arc Cathode* (Akademie-Verlag, Berlin, 1987).

[59] M. S. Benilov and N. V. Pisannaya, Sov. Phys. - Tech. Phys. **33**, 1260 (1988).

[60] M. S. Benilov, Phys. Rev. E **58**, 6480 (1998).

[61] R. Bötticher and W. Bötticher, J. Phys. D: Appl. Phys. **33**, 367 (2000).

[62] M. S. Benilov and M. D. Cunha, J. Phys. D: Appl. Phys. **36**, 603 (2003).

[63] L. Dabringhausen, O. Langenscheidt, S. Lichtenberg, M. Redwitz, and J. Mentel, J. Phys. D: Appl. Phys. **38**, 3128 (2005).

[64] G. M. J. F. Luijks, S. Nijdam, and H. v Esveld, J. Phys. D: Appl. Phys. **38**, 3163 (2005).

[65] W. W. Stoffels, A. H. F. M. Baede, J. J. A. M. van der Mullen, M. Haverlag, and G. Zissis, Meas. Sci. Technol. **17**, N67 (2006).

[66] P. G. C. Almeida, M. S. Benilov, and M. D. Cunha, J. Phys. D: Appl. Phys. **41**, 144004 (9pp) (2008).

[67] P. G. C. Almeida, M. S. Benilov, and M. D. Cunha, IEEE Trans. Plasma Sci. **36**, 1032 (2008).

[68] P. G. C. Almeida, M. S. Benilov, and M. J. Faria, Plasma Sources Sci. Technol. **19**, 025019 (13pp) (2010).

[69] P. G. C. Almeida, M. S. Benilov, and M. J. Faria, IEEE Trans. Plasma Sci. **39**, (2011, to appear).

[70] P. G. C. Almeida, M. S. Benilov, and M. J. Faria, Bull. Amer. Phys. Soc., Proc. 63rd Gaseous Electronics Conf. and 7th Int. Conf. on Reactive Plasmas **55**, 166 (2010).

[71] I. Brauer, C. Punset, H.-G. Purwins, and J. Boeuf, J. Appl. Phys. **85**, 7569 (1999).

[72] B. Bernecker, T. Callegari, S. Blanco, R. Fournier, and J. P. Boeuf, Eur. Phys. J. Appl. Phys. **47**, 22808 (2009).

[73] B. Bernecker, T. Callegari, and J. P. Boeuf, in *Proc. 12th HAKONE (Bratislava, September 2010)*, edited by J. Országh, P. Papp, and Š Matejčík (Soc. Plasma Res. Appl., Library and Publishing Centre CU, ISBN 978-80-89186-72-3, Bratislava, 2010) pp. 19–30.

[74] P. G. C. Almeida, M. S. Benilov, M. D. Cunha, and M. J. Faria, J. Phys. D: Appl. Phys. **42**, 194010 (21pp) (2009).

[75] M. A. Biondi and L. M. Chanin, Phys. Rev. **94**, 910 (1954).

[76] G. J. M. Hagelaar and L. C. Pitchford, Plasma Sources Sci. Technol. **14**, 722 (2005).

[77] J. Meunier, P. Belenguer, and J. P. Boeuf, J. Appl. Phys. **78**, 731 (1995).

[78] A. Fridman and L. A. Kennedy, *Plasma Physics and Engineering* (Taylor and Francis, New York, 2004).

[79] M. S. Benilov, Phys. Rev. A **45**, 5901 (1992).

[80] H. Haken, *Synergetics, An Introduction*, Springer Series in Synergetics, Vol. 1 (Springer, Berlin, 1978).

[81] C. H. Thomas and O. S. Duffendack, Phys. Rev. **35**, 72 (1930).

[82] K. G. Müller, Phys. Rev. A **37**, 4836 (1988).

[83] M. J. Faria, P. G. C. Almeida, M. S. Benilov, and V. V. Mikhailenko, in *Proc. 63rd Gaseous Electronics Conf. and 7th Int. Conf. on Reactive Plasmas*, Bull. Amer. Phys. Soc., Vol. 55 (2010) p. 84.

[84] L. C. Pitchford, J. Kang, C. Punset, and J. P. Boeuf, J. Appl. Phys. **92**, 6990 (2002).

[85] A. N. Bhoj and M. J. Kushner, J. Phys. D: Appl. Phys. **37**, 2510 (2004).

[86] J. P. Boeuf, L. C. Pitchford, and K. H. Schoenbach, Appl. Phys. Lett. **86**, 071501 (2005).

[87] E. A. Bogdanov, A. A. Kudryavtsev, R. R. Arslanbekov, and V. I. Kolobov, J. Phys. D: Appl. Phys. **37**, 2987 (2004).

[88] E. Muñoz-Serrano, G. Hagelaar, T. Callegari, J. P. Boeuf, and L. C. Pitchford, Plasma Phys. Control. Fusion **48**, B391 (2006).

[89] E. Muñoz-Serrano, J. P. Boeuf, and L. C. Pitchford, in *Proc. 29th Int. Conf. On Phenomena in Ionized Gases (Cancun, Mexico, July 12th - 17st, 2009)* (Universidad Autónoma de México, Cancun, 2009).

[90] M. Hayashi, NIFS - Data **79** (2003).

[91] L. Vriens and A. H. M. Smeets, Phys. Rev. A **22**, 940 (1980).

[92] M. Hayashi, NIFS - Data **72** (2003).

[93] G. M. Petrov and C. M. Ferreira, Private communication (2010).

[94] P. G. C. Almeida, M. S. Benilov, and G. V. Naidis, J. Phys. D: Appl. Phys. **35**, 1577 (2002).

[95] K. Makasheva, E. Muñoz-Serrano, G. Hagelaar, J. P. Boeuf, and L. C. Pitchford, Plasma Phys. Control. Fusion **49**, B233 (2007).

[96] T. Deconinck and L. L. Raja, Plasma Processes Polym. **6**, 335 (2009).

[97] X. Zhang, X. Wang, F. Liu, and Y. Lu, IEEE Trans. Plasma. Sci. **37**, 2055 (2009).

[98] A. V. Phelps, (2008), http://jilawww.colorado.edu/~avp/collision_data/electronneutral/ELECTRON.TXT, Last modified 24-Jun-2008.

[99] Y. Sakiyama and D. B. Graves, J. Phys. D: Appl. Phys. **39**, 3451 (2006).

[100] R. Bötticher, W. Graser, and A. Kloss, J. Phys. D: Appl. Phys. **37**, 55 (2004).

[101] R. Bötticher and M. Kettlitz, J. Phys. D: Appl. Phys. **39**, 2715 (2006).

[102] L. E. Cram, J. Phys. D: Appl. Phys. **16**, 1643 (1983).

[103] R. Bötticher and W. Bötticher, J. Phys. D: Appl. Phys. **34**, 1110 (2001).

[104] Y. S. Touloukian, R. W. Powell, C. Y. Ho, and P. G. Clemens, *Thermal Conductivity. Metallic Elements and Alloys.*, Thermophysical Properties of Matter, vol. 1 (IFI/Plenum, New York-Washington, 1970).

[105] H. Moench, C. Deppe, U. Hechtfischer, G. Heusler, and P. Pekarski, in *Proceedings of the 10th International Symposium on the Science and Technology of Light Sources, July. 2004*, edited by G. Zissis (Institute of Physics Publishing, Toulouse, France, 2004) pp. 171–172.

[106] G. Derra, E. Fischer, H. G. Ganser, and H. Moench, Patent US5608294.

[107] X. Aubert, G. Bauville, J. Guillon, B. Lacour, V. Puech, and A. Rousseau, Plasma Sources Sci. Technol. **16**, 23 (2007).

[108] J. Greenan, C. M. O. Mahony, D. Mariotti, and P. D. Maguire, Plasma Sources Sci. Technol. **20**, 025011 (2011).